Understanding Of Silicate-based Corrosion Inhibitor For Controlling Lead Release And Water Quality In Drinking Water Distribution Systems

by

Bofu Li

Submitted in partial fulfilment of the requirements
for the degree of Doctor of Philosophy

at

Dalhousie University
Halifax, Nova Scotia
November, 2020

Table of Contents

Table of Tables

Table of Figures

Abstract

Sodium silicates have been used in drinking water treatment for decades, both as sequestrants and as corrosion inhibitors. For the latter purpose they are poorly understood; a lack of information contributes uncertainty and risks drinking water quality. This work explored three approaches to investigate the effectiveness and mechanisms of sodium silicate on lead release control: lead release of corroded coupons, dissolution rate of lead carbonate, and lead release in a pilot-scale distribution system. Here, silicate treatment did not effectively mitigate the lead release, except for the impact of elevated pH with its use. Sodium silicate also provided minimal protection for galvanic corrosion while orthophosphate effectively mitigated lead release. Impact of silicate adsorption on lead carbonate dissolution was negligible and direct interaction between sodium silicate and lead appears unlikely. Lead carbonates are the major corrosion scales of lead pipes and lead coupons in silicate-treated systems. Although silicate formed a nanometer-thick coating on the top surface of corrosion scales, this mechanism appeared to be negligible in term of lead release. As a sequestrant, sodium silicates dispersed the colloidal metals (e.g., iron, manganese and aluminum) which in turn elevated the lead concentration. Elevated pH is the major mechanism by sodium silicate for lead corrosion mitigation.

List of Abbreviations Used

LSLs Lead service line

PLSLs Partial lead service line

PVC Polyvinyl chloride

DIC Dissolved inorganic carbon

DOM Dissolved organic matter

NOM Natural organic matter

TOC Total organic carbon

SEC Size-exclusion chromatography

HPLC High-performance liquid chromatography

ICP-MS Inductively coupled plasma mass spectrometry

UV254 Ultraviolet absorbance at 254 nm

SD Standard deviation

IQR Interquartile range

CPS Counts per second

CI Confidence interval

HDPE High-density polyethylene

Pt-Co Platinum cobalt

NTU Nephelometric turbidity units

XPS X-ray photoelectron spectroscopy

FFF Field flow fractionation

SEM-EDS Scanning electron microscopy/energy-dispersive X-ray spectroscopy

XRD X-ray diffraction

FTIR Fourier transform infrared spectroscopy

CSTRs Continuous stirred tank reactors

Acknowledgment

This thesis was completed with help from professors, colleagues and organizations. First, I acknowledge the financial support provided by NSERC / Halifax Water Industrial Research Chair program, NSERC CRD Grant with National Silicates, Coldblock Technologies and Killam Trusts. I also thank the cooperation from Halifax Water. I acknowledge the reproduction reproduced from Li, B., Trueman, B. F., Rahman, M. S., Gao, Y., Park, Y., & Gagnon, G. A. (2019). Understanding the impacts of sodium silicate on water quality and iron oxide particles. Environmental Science: Water Research & Technology, 5(8), 1360-1370. (20th reference) with permission from the Royal Society of Chemistry.

Second, I thank my colleagues who assisted me in completing papers and experiments. Dr. Benjamin Trueman offered me the great help in writing, experimental design and statistics. Fellow graduate students Sebastian Munoz and Javier Locsin provided important works in experiments. I also recognize the technical and administrative support provided by Dr. Yuri Park; lab technicians Heather Daurie, and Tarra Chartrand.

Third, my supervisor, Dr. Graham Gagnon, and my supervisory committee—Drs. Margaret Walsh and Jennie Rand provided me the guidance and encouragement at different stages during my program.

Finally, my parents and Shijun also inspired me to complete this work.

1 Chapter 1 Introduction

1.1 Health effects of lead exposure from drinking water

Health risks from lead (Pb) exposure through drinking water have been recognized. Blood lead levels have been shown to be positively correlated with the elevated lead concentration in drinking water.[1,2] Blood lead levels link with the risks of cardiovascular disease mortality,[3] hypertension, and renal dysfunction.[4,5] Childhood blood lead levels are also correlated with cognitive deficits.[6,7]

1.2 Regulation of lead control

Lead concentration of drinking water is regulated under Lead and Copper Rule in the United States, which specifies the action level of 15 μg/L for the 90th percentile level of tap water samples.[8] In Canada, the maximum acceptable concentration of total lead is 5 μg/L.[9]

1.3 Research motivation

Phosphate-based corrosion inhibitors are the most widely used practices in lead exposure control. Phosphate (i.e, orthophosphate) may limit lead release by forming low solubility lead phosphate solids (i.e., hydroxylpyromorphite and chloropyromorphite)[10] or mitigate dissolution of lead carbonate by the adsorption.[11] There are, however, several potential issues regarding the use of phosphate-based corrosion inhibitors: a) demand for phosphorus will increase (e.g., fertilizer in agriculture) in the future while the price is volatile.[12,13] For example, the price of phosphate rock increased ~800% in 2007-2008.[14] b) the addition of phosphate-based corrosion inhibitors increases the phosphorus loading in wastewater while wastewater treatment plants are struggling to eliminate phosphorus at great cost. c) phosphorus also acts as a nutrient for microbial growth in distribution systems or eutrophication.

Due to the considerable public health and economic benefits, the water industry, suppliers, and researchers are paying attention to the potential alternatives to phosphate-based corrosion inhibitors.

1.4 A suggested alternative—silicate-based corrosion inhibitor

Besides phosphate-based corrosion inhibitors, silicate-based corrosion inhibitors may be the most frequently mentioned in literature, especially in the reviewing of existing corrosion inhibitors for lead. However, the effectiveness and mechanisms have not been well-documented. Schock et al. [10] reported a decrease (55 - 95%) in lead concentration by replacing polyphosphate with sodium silicate in a medium-size distribution system. Lintereur et al. [15] indicated that the increase in sodium silicate dosage from 3 to 12 mg/L resulted in the lead concentration below the action level of 15 µg/L. These studies indicate that sodium silicate is a promising corrosion inhibitor for lead release control. But, in these studies, the effect of pH and dosage of silicate-based corrosion inhibitors were confounded.

Previous studies also indicate that sodium silicate does not have a good performance on the lead release control. For instance, Kogo et al. [16] indicated that sodium silicate did not effectively decrease lead release for galvanic corrosion. Woszczynski et al. [17] indicated phosphate treatment performed better than sodium silicate treatment in a pilot-scale system. Pinto et al. [18] demonstrated that pH and alkalinity adjustment were more effective than the silicate treatment. In these studies, the phosphate treatment was better than the silicate treatment.

Also, sodium silicates are widely used as sequestrants to solve aesthetic issues caused by iron and manganese.[19,20] Disperse impact of sodium silicate on lead release is still poorly understood.

Recently, the failure of a silicate-treated system—Newark, New Jersey—came to public attention in 2017.[21,22] The lack of understanding about silicate treatment raised important questions about the appropriate use and the potential misuse in lead control. However, few answers can be found in the peer-reviewed literature.

1.5 Possible mechanisms of silicate treatment

Sodium silicates may form a thin coating on the internal surface of lead pipes,[23,24] or contribute to passive scale formation,[16,25,26] but little evidence exists to support these possibilities. The effect of sodium silicate is often confounded with the increase in pH that accompanies its use,[10,15,25,27] which decreases lead carbonate solubility in most cases. Silicate-aluminum and quartz were frequently observed in drinking distribution systems,[28,29] indicating that a non-lead diffusion barrier may contribute to the lead release control. Previous studies[11,30] also indicate ion adsorption can inhibit the dissolution rates of minerals (e.g., lead carbonate) when the chemical equilibrium state is not reached.

1.6 Organization of thesis

The goal of the thesis is to comprehensively understand and evaluate the performance of silicate-based corrosion inhibitors on lead release control in drinking water distribution systems. There are six chapters:

Chapter 1 introduces background information and current concerns about previous studies of silicate-based corrosion inhibitors.

Chapter 2 is to evaluate total and dissolved lead release of corroded lead coupons in silicate-treated corrosion cells, compared against an inhibitor-free control, a better-characterized inhibitor (orthophosphate), and a widely used sequestrant (polyphosphate) at two pH (7-9.5) and dissolved inorganic carbon levels (5-50 mg C/L). The estimated main effects of inhibitors (i.e., sodium silicate, orthophosphate, polyphosphate) and the interaction effects combined with pH and dissolved inorganic carbon levels were estimated by the linear regression and the factorial experiment design. This study also characterized the possible passive corrosion scales and the silicate-related coating on the surface of silicate-treated lead coupons (Figure 1).

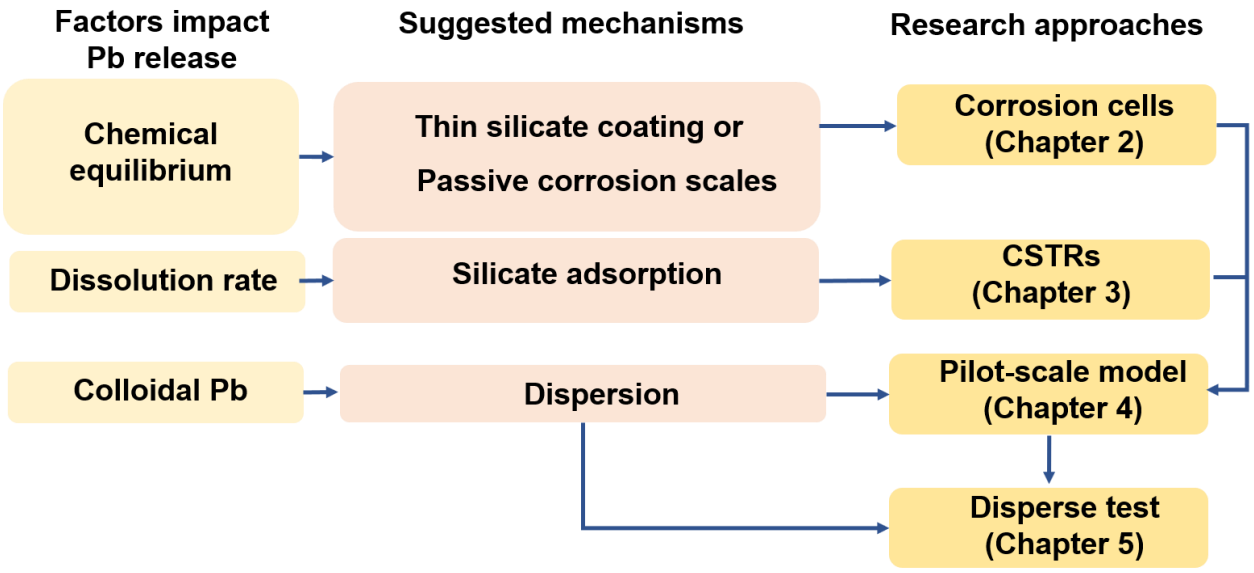

Figure 1 Suggested mechanisms and research approaches.

Chapter 3 focuses on the effect and efficiency of silicate-based inhibitors in the scenario - lead concentration does not meet the chemical equilibrium when dissolution rate controls lead release. This study using continuous-flow stirred tank reactors (CSTRs) to investigate whether silicate adsorption can block active sites and slow the dissolution rate of lead carbonate. The interaction effects of silicate treatment and the dissolution rates of lead carbonate were estimated by a factorial experimental design. The changes in the chemical and structural properties of lead carbonate and the mechanisms were described to explain these observations.

Chapter 4 is to evaluate the performance of sodium silicate in a pilot-scale model distribution system, especially compared against two common corrosion inhibitors—orthophosphate and zinc orthophosphate. Besides the effect of sodium silicate on lead release, the impacts of municipal main pipes (cast iron and PVC) and the lead service pipes types (galvanic and uniform) were evaluated by a generalized additive mixed model. In this chapter, the release of colloidal metals (iron, lead, copper, etc.) was also investigated by the field flow fractionation.

Chapter 5 aims at the disperse impact of sodium silicate. This study focuses on the interaction between sodium silicate and iron particles under various water quality

conditions (i.e., pH, dissolved organic carbon, and natural organic matter). This would help to understand the co-transportation of lead and other metals (i.e., iron, aluminum, etc.) in future studies.

Chapter 6 is the conclusions and recommendations.

Appendix A - D provides supplementary information for the individual chapter

2 Chapter 2 Controlling lead release due to uniform and galvanic corrosion—an evaluation of silicate-based inhibitors

This chapter reproduced from Li, B., Trueman, B. F., Rahman, S. M., & Gagnon, G. A. (2020). Controlling lead release due to uniform and galvanic corrosion—an evaluation of silicate-based inhibitors. Journal of Hazardous Materials.
https://doi.org/10.1016/j.jhazmat.2020.124707

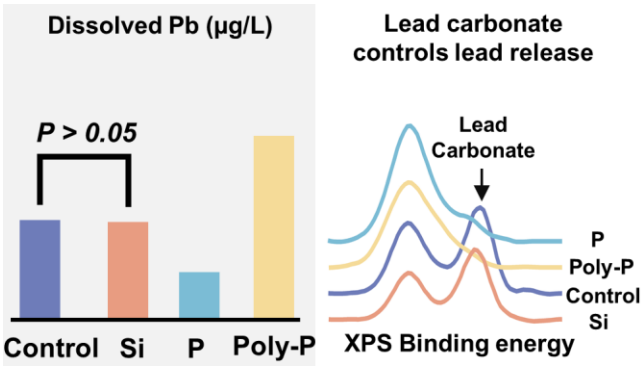

Figure 2 Artwork of evaluating sodium silicate, orthophosphate and poly-phosphate on dissolved lead; lead carbonate appeared in the silicate-treated system.

2.1 Abstract

Silicates have been added to drinking water for decades, both to sequester iron/manganese and as a corrosion control treatment for lead. However, the mechanisms by which they might act to limit lead release are not well understood, which has contributed to lead contamination in practice. The effects of two silicate formulations on lead release were evaluated due to uniform and galvanic corrosion over a wide range of pH and dissolved inorganic carbon (DIC) concentrations. These results were compared to better-characterized systems, with added ortho- or polyphosphate and in an inhibitor-free control. Independent of pH, silicates did not mitigate lead release due to

either uniform or galvanic corrosion. Furthermore, lead carbonates appeared to determine lead solubility in the presence of sodium silicate. While silicate treatment did promote the formation of a nanometer-thick silicon layer on lead and a decrease in crystallite size at the scale surface, these changes were not strongly protective. However, unlike polyphosphate—which is known to form soluble complexes with lead and disperse particulate metals—high ratio silicate did not exacerbate lead release. Conversely, metasilicate did, especially at pH 7.5 and 5 mg DIC/L; this suggests that silicate formulation may play an important role in corrosion control.

2.2 Introduction

Water utilities rely on two primary strategies—often simultaneously—to minimize lead in drinking water: careful control of distributed water chemistry and lead service line replacement.[31–34] Controlling water chemistry often means adding a corrosion inhibitor, and orthophosphate is the most frequent choice.[31] Sodium silicates represent an alternative[31]; for example, the city of Newark, New Jersey, used a sodium silicate to control lead release beginning in the mid-1990s. Newark switched to orthophosphate after its lead in water crisis came to public attention in 2017,[21,22] prompting questions on the appropriate use of silicates. A lack of research meant that there was little guidance for utilities, and almost no information on the mechanisms by which silicates might act.[26]

Two general mechanisms have been proposed to explain the inhibition of lead release attributed to sodium silicates. First, they may form a passive corrosion scale on lead pipes—either a thin coating or a mineral solid—but this has not been conclusively demonstrated.[15,16,23,24] Second, they increase water pH,[10,15] which decreases lead carbonate solubility in most cases.[35]

Sodium silicates are better understood as sequestrants for controlling aesthetic issues due to iron and manganese.[19,20] But this application carries a potential risk: when polyphosphates are used for the same purpose, they can exacerbate lead release by dissolving lead scale and dispersing colloidal lead.[10,36–38] Given the known dispersive properties of sodium silicates,[20,39] careful evaluation is warranted to ensure that similar unintended consequences do not result from silicate-based sequestration.

The choice of corrosion inhibitor also has implications for the other main approach to lead control, lead service line replacement. When lead pipe is partially replaced with copper, the result is often a galvanic couple that can be a persistent source of lead and may even elevate lead levels above those that occurred pre-replacement.[32,40–43] A galvanic joint can shift water quality dramatically in its immediate vicinity,[44,45] and effective corrosion control appears to be critically important in minimizing the excess lead release caused by partial lead pipe replacement.[32] The impacts of sodium silicates in this scenario are not well described.

Here, silicates were evaluated as inhibitors of lead release due to uniform and galvanic corrosion, comparing them against two well-characterized referential treatments, ortho- and polyphosphate. A wide pH (7–9.5) and DIC range (5–50 mg C/L) was tested, and the surface chemistry of silicate-treated corrosion scale was characterized to understand the scale-water interface. These findings will improve understanding and aid decision making regarding silicate-based corrosion control treatment.

2.3 Materials and methods

2.3.1 Uniform corrosion cells

New lead coupons (11 mm × 13 mm × 1.5 mm) were preconditioned in a 35 mg/L $NaHCO_3$ solution for 24 hours;[46] this step was repeated six times with fresh solution to generate corrosion scale on the surface of lead coupons. After preconditioning, lead coupons were two-thirds submerged in 100 mL of electrolyte solution held in 200 mL screw-top glass jars (Figure 3a).[46,47]

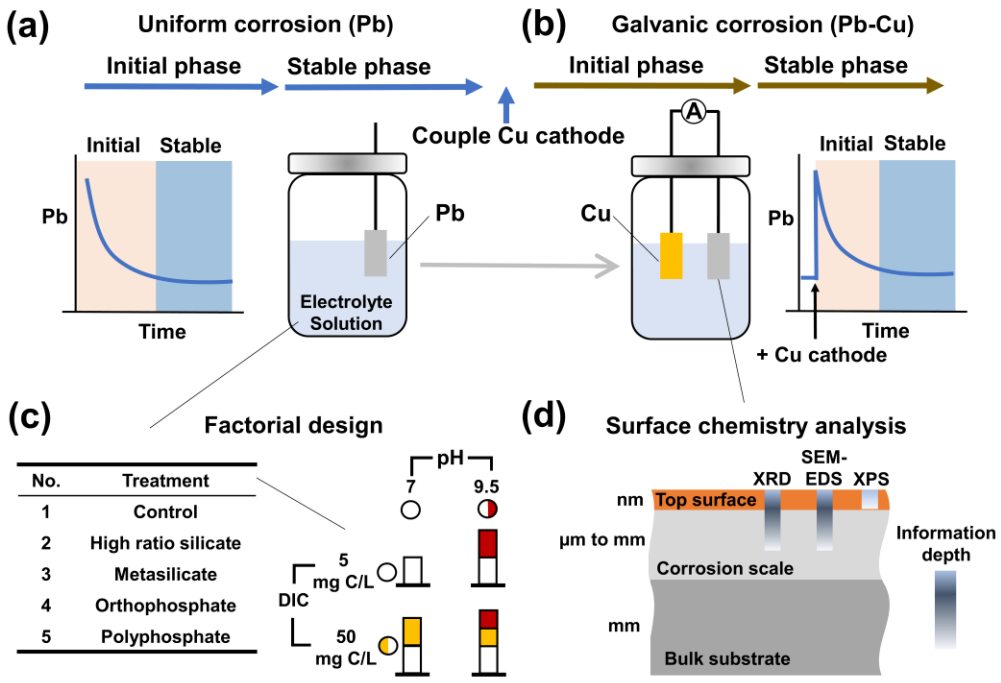

Figure 3 Lead release due to (a) uniform and (b) galvanic corrosion was divided into initial and stable phases. (c) Four corrosion inhibitors and one inhibitor-free control were investigated using a mixed level factorial design. (d) Lead coupons were examined by XRD, SEM-EDS, and XPS.

The stagnation time was set at 48 h to approximate equilibrium[48] with each change of room temperature (21°C ± 1°C) electrolyte solution. Lead release was monitored over time until it reached a steady-state. This was defined by calculating the local slope (rate of change) of the lead concentration time series using local linear regression.[49] When its 95% confidence interval included 0 µg/L per unit time (refill), the system was considered stable. An example is shown in Figure 4 (orthophosphate at pH 7 and DIC 50 mg/L).

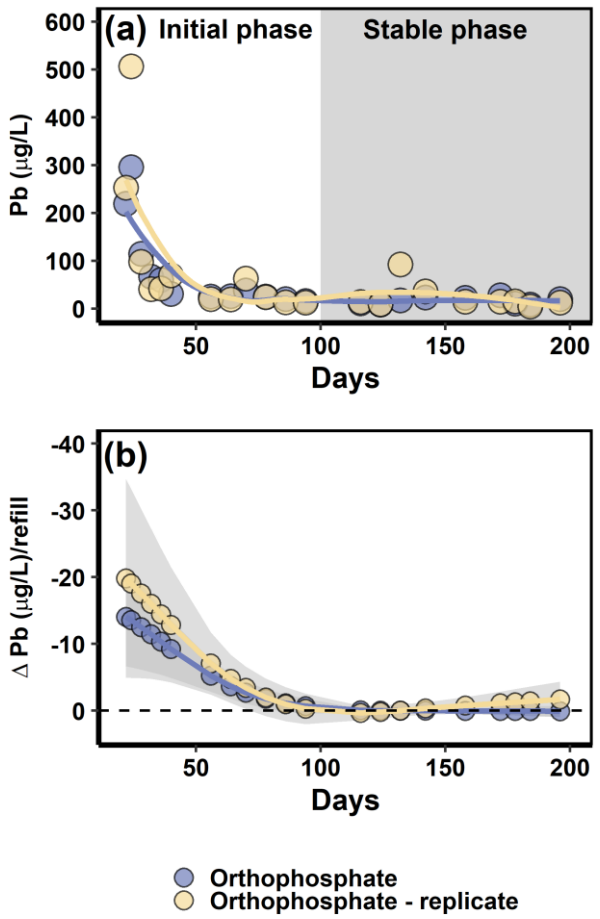

Figure 4 In the presence of orthophosphate at pH 7 and 50 mg C/L, time series of (a) lead concentration along with a local linear fit and (b) the rate of change in lead concentration. Stable-phase was defined using the rate of change in lead, ΔPb; when its 95% confidence interval (grey shaded region) included 0, the system was considered stable.

2.3.2 Galvanic corrosion cells

After lead release due to uniform corrosion had stabilized and sufficient data had been collected, a copper coupon (40 mm × 10 mm × 1 mm; two-thirds submerged) was coupled with the lead to form a galvanic connection (Figure 3b).[46,50] The electrolyte solution was changed as usual to reach a stable state, and galvanic current was measured at 1, 24, and 48 h using a digital multimeter (PeakMeter MS8236, China).

Current measurements were integrated on the intervals 0-1, 1-24, and 24-48 h to estimate lead oxidized by galvanic corrosion (using Faraday's law).

While redox reactions (e.g., oxygen reduction), lead carbonate precipitation, and lead hydroxide/carbonate complexation can alter water chemistry in a closed galvanic system.[51–53] pH and DIC settings represent initial values and were allowed to vary over the 48 h reaction period, as they would during stagnation in a lead pipe.

The change in pH was measured due to galvanic corrosion after the systems had stabilized (Appendix A, Figure 38b). At an initial pH of 9.5 (DIC 5 mg C/L), pH decreased by more than an order of magnitude—from 9.5 to approximately 8. This may be linked to the formation of soluble complexes that contain OH^- (e.g., $Pb_3(OH)_4^{2+}$).[53–55] The reverse trend was observed at an initial pH of 7 (DIC 50 mg C/L). That is, final pH increased to approximately 8.3, which may be caused by the overall redox reaction involving metallic lead, dissolved oxygen, and bicarbonate.[51] During the uniform corrosion phase of the experiment, solution pH was stable over the 48 h stagnation period (Appendix A, Figure 38a).

2.3.3 Experimental design and statistical analysis

Four inhibitors were evaluated—orthophosphate (2 mg P/L), polyphosphate (2 mg P/L), high ratio sodium silicate (25 mg SiO_2/L, SiO_2:Na_2O = 3.6), and sodium metasilicate (25 mg SiO_2/L, SiO_2:Na_2O = 1) — against a control at two pH (7 and 9.5) and two DIC levels (5 and 50 mg C/L) (Figure 3c). Each pH and DIC combination was evaluated for each of the four inhibitors and the control (Appendix A, Figure 39).[56,57] This amounted to 20 treatments, each of which was duplicated (40 cells = 5 inhibitor conditions × 2 pH levels × 2 DIC levels × 2 replicates). The experimental design allows for comparison of sodium silicates against the well-characterized lead-water-carbonate and lead-water-carbonate-orthophosphate systems (Appendix A, Figure 40).[54] While sequestration was not a focus here, sequestrants influence lead release.[36,58] Polyphosphate was chosen as a reference because its effect on lead release is better characterized than that of sodium silicate.

After log-transforming the response to improve the distribution of residuals, linear regression was used to summarize the results.[56,57] The inhibitor-free control at pH 7 and DIC 5 mg/L was defined here as the reference condition,[56,57,59,60] and all effects were estimated as ratios of geometric mean lead concentration, with the reference condition as the denominator. That is, each main effect (pH, DIC, and each inhibitor) represents the ratio of lead release in that treatment group and lead release in the reference group. Due to the log transformation, effects in the original units are multiplicative; for instance, the ratio of lead release at high pH and high DIC is the product of three numbers: each main effect and the pH × DIC interaction effect. Ratios greater and less than one identify factors that increase and decrease lead release, respectively.

2.3.4 Chemical reagents

All solutions were prepared with ultrapure water. Dissolved inorganic carbon (DIC) was dosed as $NaHCO_3$ (Fisher Scientific, USA), and solution pH was adjusted using NaOH and HNO_3. Orthophosphate (as H_3PO_4, Fisher Scientific, USA), polyphosphate ($Na(PO_3)_6$, Alfa Aesar, USA), sodium silicate (high ratio) (SiO_2:Na_2O = 3.6:1, National Silicates, Canada), and sodium metasilicate (SiO_2:Na_2O = 1:1, Fisher Scientific, USA) were acquired commercially.

2.3.5 Analytical methods

2.3.6 Inductively coupled plasma-mass-spectrometry (ICP-MS)

Metals were quantified by inductively coupled plasma-mass spectrometry (ICP-MS, X Series II, Thermo Scientific, reporting limits: Pb = 0.4 µg/L and Cu = 0.7 µg/L). At 48 h, coupons were carefully removed and the corrosion cells were vigorously agitated to mix the cell contents and resuspend colloidal/particulate metals. A 10 mL aliquot was removed from each cell, acidified with concentrated HNO_3 (to a pH < 2.0), held for a minimum of 24 h in a polypropylene tube, and analyzed for total lead. A second 10 mL aliquot was passed through a 0.45 µm cellulose nitrate membrane filter with a syringe filter cartridge and preserved in the same manner. After sampling, the electrolyte solution was refreshed and the coupons returned to each cell. These steps took less than 2 minutes to prevent scale dehydration.

2.3.7 X-ray diffraction (XRD)

XRD was used to identify crystalline phases on the surface of lead coupons that had been dried at room temperature (21°C $\pm$ 1°C).[61,62] XRD scans were acquired on a Siemens D500 diffractometer equipped with a Cu anode and a diffracted beam monochromator (wavelength = 1.5406 Angstroms). Data were acquired in step scan mode using a step size of 0.04 degrees (2θ) and a dwell time of 3.0 seconds.

2.3.8 X-ray photoelectron spectroscopy (XPS)

A Thermo VG Scientific Multilab 2000 was used to determine the elemental composition of corrosion scales. An aluminum X-ray source (1486.6 eV) was used under high vacuum ($1 \times 10^{-9} < P < 1 \times 10^{-8}$ torr), and a CLAM4 hemispherical analyzer (r = 150 mm) with a multichannel detector was used to detect photoelectrons. Survey scans were acquired with a pass energy of 100 eV, an energy step of 1.0 eV, and a spot size of 0.6 mm. High-resolution scans were acquired at a pass energy of 30 eV with an energy step size of 0.1 eV.

2.3.9 Scanning electron microscopy/energy-dispersive X-ray spectroscopy (SEM-EDS)

A Hitachi S-4700 scanning electron microscope (SEM) was used for imaging and elemental analysis. Dried coupons were attached to metal stubs with conductive carbon tape, placed in a holder, and loaded for imaging. Elemental composition data were acquired over an area of 900 mm^2 per sample.

2.3.10 Data analysis

Data were analyzed and visualized using R (version 4.0.0)[63] and a collection of widely-used contributed packages.[64–73]

2.4 Results and discussion

2.4.1 Lead release due to uniform corrosion

Sodium silicates did not strongly influence lead release due to uniform corrosion; representative steady-state lead concentrations in the bulk water (total) and filtrate (<0.45 µm) are shown in Figure 5 (Appendix A, Figure 41-42), along with the effect estimates for each experimental factor (inhibitors, pH and DIC). In the control system, total lead ranged from 46 - 90 µg/L and filtrate lead from 32 - 57 µg/L (21 - 57% particulate). High ratio silicate had a minimal impact on total and filtrate lead; concentrations ranged from 67 - 108 and 42 - 65 µg/L, respectively (13 - 55% particulate). This was also generally true of metasilicate, although at low pH and DIC, metasilicate tended to increase total lead release compared to the control.

Accordingly, the main effects of high ratio silicate on total and filtrate lead were not statistically significant ($p > 0.05$) (Appendix A, Figure 42). The main effects of metasilicate were also not significant, except at pH 7 and DIC 5 mg C/L, where metasilicate caused a statistically significant increase in total—but not filtrate—lead. This increase was due to particles: lead in 0.45 µm filtrate accounted for just 27% of total lead in the presence of metasilicate compared with 63% in the control system (both at pH 7, 5 mg C/L).

As expected, orthophosphate decreased lead release (6 - 37 µg/L total; <0.4 - 22 µg/L in filtrate) while polyphosphate increased lead release (615 - 1052 µg/L in total; 703 - 1194 µg/L in filtrate). These effects are consistent with a large body of work demonstrating the efficacy of orthophosphate and the risks of polyphosphate in terms of lead solubility and release.[31,35,36,58,74–76] Increasing pH to 9.5 or DIC to 50 mg C/L did not have a statistically significant impact on total lead in the control system (Figure 5a; Appendix A, Figure 42). Nevertheless, the effect estimates—being less than one—are consistent with the expected trends in lead solubility under the control of lead carbonate phases (Appendix A, Figure 40).[10,11,54]

The two- and three-way interactions are also consistent with expectations based on equilibrium solubility. For instance, the two-way interactions between orthophosphate

and high pH or high DIC were greater than one (Figure 5). This agrees with the expected increase in solubility of hydroxylpyromorphite with increasing pH and DIC (Appendix A, Figure 40).[54,77,78] The two way-interactions between metasilicate and pH or DIC—both less than one—indicate that the unusually high particulate lead release in the presence of metasilicate was confined to the low pH, low DIC condition. Changes in DIC and pH were not significant in the cells treated with high ratio silicate or polyphosphate, as indicated by the insignificant interaction effects involving these inhibitors.

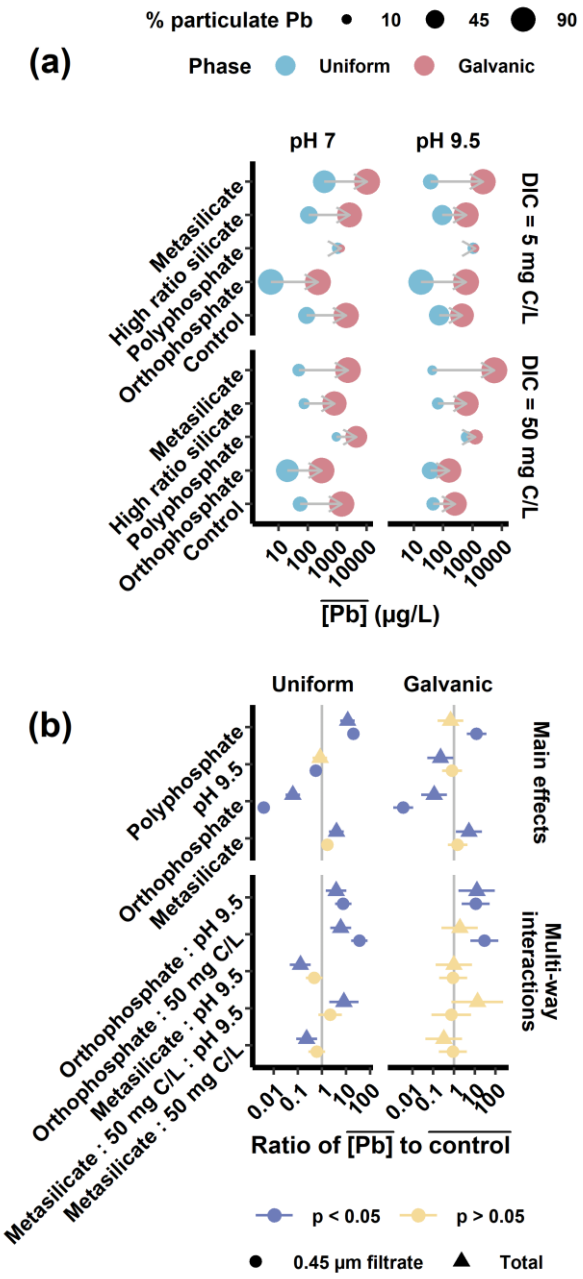

Figure 5 (a) Geometric mean lead release due to uniform (stable phase) and galvanic corrosion (initial phase) at two pH and DIC levels. Arrows indicate the increase in lead release due to coupling lead and copper. (b) Linear model coefficients estimate the ratio of geometric mean lead in each treatment group (e.g., pH, DIC, or orthophosphate) to that of the reference group (pH 7 + 5 mg C/L, no inhibitor). Points represent coefficient magnitudes and error bars span the 95% confidence intervals; a ratio greater than 1

indicates an increase in mean lead release in the associated treatment group. Only the treatments with statistically significant effects on either total or filtrate lead are shown here; the full linear model is detailed in Appendix A, Figure 42.

2.4.2 Lead release due to galvanic corrosion (initial phase)

While coupling lead and copper invariably caused lead levels to spike (Figure 5a; Appendix A, Figure 41), silicate treatment fared poorly in comparison with both orthophosphate and the inhibitor-free control. Over the initial galvanic phase—the first 29 solution changes (48 days) after introducing copper—total lead in the control system ranged from 250 - 2005 µg/L while filtrate lead remained comparable with levels due to uniform corrosion: 47 - 105 µg/L. Total and filtrate lead levels in the presence of high ratio silicate were similar, ranging from 600 - 2657 and 58 - 252 µg/L, respectively. Accordingly, the effects of high ratio silicate on total and filtrate lead were not statistically significant. Metasilicate, on the other hand, increased particle release dramatically. Total lead in the metasilicate-treated cells ranged from 2248 - 10457 µg/L, while filtrate levels were comparable with other treatments, at 42 - 157 µg/L. The effect of metasilicate was statistically significant, and greater than one, at low pH and DIC.

Metasilicate was no better—and perhaps worse—than polyphosphate, which was associated with total and filtrate lead levels ranging from 1227 - 4487 and 905 - 1467 µg/L. The main effect of polyphosphate on total lead release was not significant, while its effect on filtrate lead remained so, with a ratio greater than one. This is due to the large release of particles in most cells without polyphosphate, which obscured the effect of polyphosphate on lead solubility. The significant effect of polyphosphate on filtrate lead is likely explained by strong complexation of lead oxidized in galvanic corrosion.

Orthophosphate was alone among inhibitors in causing a significant decrease in lead release relative to the control (Figure 5b). In the presence of orthophosphate, total and filtrate lead ranged from 160 - 353 and <0.4 - 23 µg/L.

2.4.3 Lead release due to galvanic corrosion (stable phase)

A new galvanic couple typically causes a spike in lead release followed by stabilization, sometimes at an elevated baseline.[79] The stable galvanic phase baseline in the metasilicate-treated cells was particularly elevated: even 30+ solution changes (60+ days) after introducing copper, lead release due to galvanic corrosion was greater than that due to uniform corrosion by a factor of more than 20 at both 5 (pH 9.5) and 50 mg C/L (pH 7) (Figure 6). This was largely due to the elevated release of particles, which accounted for 90-91 % of total lead (Appendix A, Figure 43).

In most of the other treatment groups, stable-state lead release due to galvanic corrosion was greater than that due to uniform corrosion by a factor of 1.1 - 10.8 (Figure 6). This is comparable with the 5 – 7-fold increase in lead release due to galvanic corrosion reported elsewhere.[43] The exceptions to this trend were the orthophosphate-treated cells at pH 9.5 and 50 mg C/L and the polyphosphate-treated cells (pH 7 + 5 mg C/L and pH 9.5 + 5 or 50 mg C/L), which exhibited slightly lower lead levels during the stable galvanic phase. In the case of orthophosphate, this is likely due to long-term passivation (i.e., hydroxylpyromorphite formation). Hydroxylpyromorphite may have contributed to a declining trend in lead release in the presence of polyphosphate as well, but given the high overall lead levels in polyphosphate-treated cells, this is not likely to be practically relevant.

In all but the cells treated with polyphosphate, the effect of galvanic corrosion on lead was especially pronounced at 5 mg C/L and pH 7. This may be due to the lack of buffering capacity at low DIC against a local pH drop at the lead surface driven by galvanic corrosion.[52] This effect has been reported elsewhere, and high DIC can sometimes mitigate it.[44,45] Without sufficient buffering capacity, low pH at the corroding surface inhibits passive scale formation and increases lead solubility.[53]

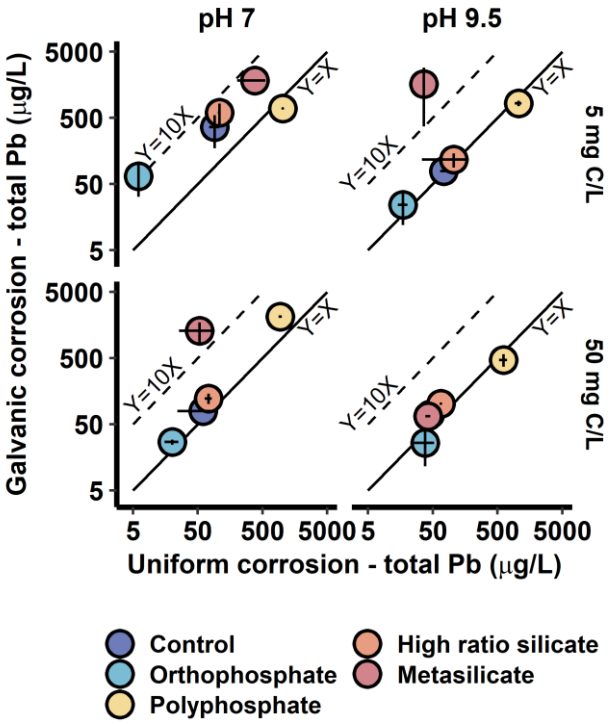

Figure 6 Comparison of mean total lead concentration over the stable uniform and stable galvanic corrosion phases of the experiment. Error bars span one standard deviation about the mean.

2.4.4 Lead release as a function of galvanic current

In the presence of sodium silicate, a relatively large fraction of the lead oxidized by galvanic corrosion was released to water. Over the initial and stable galvanic phases (4 - 158 days after introducing copper), an estimated 52% of oxidized lead was released to water treated with metasilicate, while just 5% of oxidized lead was released to water treated with orthophosphate. Fractional releases to high ratio silicate- and polyphosphate-treated waters were comparable, at 29 and 33%, while release to the control cells was intermediate, at 24% (estimates by linear regression).

High initial galvanic currents were observed in all treatment groups and these nearly always resulted in elevated lead release. However, lead release in orthophosphate-treated corrosion cells fell relatively quickly following the introduction of a copper cathode (Figure 7). After day 100, just 0.2 - 4.6% of oxidized lead was released to water

in the presence of orthophosphate. The inhibitor-free controls also exhibited relatively small fractional releases of 0.9 - 5.6%. Consistent with previous studies,[16,80,81] decreases were attributed in the ratio of observed-to-oxidized lead to scale formation.

Cells treated with metasilicate, high ratio silicate, or polyphosphate exhibited a less pronounced decrease—or even an increase—in the fraction of galvanically corroded lead released to water (1.9 - 85% after day 100). That is, scale formed under these conditions had less capacity to store lead oxidized by galvanic corrosion, especially at low pH and DIC. This may be explained by detachment or dispersion of particles originating on the scale surface; accordingly, high particulate lead levels were observed in silicate-treated cells (Appendix A, Figure 43). At low DIC, metasilicate was comparable with polyphosphate in failing to consistently diminish fractional lead release over time (Figure 7).

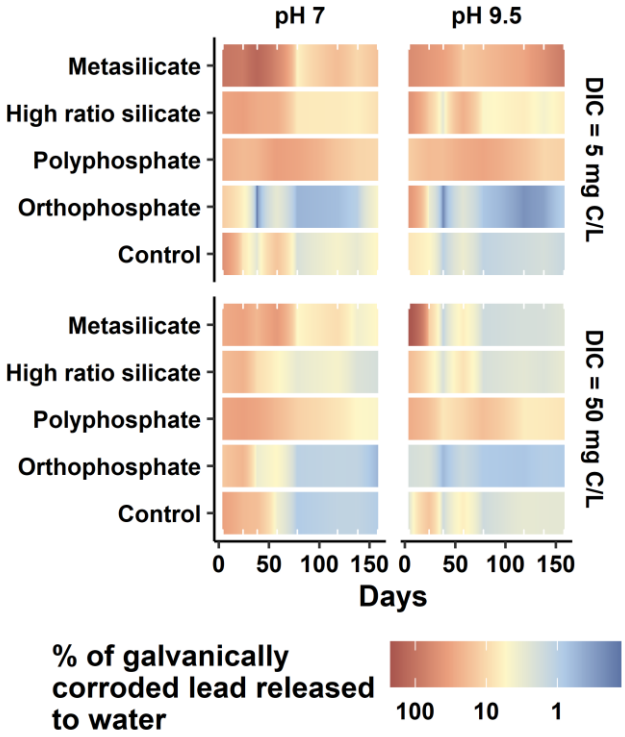

Figure 7 Linearly interpolated ratios of measured total lead to predicted lead calculated by Faraday's Law over time, grouped by inhibitor, pH, and DIC concentration. The x-axis indicates time since galvanic coupling was initiated, and the white ticks represent days when galvanic current was measured.

2.4.5 Corrosion scale structure, morphology, and elemental analysis

At low pH and DIC (pH 7 + 5 mg C/L), neither silicate formulation yielded a crystalline lead-silicate phase (e.g., $PbSiO_3$) identifiable by XRD (Figure 8). Rather, the phase composition of corrosion scale was consistent with expectations based on solubility in the lead-water-carbonate system.[10,35] Cerussite ($PbCO_3$) was predominant in the control system (Figure 8a), and in the two silicate-treated systems, scale also included hydrocerussite ($Pb_3(CO_3)_2(OH)_2$). Silicate-treatment yielded diffraction patterns that were consistent with the presence of quartz (SiO_2) as a minor phase, but the associated signal was relatively weak and the match to quartz is somewhat uncertain. The principal peaks in diffraction patterns representing silicate systems were also wider than those representing the control system, which may be due to inelastic scattering by small crystallites.[82,83]

Scale morphology was generally consistent with the XRD patterns: scanning electron micrographs of scale formed in the control system exhibited morphology characteristic of cerussite (Figure 9a).[84,85] In the silicate-treated systems, hexagonal, platy crystals were apparent—consistent with the presence of hydrocerussite[62,86,87]—although most of these lacked a well-defined shape. Silicate treatment accompanied an approximate order-of-magnitude decrease in the grain size of accumulated crystals relative to the control system (Figure 9). This is consistent with the increase in the width of diffraction peaks due to silicate (Figure 8a-b) and suggests that silicates promote microcrystallization of cerussite or hydrocerussite. In the presence of meta- and high ratio silicates, the silicon contents of the respective corrosion scales were 0.42% and 0.58% by weight (Table 1).

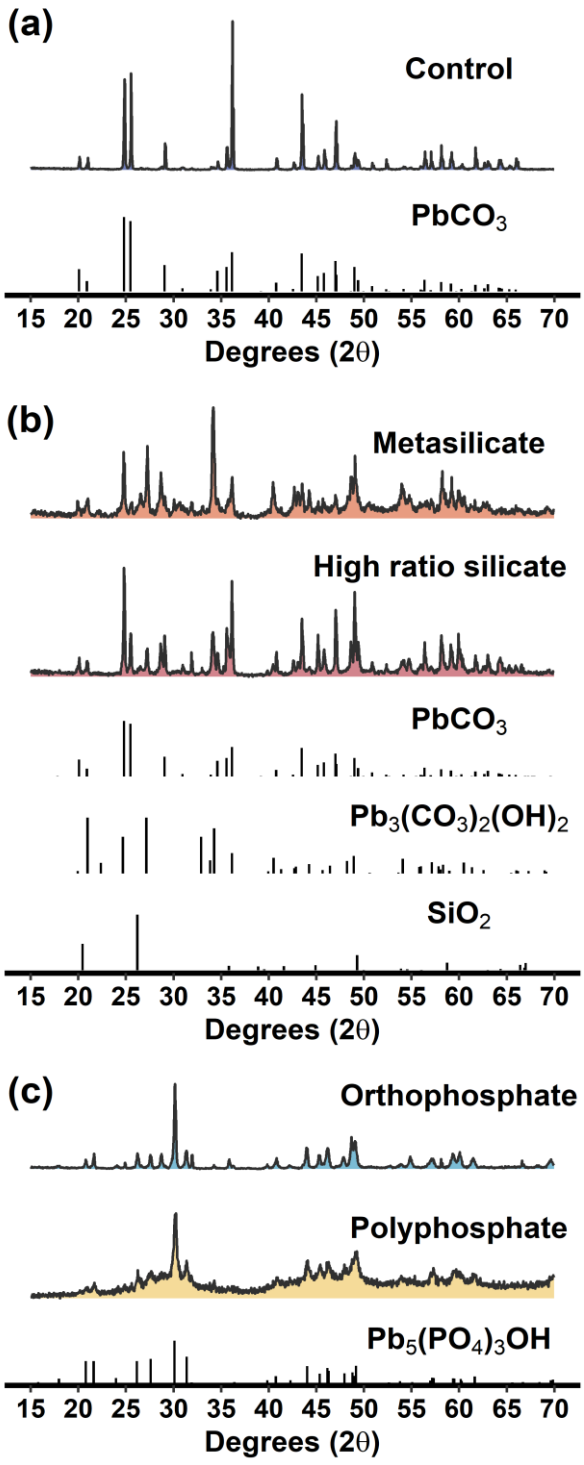

Figure 8 X-ray diffraction (XRD) patterns representing the (a) control, (b) metasilicate, high ratio silicate, (c) orthophosphate, and polyphosphate systems at pH 7 and DIC 5 mg/L. Standard patterns are labelled according to their chemical formulas.

Hydroxylpyromorphite ($Pb_5(PO_4)_3OH$) was predominant in XRD patterns representing the ortho- and polyphosphate-treated systems (Figure 8c). In the case of orthophosphate, this was expected based on equilibrium solubility and previous observations.[35,88,89] Polyphosphate yielded a diffraction pattern with a lower signal-to-noise ratio, and hydroxylpyromorphite formation here is likely due to partial reversion of poly- to orthophosphate during stagnation.[90]

In agreement with the XRD data, scale in the presence of orthophosphate exhibited a needle-like morphology characteristic of hydroxylpyromorphite.[91,92] In the presence of polyphosphate, scale exhibited irregular platy and globular characteristics. Ortho- and polyphosphate treatment yielded corrosion scale with phosphorus weight percentages (5.58% and 8.98%, respectively) that are comparable with the phosphorus content of hydroxylpyromorphite (6.95%). Copper was 8.5% in the polyphosphate-treated system, which is explained by high copper release under these conditions (Appendix A, Figure 44).

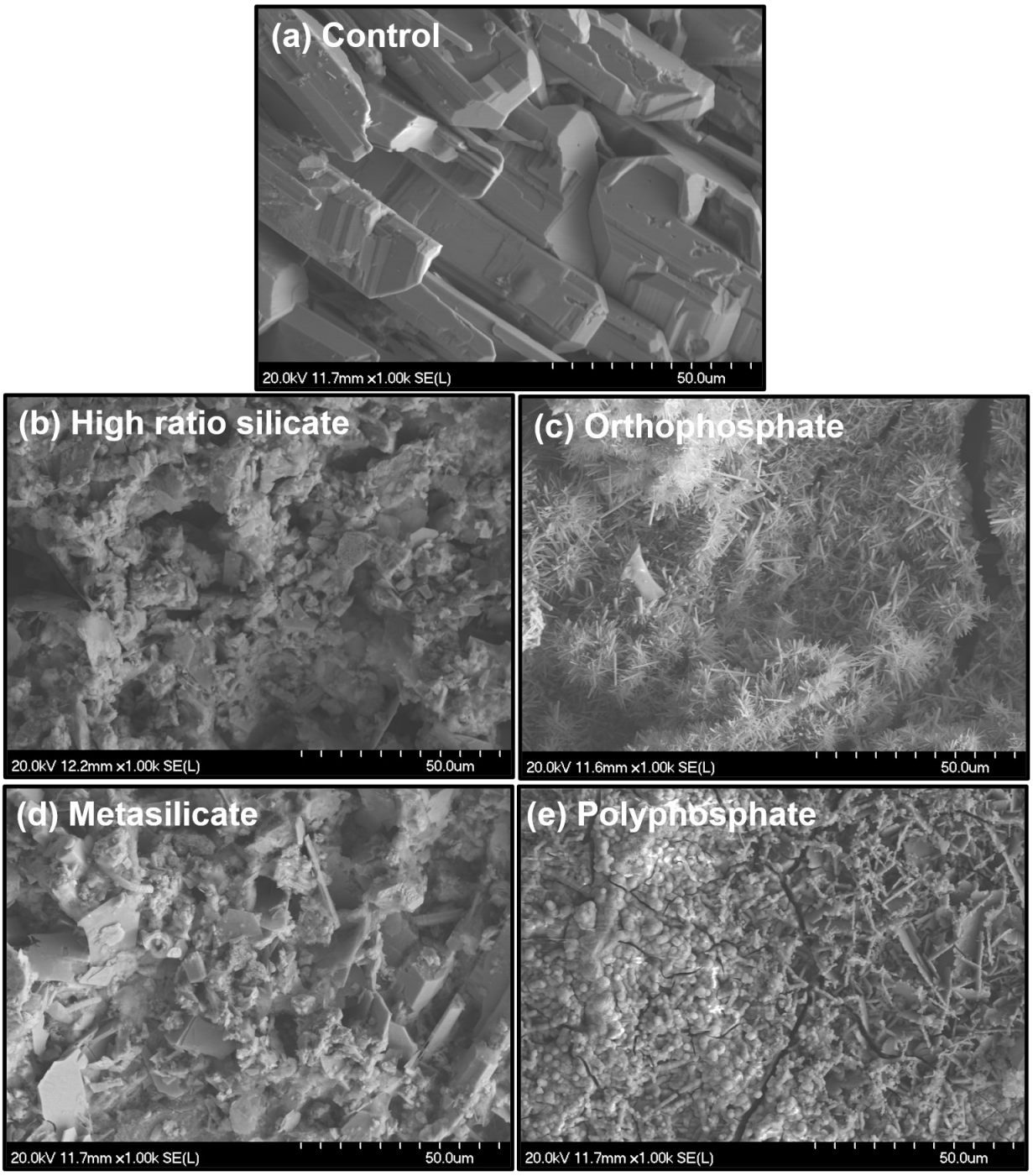

Figure 9 SEM micrographs of corrosion scale in the (a) control, (b) high ratio silicate, (c) orthophosphate, (d) metasilicate, and (e) polyphosphate systems at pH 7 and DIC 5 mg/L.

Table 1 Elemental analysis (weight %) by SEM-EDS of corrosion scale at pH 7 and DIC 5 mg/L (ND = nondetect).

Treatment	O	C	Pb	P	Si	Cu
Control	25.8	12.84	61.37	ND	ND	ND
High ratio silicate	19.84	6.79	72.79	ND	0.58	ND
Metasilicate	21.79	8.15	69.64	ND	0.42	ND
Orthophosphate	19.78	7.56	67.08	5.58	ND	ND
Polyphosphate	25.31	3.61	53.61	8.98	ND	8.5

2.4.6 Surface chemistry of lead coupons

Formation of a thin (e.g., ~nm) coating has been proposed as an explanation for silicates' purported beneficial effect on lead release.[23,24] To investigate this possibility, the top few nanometers of scale depth was characterized using XPS. By contrast, XRD and EDS penetrate to a depth of several micrometers (Figure 3d; Figure 8; Table 1),[93–95] which, given the age of the system, amounts to a bulk characterization of scale.

XPS data suggest that, in the silicate-treated systems, a carbonate mineral was present at the solid-solution interface and likely controlled solubility (Figure 10c). While the Si 2p band (~102.8 eV) (Figure 10b) does indicate some degree of interaction between inhibitor and scale in the silicate-treated cells, the prominent secondary C 1s peak (289.28 eV) in the control and silicate-treated systems is attributable to carbonate.[96,97]

The ortho- and polyphosphate spectra exhibited much less evidence of carbonate, due probably to the formation of hydroxylpyromorphite ($Pb_5(PO_4)_3OH$). The minimal carbonate signal in the presence of phosphate suggests that hydroxylpyromorphite was predominant in the top few nanometers of scale and likely determined the exchange of lead between the scale surface and the solution. Conversely, the significant carbonate peak in the control and silicate-treated systems suggests that here solubility was controlled by lead carbonate. The comparable dissolved lead concentration (Appendix A, Figure 41) of these two systems also supports this observation. That is, under the conditions studied, sodium silicate does not appear to provide a protective film on the coupon surface in the same manner that orthophosphate does.

More generally, the principle photoelectron peaks in the XPS survey (Appendix A, Figure 45) matched the elemental composition reported by SEM-EDS. The Pb 4f 7/2 and Pb 4f 5/2 binding energies, 138.81 eV and 143.67 eV respectively, were similar to values for cerussite reported in literature,[96,97] and the P 2s band (~190.7 eV) was prominent in ortho- and polyphosphate-treated cells and absent otherwise (Figure 10a).

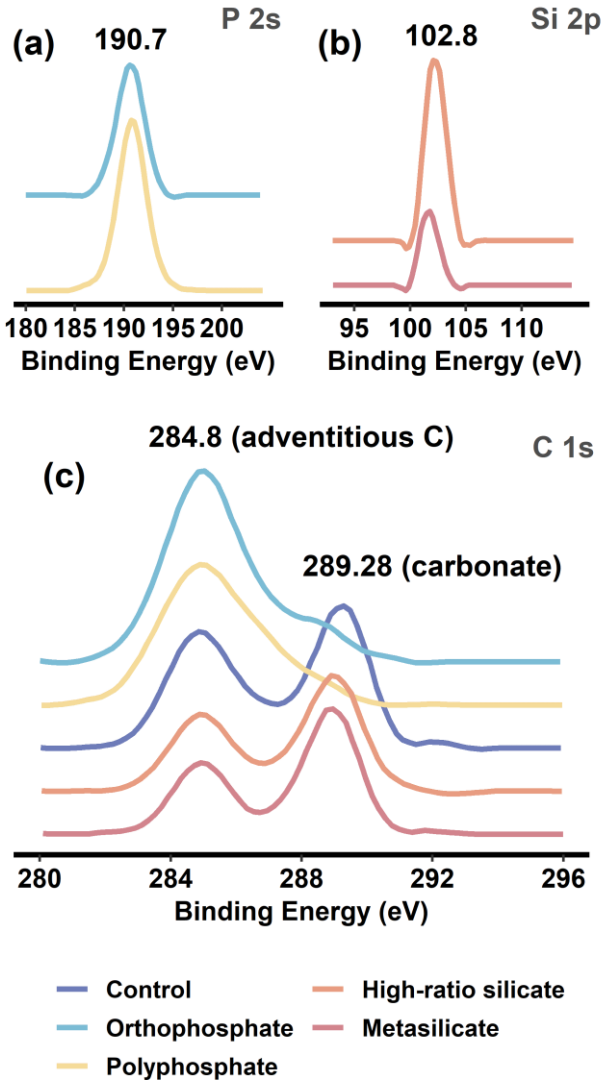

Figure 10 High resolution XPS scans of (a) P 2s, (b) Si 2p and (c) C 1s at pH 7 and DIC 5 mg C/L. The primary C 1s peak (adventitious C at 284.8 eV) is attributable to air exposure.[98] No P 2s signal was observed in the silicate-treated systems, and no Si 2p signal was observed in the non-phosphate systems.

2.5 Conclusions

Despite of decades of use, fundamental knowledge gaps concerning the proper use of sodium silicates remain. Two silicate formulations were evaluated over a representative pH and DIC range, comparing them against a well-studied inhibitor and sequestrant (orthophosphate and polyphosphate, respectively). The results suggest the following:

1. The effect of sodium silicate on lead release is explained mainly by its tendency to increase pH. While silicate-treated cells did release less lead than their corresponding controls under some conditions, these differences were generally small and inconsistent. For example, metasilicate performed best at high pH and low DIC (pH 9.5 with 5 mg C/L): total lead release under these conditions was 50% of that in the corresponding control system. But once a galvanic couple was established, metasilicate-treated cells released 5.1 times the lead of the high pH and low DIC control cells.

2. Compared with sodium silicate, orthophosphate is an efficient lead corrosion control treatment. Except for the high pH and DIC setting (pH 9.5 with 50 mg C/L), orthophosphate was effective in controlling lead release due to uniform and galvanic corrosion.

3. Direct interaction between silicate and lead appears unlikely: although silicates influence the morphology and grain size of corrosion scale and yield a nanometer-thick silicon coating, lead carbonates appear to control lead release in silicate-treated systems. Sodium silicate may react differently with a complex scale rich in other elements, but without further research this is not practically relevant.

3 Chapter 3 Evaluation of cerussite $Pb(CO_3)$ dissolution by sodium silicate

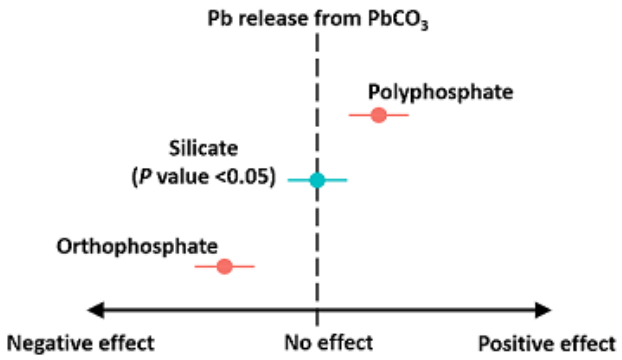

Figure 11 Artwork of main effect of sodium silicate, orthophosphate and poly-phosphate on dissolution of cerussite.

3.1 Abstract

Silicates have been added to drinking water for decades, mainly to control colour by dispersing oxidized iron and manganese. Silicates have been used occasionally to control lead release, but there is no consensus on whether they do so effectively. Moreover, there are concerns that silicates may disperse particulate lead. The effect of sodium silicate on lead release from a model lead(II) carbonate powder was evaluated using a continuous-flow stirred-tank reactor. A wide range of pH (7.5 and 9) and dissolved inorganic carbon (DIC) concentrations (5 and 50 mg C/L) was tested. Sodium silicate is compared against against an inhibitor-free control, a better-characterized inhibitor (orthophosphate), and a widely used sequestrant (polyphosphate). Sodium silicate did not have a statistically significant impact on lead release at pH 7.5, regardless of the DIC concentration. At pH 9 it accompanied 58% more lead release at 5 mg C/L and 21% less lead release at 50 mg C/L, compared with controls at matched pH and DIC settings. Sodium silicate did not influence the crystalline phase composition, but it did adsorb to lead(II) carbonate. This may account for its effects at pH 9. Orthophosphate was the more effective inhibitor, yielding 38 - 96% less lead release relative to matched controls. Orthophosphate inhibition was attributed to

conversion from lead(II) carbonate to hydroxylpyromorphite ($Pb_5(PO_4)_3OH$) and adsorption to lead(II) carbonate in the absence of a phase conversion (i.e., at pH 9 with 50 mg C/L). Polyphosphate increased lead release by 540 - 3600%, likely due to aqueous complexation and possibly due to colloidal dispersion.

3.2 Introduction

Silicates are recognized as effective sequestrants, added to drinking water to prevent colour caused by oxidized iron and manganese.[19,20,39] Silicates have also been used to control corrosion. Newark, New Jersey, for instance, used a sodium silicate corrosion inhibitor from the mid-1990s until 2019, when, following a lead-in-water crisis, the city switched to orthophosphate.[21,22] This event raised concerns regarding the appropriate use of sodium silicates for lead corrosion control treatment.[21]

While there is no consensus on how, or even if, silicates control lead release, several mechanisms have been proposed. First, silicates may form a protective film or diffusion barrier on the interior surface of lead pipes. This may be an amorphous coating or a mineral solid,[15,16,23,24] but the formation of such a film has not been conclusively demonstrated. Second, silicate species may adsorb to lead mineral surfaces, blocking active sites and slowing dissolution. Orthophosphate may function analogously in systems that do not reach equilibrium, or where the solution remains undersaturated with respect to all possible lead-phosphate solids.[11,99,100] Third, silicates increase pH, which decreases the equilibrium solubility of common lead carbonates under most conditions.[10,15]

But there is a potential drawback to silicate corrosion control treatment: the properties that make silicates effective at sequestering metals[20,39,101] may result in dispersion of particulate or colloidal lead. This is analogous to the negative side effects of polyphosphates—another common class of sequestrants—which are known to mobilize lead.[10,36,38,102] Whether silicates are used as sequestrants or corrosion inhibitors, a comprehensive evaluation is needed to guarantee drinking water safety.

Here, lead release was evaluated in the presence of sodium silicate, quantified as the net conversion rate from lead(II) carbonate to dissolved species and small colloids (<

0.2 or 0.45 µm). A continuous-flow stirred-tank reactor was used with a hydraulic retention time of 30 minutes, chosen to match the stagnation periods of regulatory sampling protocols in Canada and the United Kingdom.[103,104] The effect of sodium silicate was compared against that of orthophosphate, as a reference inhibitor, and polyphosphate, as a reference sequestrant. Changes in the chemical and structural properties of lead(II) carbonate due to each inhibitor/sequestrant and water quality setting, proposing mechanisms were described to explain these observations. These findings will inform corrosion control and sequestration strategies and improve understanding of sodium silicate's impacts on drinking water.

3.3 Materials and methods

3.3.1 Continuous-flow stirred-tank reactors (CSTRs)

Experiments were conducted at room temperature (21°C ± 1°C) in continuous-flow stirred-tank reactors made with glass chromatography columns (Kimble, Rockwood, USA) (diameter × length = 2.5 cm × 30 cm) (Figure 12a). Similar reactors have been used previously to investigate the release of lead from representative solids.[11,100,105,106] Columns, tubing, and other containers were immersed in HNO_3 (approximately 1.6 M) for at least 24 h and rinsed at least four times with ultrapure water before each experiment. Reactor influent was maintained by a peristaltic pump at 4.9 mL/min to achieve a hydraulic retention time of 30 minutes, and all experiments were completed within 40 hours.

Lead(II) carbonate was suspended at 1 g/L, to ensure oversaturation, in solutions containing either no inhibitor (the control), orthophosphate (1 mg P/L), polyphosphate (1 mg P/L), or sodium silicate (32 mg SiO_2/L). Lead carbonate particles were retained by a 0.45 µm cellulose nitrate membrane filter (Figure 12a)).[11] Reactor effluent was then filtered through a 0.2 µm cellulose nitrate membrane filter using a syringe-mounted apparatus.[100,106,107] Filtered effluent was sampled periodically and preserved for analysis with concentrated nitric acid.

Lead release was determined as the net conversion rate from lead carbonate to dissolved lead and small colloids (<0.2 or 0.45 µm). Lead release was highly variable

during the first 40 retention times but did eventually stabilize (Appendix B, Figure 46). This has been noted previously and has been attributed to an uncharacteristically labile surface phase.[11,42,100,106,108] Here, stability was defined as less than 30% variation (standard deviation/mean) over at least four consecutive effluent samples spanning at least eight hydraulic retention times.[11]

Once reactor effluent had stabilized, the net conversation rate was calculated according to Equation (1).[11,108]

$$r_{exp} = \frac{Q C_{ss}}{V_R A[solids]} = \frac{Css}{\tau\ A[solids]}$$

where r_{exp} is the net conversation rate (mol/m^2 min); Q is the flow rate (L/min); C_{ss} is the lead concentration measured after satisfaction of the stability criterion; V_R is the volume of the reactor (L); A is the specific surface area of lead carbonate, determined by BET-N_2 adsorption analysis at 0.72 m^2/g; [solids] is the mass of solids (g/L); and τ is the hydraulic retention time in minutes (i.e., V_r/Q).

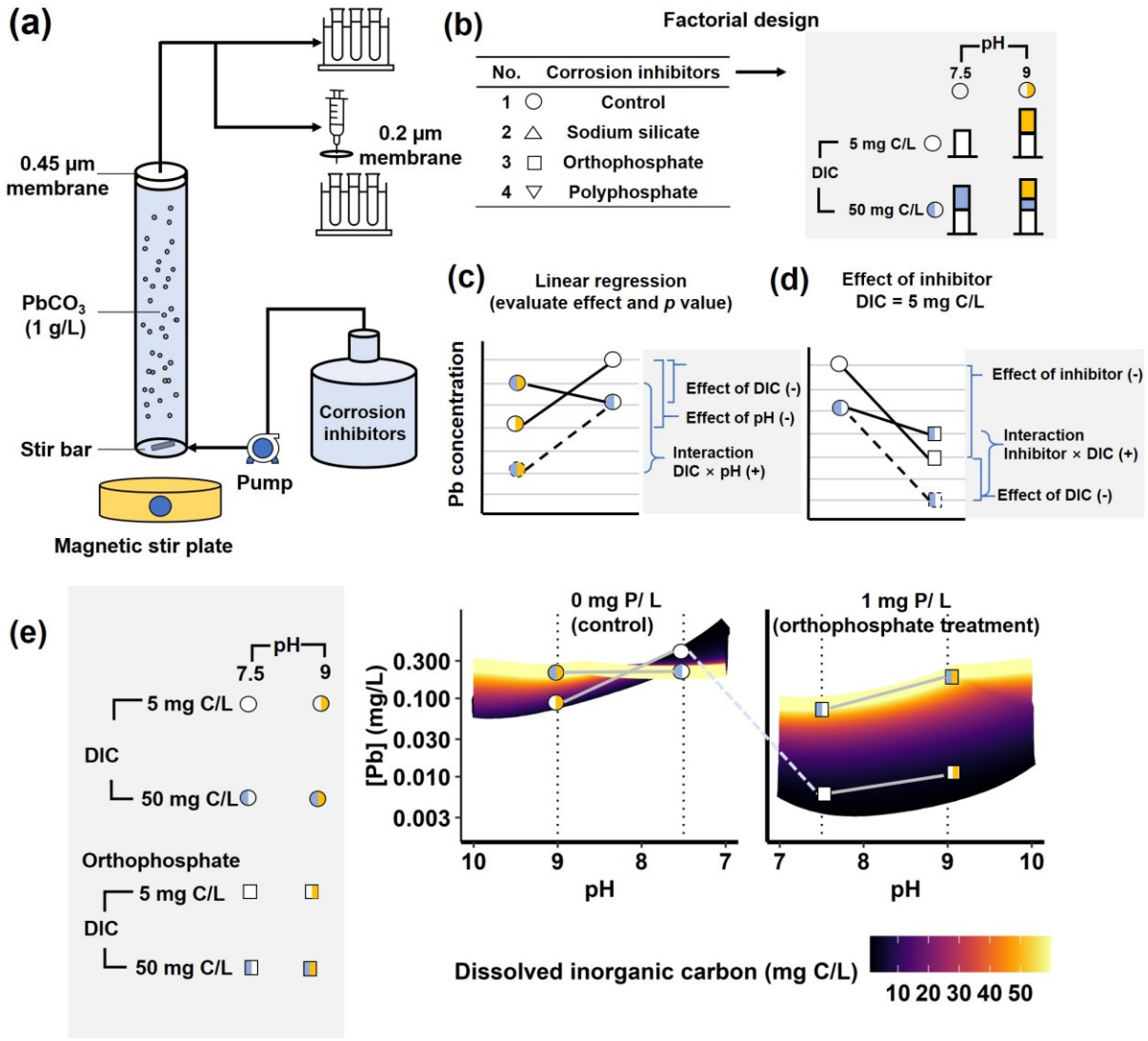

Figure 12 (a) Schematic diagram of continuous-flow stirred-tank reactors. (b) Three corrosion inhibitors and one inhibitor-free control were investigated using a 4 × 2 × 2 mixed-level factorial design. (c) Conceptual diagram of the factorial design for effect and interaction evaluation; + indicates an increase in lead concentration; - indicates a decrease. (d) Effects and interaction estimation for inhibitor and pH. (e) A factorial design can approximate the equilibrium solubility of lead as a function of pH, dissolved inorganic carbon concentration, with cerussite and hydrocerussite (0 P mg/L) or hydroxylpyromorphite (1 mg P/L) as possible phases. Thermodynamic data are due to Schock et al. [54] and solubility calculations were made with tidyphreeqc.[109]

3.3.2 Experimental design and statistical analysis

A 4 × 2 × 2 mixed-level factorial design was used to compare sodium silicate against better-characterized reference treatments (Figure 12b). Three inhibitors were evaluated—sodium silicate (32 mg SiO_2/L, SiO_2:Na_2O = 3.6), orthophosphate (1 mg P/L), and polyphosphate (1 mg P/L)—against a control at two pH (7.5 ± 0.3 or 9.0 ± 0.3 in effluent) and two DIC levels (5 and 50 mg C/L). This amounted to 16 settings (4 inhibitors × 2 pH levels × 2 DIC levels), each of which was duplicated at a minimum ($n \geq 2$).

Factorial designs are used widely to evaluate the synergies among factors in complex systems.[56,57] In the lead-water-carbonate system, for example, pH and DIC have non-additive effects on lead solubility (Figure 12c and e), which can be approximated by two main effects and an interaction term.[56,57] The effect of an inhibitor and its interactions with pH and DIC can be evaluated in the same way (Figure 12d and e). For instance, increasing DIC decreases lead concentration at pH 7, but it has the opposite effect in the presence of orthophosphate, leading to a non-negligible orthophosphate-DIC interaction term (Figure 12e).[11,54]

Here, the main effects and interactions were summarized using linear regression, after log-transformation to improve the distribution of the model residuals.[56,57] The inhibitor-free control at pH 7.5 and DIC 5 mg C/L was defined as the reference condition[56,57,59,60] and all effects were estimated as ratios of geometric mean lead release, with the reference condition as the denominator. Ratios greater and less than one indicate factors or interactions that accelerate or slow lead release, respectively. Due to the log-transformation, effects in the original units are multiplicative: for example, lead release in the presence of orthophosphate at pH 9 and DIC 50 mg C/L is estimated as the product of five numbers: lead release under the reference condition; each main effect; the two-way interactions among orthophosphate, pH, and DIC; and the three-way interaction.

3.3.3 Chemical reagents

All solutions were prepared in ultrapure water. Dissolved inorganic carbon (DIC) was dosed as $NaHCO_3$ (Fisher Scientific, USA), and solution pH was adjusted with NaOH and HNO_3. Sodium silicate, orthophosphate, and polyphosphate were dosed as high-ratio ($NaO:SiO_2$=1:3.6) sodium silicate product (National Silicates, Canada), phosphoric acid (H_3PO_4) (Fisher Scientific, USA), and sodium hexametaphosphate ($(NaPO_3)_6$) (Alfa Aesar, USA). Lead carbonate (Alfa Aesar, USA) was used as a model for lead corrosion scale in the reactors; an X-ray diffractorgram of the unreacted powder is shown in Appendix B, Figure 48.

3.3.4 Inductively coupled plasma mass spectrometry (ICP-MS)

Metals were quantified by inductively coupled plasma-mass spectrometry (ICP-MS, X Series II, Thermo Scientific). Filtered samples (0.2 and 0.45 µm) were acidified with HNO_3 to pH < 2 and held for a minimum of 24 hours before analysis.

3.3.5 X-ray diffraction (XRD)

A Rigaku Ultima IV X-ray Diffractometer (XRD) with a copper Kα source was used to identify crystalline phases present in the reactor solids. The X-ray tube was operated at 45 kV and 40 mA. Scans were performed over the range 10° to 80°/90° (2-theta) with a step size of 0.05° and a scan speed of 1 degree/min.

3.3.6 X-ray photoelectron spectroscopy (XPS)

A Thermo VG Scientific Multilab 2000 instrument was used to examine the chemical states of elements. An aluminum X-ray source (1486.6 eV) was used under high vacuum: $1 \times 10^{-9} < P < 1 \times 10^{-8}$ torr. Photoelectrons were detected using a CLAM4 hemispherical analyzer (r = 150mm) with a multi-channel detector. Survey scans were collected using a pass energy of 100eV, an energy step of 1.0 eV, and a spot size of 0.6 mm. High-resolution scans were performed at a pass energy of 30 eV and an energy step of 0.1 eV. Samples were prepared by collecting 50 mL aliquots of each suspension, centrifuging for 5 min, and evaporating the pellet on tin foil.

3.3.7 Zeta (ζ) potentials

Zeta (ζ) potential was measured using a Zetasizer-Nano-ZS (Malvern Instruments, Worcestershire, UK). Freshly prepared lead carbonate suspension (100 mL at 1 g/L) was dosed with each inhibitor for measurement according to the electrophoretic light scattering method.[110]

3.3.8 Fourier transform infrared (FT-IR)

After reaction with orthophosphate, polyphosphate, or sodium silicate, lead carbonate suspensions were characterized using Fourier transform infrared spectroscopy (FT-IR) in attenuated total reflectance mode (Bruker, USA). Spectra were collected over a wavenumber range of 400-4000 cm^{-1} with a resolution of 4 cm^{-1} and 60 scans per spectrum.

3.3.9 Scanning Electron Microscopy (SEM)

A Hitachi S-4700 scanning electron microscope was used for imaging analysis. After reaction, a 50 ml aliquot of each suspension was centrifuged for 5 minutes and the pellet was dried on a SEM specimen stub at 21 $\pm$ 1 °C. SEM samples were placed in a holder and loaded into the Hitachi S-4700 SEM for imaging.

3.3.10 Equilibrium solubility model and data analysis

Data were analyzed and presented using R version 4.0.0[63] and a collection of widely used contributed packages.[111–115] The thermodynamic data (Appendix B, Table 4) used in the equilibrium solubility model are due to Schock et al. [54] and the model was implemented using *tidyphreeqc*,[109] an R interface for PHREEQC.[116] Calculation of activity coefficients is described in the method described by Parkhurst and Appelo.[117]

3.4 Results and discussion

3.4.1 Effect of sodium silicate on the lead leaching of cerussite

Sodium silicate did not have a statistically significant impact on the net conversion rate of lead(II) carbonate (Figure 13b, Appendix B, Table 5- 6), except under two

circumstances. First, increasing pH from 7.5 to 9 and adding silicate resulted in 58% more lead in 0.45 μm filtrate than would be expected based on the main effects of these two factors (i.e., a significant silicate:pH interaction). Second, increasing pH from 7.5 to 9, DIC from 5 to 50 mg C/L, and adding silicate resulted in 59% less lead in 0.45 μm filtrate than would be expected based on the main effects and two-way interactions among these factors (i.e., a significant silicate:pH:DIC interaction, also significant at 0.2 μm). The latter interaction highlights the only scenario where sodium silicate yielded a lower net conversion rate than the corresponding control: lead in 0.45 μm filtrate was 21% lower in the presence of sodium silicate at pH 9 and 50 mg C/L (Appendix B, Table 6). Elevated lead associated with the former interaction may be due to colloidal dispersion by sodium silicate.

While the net conversion rate estimates representing 0.2 and 0.45 μm filtrate were similar (Figure 13a), lead colloids, defined here as particles between 0.2 and 0.45 μm, were present in reactor effluent. In the control system, rates representing 0.2 and 0.45 μm filtrate were 9 - 31 and 11.1 - 34.7 $\times$ 10^{-9} mol/m^2·min, respectively (0.2:0.45 ratio = 64 - 87%). In the presence of sodium silicate, rates ranged from 12 - 23 and 16 - 28 $\times$ 10^{-9} mol/m^2·min (0.2:0.45 ratio = 73 - 81%). Consistent with the linear model, orthophosphate yielded lower net conversion rates ranging from 0.6- 19 and 1 - 21 $\times$ 10^{-9} mol/m^2·min (0.2:0.45 ratio = 58 - 90%).

In agreement with solubility predictions for the lead-water-carbonate system (Figure 13e), increasing pH or DIC slowed lead release from lead(II) carbonate. But these two effects were non-additive: the large and statistically significant pH:DIC interaction captures the known tendency for carbonate species to decrease solubility at pH 7.5 while increasing it at pH 9 (Figure 13b). Also consistent with solubility predictions, adding orthophosphate slowed lead release at low pH (i.e., a significant main effect) but reversed the effect of increasing pH or DIC. That is, the significant two-way interactions between orthophosphate and pH or DIC counteract the negative main effects of pH and DIC. These interactions accord with the known tendency of orthophosphate to shift the lead solubility minimum to pH 7 - 8 with 0 mg C/L.[54]

In contrast to orthophosphate, polyphosphate accelerated lead release dramatically. And while the dissolution rates of lead carbonates by polyphosphate have not been well studied, this is consistent with a substantial body of literature demonstrating the risks of polyphosphate in systems with lead.[35,36,58]

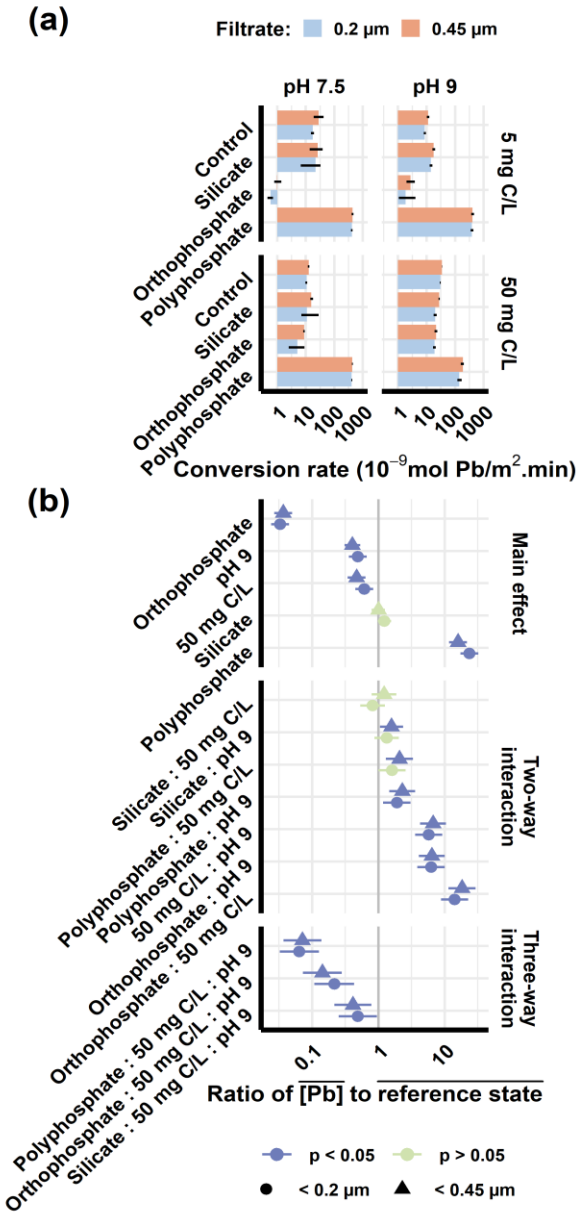

Figure 13 (a) Geometric mean net conversion rates at two pH (7.5 and 9) and DIC levels (5 and 50 mg C/ L) (log-scale). Each setting represents at least two reactor runs, and error bars span the range of measurements. (b) Main effects and their interactions estimate the ratio of geometric means at different settings. The reference state is

defined as the low pH, low DIC, inhibitor-free condition. Points indicate coefficient magnitudes and error bars span their 95% confidence intervals.

3.4.2 Dissolution rates and equilibrium solubility

While similar reactors have been used previously to study dissolving lead minerals,[11,105,106] the data they generate may not always yield pure dissolution rates. The effluent lead concentration may reach equilibrium under some water quality conditions, and transformation of mineral phases may occur.[11] To better understand these limitations, lead in reactor effluent was compared against a well-established solubility model.[54] It is assumed that cerussite or hydrocerussite controlled lead solubility in the control systems and in the presence of sodium silicate. Hydroxylpyromorphite controlled solubility in the presence of orthophosphate (Appendix B, Figure 47).

Effluent lead concentrations in the control and silicate-treated systems were lower than predicted at all pH and DIC settings (measured:predicted ratio = 24–69 %). Assuming, based on model predictions, that these systems did not reach equilibrium, the effluent lead concentrations approximate cerussite's dissolution rate (neglecting any contribution from minor phases, see *Crystalline structure and morphology*). The major exception was at pH 9 and 5 mg C/L, where hydrocerussite was prominent in the reactor solids. The latter pH/DIC setting is near the solubility minimum in the lead-water-carbonate system, where hydrocerussite is predicted to control solubility.

While solubility predictions generally captured the trends in lead release due to variation in pH and DIC, there were some notable discrepancies. Whereas predicted solubility at 50 mg C/L is approximately constant between pH 7.5 and 9, lead release increased with pH. This may be due to dissolution of cerussite, whereas the model predicts that hydrocerussite will control solubility (Appendix B, Figure 47). Under the experimental conditions, the 30-minute retention time may not get have been long enough to convert cerussite to hydrocerussite (see *Crystalline structure and morphology*).

In the presence of orthophosphate, reactor data paralleled the equilibrium hydroxylpyromorphite solubility predictions (Figure 14). But these data do not represent

pure dissolution rates; they involve at least partial phase conversion, which complicates the interpretation. In the presence of polyphosphate, lead release was much higher than predicted (629 - 1851 µg/L), and speciation was likely dominated by lead-polyphosphate complexes which are not accounted for in the solubility model.[36]

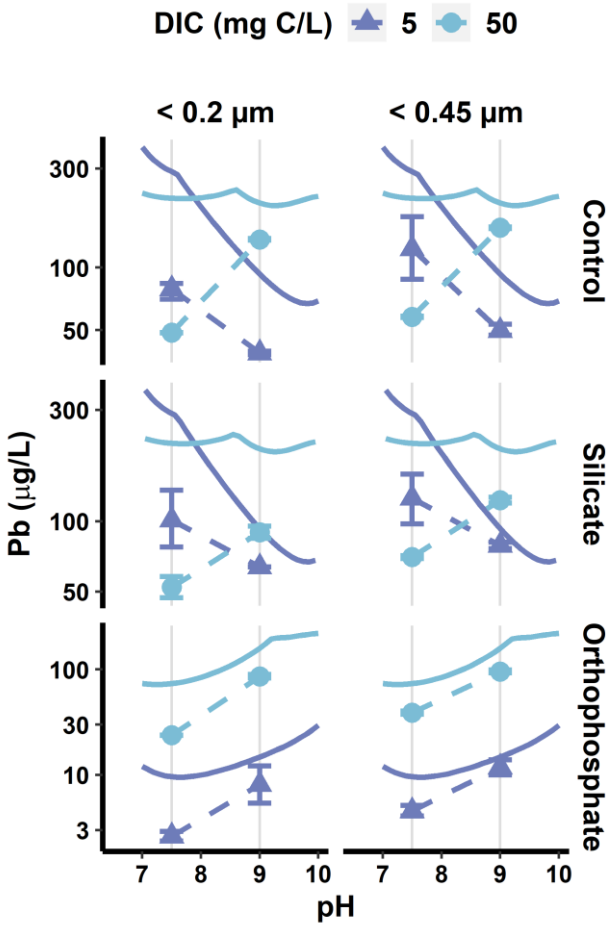

Figure 14 Lead release in the control, silicate-treated, and orthophosphate-treated systems (dashed lines), along with equilibrium solubility predictions (solid lines). Error bars span the manxium and mininum values. Thermodynamic data are due to Schock et al. [54] and solubility calculations were made with tidyphreeqc.[109]

3.4.3 Crystalline structure and morphology (XRD and SEM data)

Previous studies[15,16] suggest that silicate may form a protective layer on lead surfaces, but here, silicate did not yield a crystalline silicate solid (e.g., $PbSiO_3$) identifiable by XRD (Figure 15). Instead, cerussite and hydrocerussite appeared to control lead

release (Figure 15). These findings are consistent with model predictions that a lead carbonate phase controls solubility, regardless of the concentration of sodium silicate.[54,118]

In the control reactors, cerussite was identified as the predominant crystalline phase, although it underwent partial conversion to hydrocerussite at pH 9 and 5 mg C/L. While cerussite was predominant silicate-treated reactors as well, a small amount of hydrocerussite was detectable at all pH and DIC settings. Scale morphology generally supported the XRD patterns: scanning electron micrographs of control reactor solids exhibited morphology characteristic of cerussite (Figure 16).[84,85] In the silicate-treated systems, cerussite exhibited a new prismatic presentation,[119] suggesting that sodium silicate might influence the morphology of cerussite.

While polyphosphate did not alter the phase composition at any pH or DIC setting, orthophosphate promoted formation of low-solubility hydroxylpyromorphite (Appendix B, Figure 49). Needle-like crystals indicative of hydroxylpyromorphite[91,92] were apparent on reactor solids (Figure 16), and this phase most likely explains the slow rates of lead release in the orthophosphate-treated reactors. The exception was at pH 9 with 50 mg C/L, where cerussite remained predominant (Appendix B, Figure 49). Hydrocerussite is predicted to control solubility at high pH and DIC, but the effluent lead concentration did not reach predicted saturation with respect to hydrocerussite (Figure 14). Nevertheless, orthophosphate did limit lead release compared to the corresponding control (pH 9 with 50 mg C/L). Instead of altering the phase composition, orthophosphate may have adsorbed to lead carbonate, slowing dissolution by blocking active sites at the surface.[11]

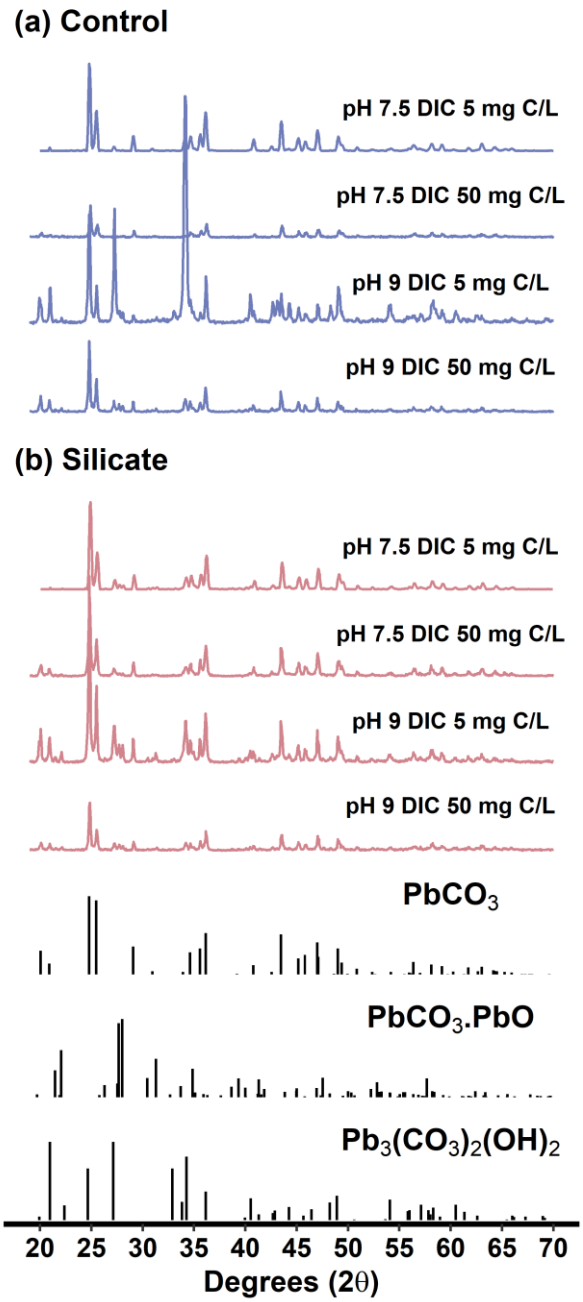

Figure 15 X-ray diffraction (XRD) patterns representing the (a) control and (b) silicate. Standard patterns are labelled according to their chemical formulas.

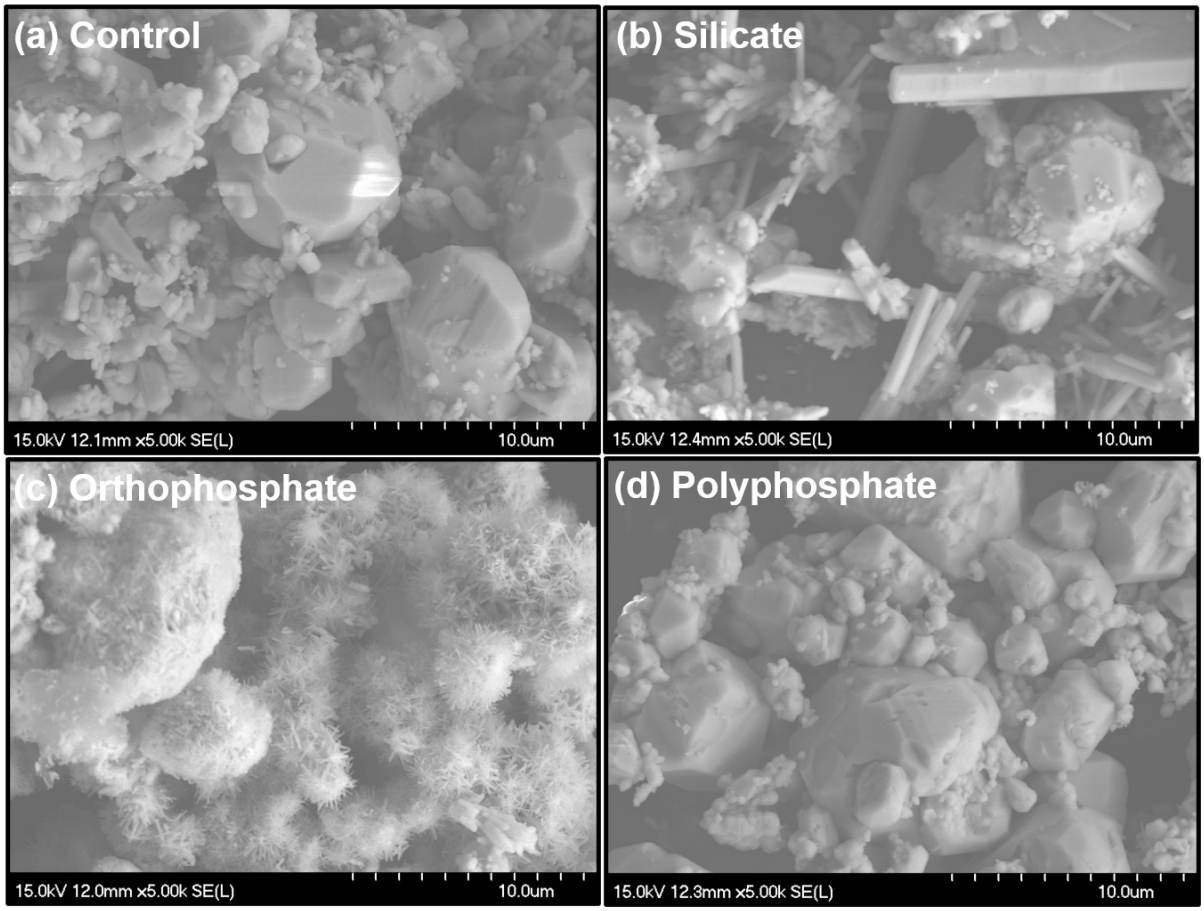

Figure 16 Scanning Electron Microscopy (SEM) of reactor solids in the (a) control, (b) silicate, (c) orthophosphate, and (d) polyphosphate systems at pH 7.5 and DIC 5 mg/L.

3.4.4 Role of silicate adsorption

Although sodium silicate did not change the crystalline structure of lead(II) carbonate in any way that clearly slowed lead release, a thin (~nm) silicate film has been proposed as a mechanism for lead control in silicate-treated systems.[23,24] Since accumulation of amorphous silicate at the surface would be difficult to detect by XRD and SEM,[23] XPS was used to quantify Si up to several nanometers below the surface in the low pH, low DIC system.[23,106,120,121] Fourier transform infrared (FT-IR) spectra was used to identify changes in functional groups under the same conditions.

Adsorption of silicate anions might conceivably slow lead release by blocking active sites at the lead carbonate surface. A similar mechanism has been proposed to explain the effect of orthophosphate on lead release at high DIC concentrations,[11] and the

inhibition of calcite dissolution by orthophosphate. In the latter system, orthophosphate chemisorbs to calcite, accumulating Ca^{2+} around the phosphate-poisoned sites and slowing the dissolution rate.[30] Here, silicate adsorbed to lead carbonate, as detected by XPS, but no evidence was found that this process slowed lead release at pH 7.5 and 5 mg C/L. Failure of silicate to chemisorb and effectively block (poison) active surface sites from releasing lead may explain these results.

Oxygen, carbon, and lead dominated the elemental composition of solids from the control reactors, which is consistent with the composition of lead carbonate (Figure 17). The FT-IR spectrum was also consistent with previous studies of cerussite,[122–125] with bands characteristic of carbonate at 673, 836, 1048, and 1730 cm^{-1}. Solids from the silicate-treated reactors had a silicon content of 5.7% at the surface, whereas solids from the control reactors did not have detectable silicon (Figure 17). A weak Si-O-Si band occurred at 994 cm^{-1} in the FT-IR spectrum (Figure 18),[126] which agrees with a previous observation of silicate in water service lines treated by sodium silicate.[23]

Phosphorus accounted for 20.7% of the surface elemental composition in solids from the orthophosphate-treated reactors (Figure 17). This is explained by hydroxylpyromorphite and perhaps by orthophosphate adsorption. Reactor solids yielded an FT-IR spectrum consistent with hydroxylpyromorphite, but carbonate bands occurred at 1334 1422, and 1388 cm^{-1}, which may be due to carbonate-substituted hydroxylpyromorphite.[92,127] Solids from the reactors treated with polyphosphate yielded an FT-IR spectrum consistent with that of the control reactor.

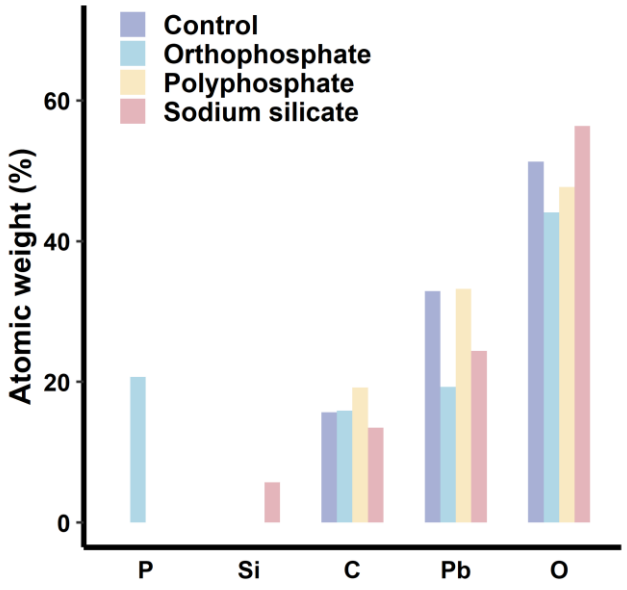

Figure 17 Elemental analysis (atomic %) by X-ray photoelectron spectroscopy (XPS) of reactor solids at pH 7.5 and 5 mg C/L.

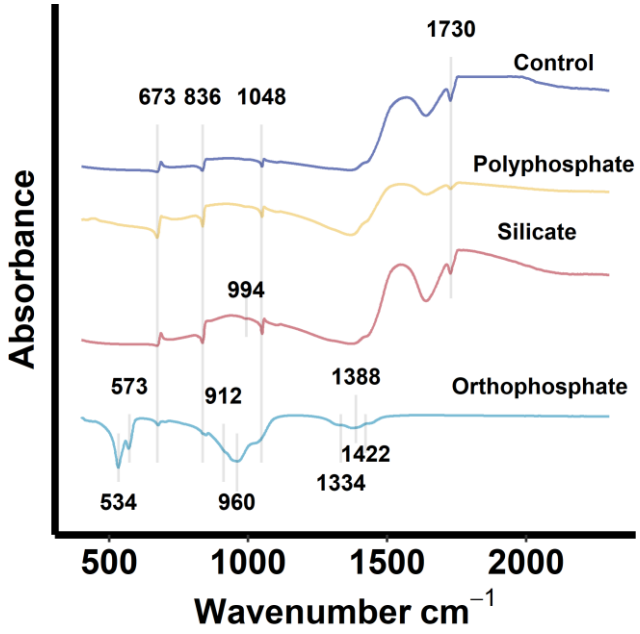

Figure 18 FTIR spectra of reactor solids after reaction with orthophosphate, polyphosphate, or sodium silicate at pH 7.5 and DIC 5 mg C/L.

3.4.5 Implications for distribution systems

Given that sodium silicate had a minimal impact on lead release from lead carbonate—especially compared with orthophosphate—pH adjustment appears from these data to be the primary mechanism by which sodium silicate controls lead release. That is, this study suggests the silicate-treated system may be approximated as a lead-water-carbonate system, provided that other impacts of silicate are negligible.

As a sequestrant, sodium silicate may avoid some of the problems associated with polyphosphate: phosphorus loading to the environment and elevated lead solubility. Like polyphosphate, however, sodium silicate can mobilize particulate and colloidal metals (e.g., lead and iron) via dispersion. Both sequestrants caused pronounced negative shifts in the zeta potentials of cerussite suspensions over a wide pH range, highlighting their dispersive properties (Figure 19). Unlike polyphosphate, sodium silicate did not cause any significant increases in lead, except at pH 9 and 5 mg C/L. But the negative shift in zeta potential that silicate induces may disperse particles or colloids at circumneutral pH in systems where lead is more easily mobilized. Similar concerns have been raised concerning orthophosphate,[128] but further study is needed to evaluate these factors and potential drawbacks.

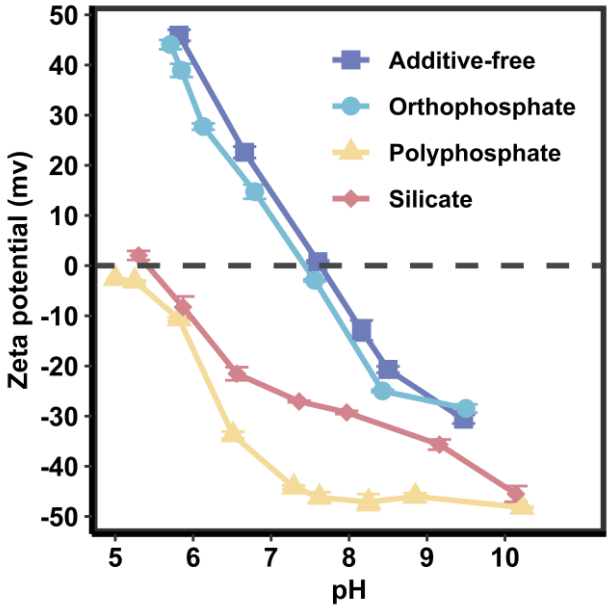

Figure 19 Zeta potential as a function of pH, characterizing newly-prepared suspensions of cerussite (1 g/L) at 5 mg C/L and 21 °C (orthophosphate 1 mg P/L; polyphosphate 1 mg P/L and sodium silicate 32 mg SiO_2/L).

Here, silicate adsorption to lead carbonate did not slow lead release, except perhaps at pH 9 with 50 mg C/L. But formation of a diffusion barrier may take longer than the time in which experiments were completed (≤ 40 hours). The long-term impact of sodium silicate is still worth investigating, as is the interaction between silicate and non-lead species. Natural silicate minerals (e.g., aluminosilicate, quartz, etc…) are frequently observed in lead corrosion scale,[28,29] and a recent study using recovered lead pipe attributed declines in lead release with silicate addition to an aluminum-rich diffusion barrier.[129]

Conversely, orthophosphate promoted formation of low-solubility hydroxylpyromorphite within the experiment's timeframe. Comparable to sodium silicate, orthophosphate slowed lead release at high pH and DIC even without altering the crystalline phase composition (perhaps via chemisorption and crystal poisoning).[11,30] At the other pH and DIC settings, the rapid action of orthophosphate relative to sodium silicate represents a distinct advantage even if future work shows silicate addition to be effective on longer timescales.

3.5 Conclusion

This study investigated lead release from lead(II) carbonate in the presence of sodium silicate, orthophosphate as a reference inhibitor, and polyphosphate as a reference sequestrant. Sodium silicate has seen some use for lead release control, but its effect is often confounded with the accompanying increase in pH. Here, pH was controlled, finding that sodium silicate had relatively little impact on lead release within the 30-minute hydraulic retention time.

Silicate treatment did not induce formation of silicate-based mineral phases or significant changes in functional groups, but it did accumulate at the lead carbonate surface, altering surface morphology. At pH 7.5, sodium silicate had a negligible impact on lead release at both low and high DIC concentrations. At pH 9, silicate had diverging effects. At 5 mg C/L, sodium silicate accelerated lead release, which may be due to its negative effect on zeta potential facilitating colloidal dispersion. At 50 mg C/L sodium silicate slowed lead release. These data suggest that future work on silicate control of lead release should focus on high pH, high DIC systems and the formation of silicate-based diffusion barriers due to interaction with non-lead species.

4 Chapter 4 Impact of sodium silicate on lead release and colloid size distributions in drinking water

This chapter reproduced from Li, B., Trueman, B. F., Munoz, S., Locsin, J. A., & Gagnon, G. A. (2020). Impact of sodium silicate on lead release and colloid size distributions in drinking water. Water Research. https://doi.org/10.1016/j.watres.2020.116709

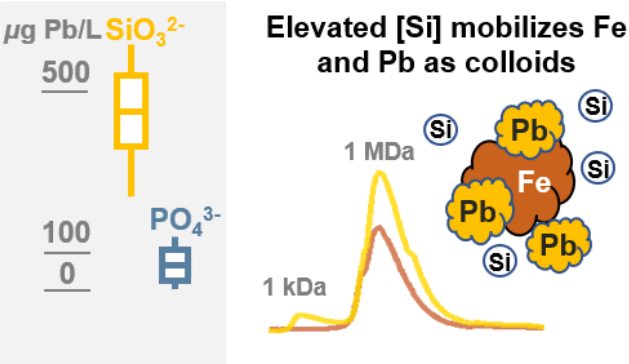

Figure 20 Artwork of impact of sodium silicate and orthophosphate on lead release; co-transport of iron and lead with addition of sodium silicate.

4.1 Abstract

Sodium silicates have been used in drinking water treatment for decades as sequestrants and corrosion inhibitors. For the latter purpose they are poorly understood, which presents a potential public health risk. A common sodium silicate formulation was investigated as a treatment for lead release and compared it to orthophosphate, a well-established lead corrosion control treatment. The size distributions of colloids generated in silicate and orthophosphate-treated systems were compared using field flow fractionation with multielement detection. Sodium silicate provided minimal protection of new lead pipes while orthophosphate effectively mitigated lead release. Moreover, an elevated sodium silicate dose (48 mg SiO_2/L) dispersed corrosion scale in cast iron pipe sections and lead service lines, resulting in a substantial release of colloidal iron and lead. Although a silicon-rich coating was observed at the lead-water interface, lead

carbonate remained the major corrosion product and appeared to control lead levels in the silicate-treated system. These data suggest that pH adjustment is the major mechanism explaining lead corrosion control by sodium silicate, and that—as with polyphosphate—excess silicate can be highly detrimental to controlling lead release.

4.2 Introduction

Sodium silicates have been used by water utilities as corrosion inhibitors and sequestrants for decades.[19–21] Orthophosphate is much more widely used for lead control,[74,75,130] but silicates are regarded as a legitimate lead control treatment.[9,131]

Limited data, however, mean that the mechanisms by which silicates might act to limit lead release are still unclear. They may form a thin silicate-based film on the internal surface of lead pipes,[23,24] or contribute to passive corrosion scale formation,[16,25] but little evidence exists to support either possibility. Moreover, the effect of silicates on lead is often confounded with the increase in pH that silicates cause.[10,15,24,25,27] Limited understanding of silicate-lead interactions leaves water systems that use silicates vulnerable to lead contamination.

Silicates are better known as sequestrants, and they are widely used to solve aesthetic issues caused by iron and manganese.[19,20,132,133] However, given the role of polyphosphate—another popular sequestrant—in exacerbating lead release,[36,58,134] careful evaluation of silicates' effect on lead is warranted. Although silicates' impacts on iron oxidation[135,136] and particle size distribution[20] have been described previously, silicates' effect on the distribution system as a whole is poorly characterized. Previous work[46,48,50,137–139] indicates that particulate iron and manganese may increase lead release. Given the dispersive effects of silicates on these metals, study of the interplay between iron/manganese, lead, and silicate species is important to avoid future water quality problems.

Here lead release control was evaluated using a common sodium silicate formulation, comparing it against orthophosphate, a well-established corrosion control treatment.[31,58,76,140] A model distribution system was used with new lead pipes and cast iron or PVC water mains to address three primary objectives: a) the effect of sodium

silicate on lead release from full and partial lead service lines (LSLs); b) its effect on colloidal metals release from both LSLs and water mains; and c) LSL scale formation in the presence of sodium silicate. This work provides new insight into silicate corrosion control and sequestration, especially for minimizing lead release.

4.3 Materials and methods

4.3.1 Model distribution system

Detailed descriptions of the pilot-scale model distribution system are available elsewhere,[46,141,142] and the relevant modifications are described here. Given the limited data on silicate-lead interactions in a drinking water context, new lead pipe was used in this study because it yields repeatable results, avoiding the peculiarities of recovered lead pipe that would have limited our ability to generalize the study findings.

The model system (Figure 21a) comprised six independent distribution main pipe loops: three PVC and tuberculated cast iron (100 and 150 mm in diameter, respectively; 1.8 m in length). Each loop supplied one partial and one full LSL section in parallel; these were constructed with 30 and 60 cm sections, respectively, of new lead pipe (≥ 99.97 % purity; 3/4 in. extra strong; Canada Metal, Montréal, Canada). Partial LSL sections included 30 cm of new copper pipe (3/4 in. type ‘K’; Wolverine, Portage, USA) coupled to the new lead with a plastic fitting (Philmac, North Plympton, Australia). Electrical continuity between lead and copper was achieved with an external copper wire and copper alligator clips.

Effluent from the six pipe loops was discharged to six independent 68 L reservoirs and pumped through the LSLs for 5 minutes each day at an approximate flow rate of 2 L/min. This resulted in a daily stagnation period of 23h 55 min, which, given the pipe diameter, approximates equilibrium.[143]

Feedwater for the model distribution system was provided by the J.D. Kline water supply plant (Halifax, Nova Scotia, Canada), which uses alum coagulation followed by dual media direct filtration (sand and anthracite). A full description of the facility is available elsewhere.[139,144] Typical total organic and inorganic carbon values were 1.5

and 5 mg C/L, while lead and iron were below their reporting limits. Feedwater was modified according to the experimental design (Figure 21a) with sodium hypochlorite (1.0 mg Cl_2/L, Altantic Chemical and Aquatic Inc., Canada), sodium silicate (12, 24 and 48 mg SiO_2/L, Na_2O:SiO_2 = 1:3.22, National Silicate, Canada), orthophosphate (1.0 mg PO_4^{3-}/L, dosed as H_3PO_4, Fisher Scientific, USA), zinc orthophosphate (1.0 mg PO_4^{3-}/L, Carus 3150, Carus Chemical Company, USA), and sodium hydroxide (pH 7.4, Fisher Scientific, USA) (Appendix C, Figure 50b). Water temperature in the model distribution system ranged from 14.5 to 23.7°C over the experiment (Appendix C, Figure 51a).

4.3.2 Experimental design

Lead release was evaluated under twelve conditions: three inhibitors (i.e., sodium silicate, orthophosphate, zinc orthophosphate), two distribution main materials (recovered cast iron and PVC), and two LSL types (full and partial, Figure 21a). A standard $3 \times 2 \times 2$ mixed level factorial design which,[56,145] under a mild assumption concerning interactions between factors (i.e., a negligible three-way interaction), yields a multiple-degree-of-freedom estimate of error. The effect of sodium silicate was evaluated using data from at least eight pipe sections, and the effect of LSL type was evaluated using data from all twelve pipe sections (Figure 21a).

To prevent the confounding of pH and silicate dose noted in previous studies, the LSL influent water pH was maintained at 7.4 (Figure 21a; Appendix C, Figure 50b) throughout the experiment and under all water quality conditions. Stagnated LSL effluent pH was 6.99 (Figure 21b; Appendix C, Figure 51b and c) at 24 and 48 mg SiO_2/L. Silicate doses were selected based on previous studies[10,15,16] and the current NSF/ANSI/CAN standard.[131]

4.3.3 Conditioning and sampling

The model distribution system was operated for 84 weeks (Figure 21b), the first 44 of which were devoted to conditioning under the parameter settings described above. Lead in LSL effluent was measured sporadically during conditioning, while control parameters were measured consistently. Regular sampling began at week 45; LSL effluent was collected almost every week in 250 mL polyethylene (HDPE) bottles

following 23 h 55 min of stagnation. Samples of influent to the LSLs were collected from the 68 L reservoirs in polypropylene tubes. HDPE bottles and caps were prepared for use by immersion for at least 24 h in ~2M HNO_3, followed by thorough rinsing with ultrapure water. At the end of experiment, full LSL pipes were retrieved and prepared for surface analysis (i.e., XRD, SEM-EDS, and XPS).

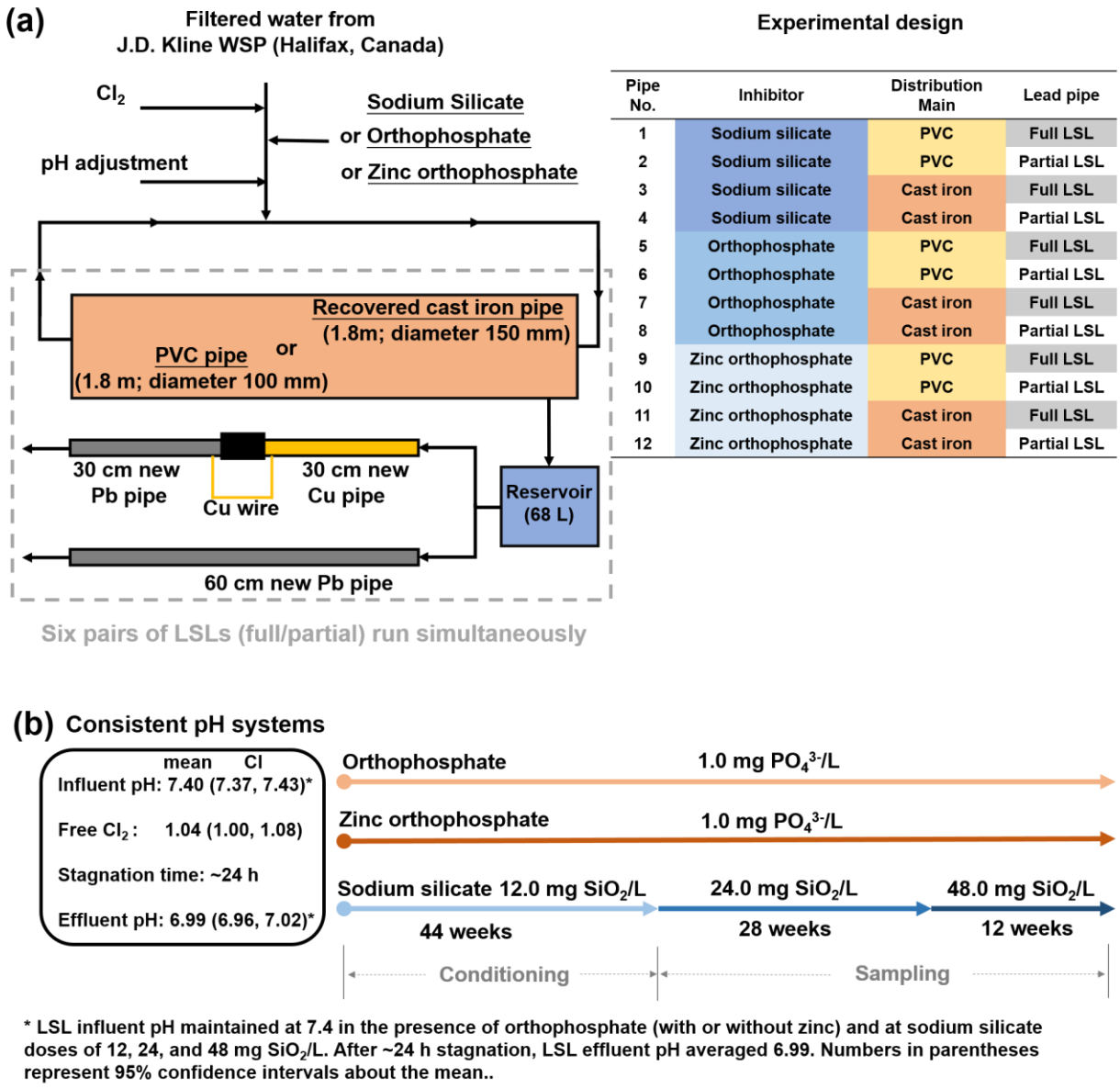

Figure 21 (a) A description of the model system: a PVC or recovered cast iron pipe loop, a set of full and partial LSL sections, and the experimental design. (b) Experimental timeline of the constant pH system.

4.3.4 On-site water quality analysis

Free chlorine, orthophosphate, and sodium silicate were measured on-site in pipe loop effluent using the N,N-diethyl-p-phenylenediamine (DPD), molybdate colorimetric, and silicomolybdate methods, respectively, with a UV-Vis spectrometer (DR6000, Hach, USA).[146] Temperature was measured using a glass thermometer (Fisher Scientific, USA) and pH using a combination electrode (Accumet Excel XL25, Fisher Scientific, USA).

4.3.5 Inductively coupled plasma-mass-spectrometry (ICP-MS)

Metals were quantified by inductively coupled plasma-mass spectrometry (ICP-MS, X Series II, Thermo Scientific).[147] Samples of LSL influent were preserved for total metals analysis by acidifying with trace metal grade nitric acid (Fisher Scientific, USA) to pH < 2.0 and holding for a minimum of 24 h. Ten ml aliquots from a subset of effluent samples were passed through 0.45 µm cellulose nitrate membrane filters with a syringe filter cartridge and preserved in polypropylene tubes for quantification of dissolved/colloidal metals. The remaining volume of each effluent sample was preserved in the original bottle and held for a minimum of 24 h. Afterwards, a 10 ml aliquot from each was decanted to a polypropylene tube for total metals analysis.

4.3.6 Field flow fractionation (FFF)

Colloidal metals were characterized in LSL effluent from the silicate- and zinc orthophosphate-treated systems by asymmetric flow field flow fractionation.[148–152] Samples were filtered at 0.45 µm with a cellulose nitrate membrane immediately before analysis, and details of the method are described elsewhere.[138]

4.3.7 X-ray diffraction (XRD)

A Siemens D500 diffractometer equipped with a copper anode and a diffracted beam monochromator (wavelength = 1.5406 Angstroms) was used to identify crystalline phases on the internal surfaces of lead pipes. Measurements were made in step scan mode using a step size of 0.04 degrees (2θ) and a dwell time of 3.0 seconds. Samples were dried at 21°C $\pm$ 1°C before analysis.

4.3.8 X-ray photoelectron spectroscopy (XPS)

A Thermo VG Scientific Multilab 2000 was used to determine the elemental composition of corrosion scale. An aluminum X-ray source (1486.6 eV) was used under high vacuum (1 x 10-9 < P < 1 x 10-8 torr), and a CLAM4 Hemispherical Analyzer (r = 150mm) with a multichannel detector was used to detect photoelectrons. High-resolution scans were performed at pass energy of 30 eV with a step size of 0.1 eV, and survey scans were performed at a pass energy of 100 eV with a step size of 1.0 eV. Samples were dried at 21°C $\pm$ 1°C. Binding energy was calibrated using the C 1s line (285.0 eV), due to adventitious carbon; binding energies drawn from literature were adjusted based on this calibration.

4.3.9 Scanning electron microscopy/energy-dispersive X-ray spectroscopy (SEM-EDS)

The morphology and elemental composition of corrosion scale was characterized using a Hitachi S-4700 scanning electron microscope, operated at 10 kV and an 11-12 mm working distance. Samples were dried at 21°C $\pm$ 1°C, attached with conductive carbon tabs to aluminum stubs, and loaded into the SEM for imaging.

4.3.10 Galvanic current measurement

Galvanic current between the lead and copper comprising partial LSLs was measured, before sampling the effluent, using a digital multimeter (PeakMeter MS8236, China).

4.3.11 Data analysis and modeling

The experimental data was analyzed using R (version 4.0.0),[63] along with a collection of widely-used contributed packages.[64–67,153] An additive mixed model[153] was fitted to the LSL effluent data, describing lead release as a smooth non-parametric function of effluent iron concentration (a thin plate regression spline). LSL type (full or partial) and inhibitor type was modeled as parametric effects, and the model was estimated using restricted maximum likelihood.

To account for the differences in length of lead pipe between full and partial LSLs, lead release was expressed as mass released per unit length of lead pipe (µg Pb/cm). This quantity is a function of the lead concentration in LSL effluent, the volume of water contained within the LSL section, and the length of lead pipe.

Autocorrelation was modeled for each LSL section as a continuous time first order autoregressive process (CAR(1)) (Appendix C, Figure 54d).[154,155] The basic form of the model is described in Pedersen et al. (model G),[156] and the autocorrelation structure is described in Simpson.[154] The model is summarized by Equation (2):

$$log(\text{Pb}) = \beta_o + \beta_1 x_{partial\ LSL} + \beta_2 x_{zinc\ orthophosphate} + \beta_3 x_{sodium\ silicate} + f(log(\text{Fe})) + e$$

where log is the natural log transformation, Pb is the mass of lead released per unit length of lead pipe (µg Pb/cm), Fe is the iron concentration in LSL effluent (µg Fe/L), e is the error term, f is a smooth function, and the x are 0/1 dummy variables where $x = 0$ is the reference state ($x_{partial\ LSL}$: 0 = full LSL, 1 = partial LSL; $x_{zinc\ orthophosphate}$: 0 = absent, 1 = present; $x_{sodium\ silicate}$: 0 = absent, 1 = present; and $x_{zinc\ orthophosphate}$ = $x_{sodium\ silicate}$ = 0 indicates the orthophosphate system).

4.4 Results and discussion

4.4.1 Effect of sodium silicate on lead release from LSLs

Sodium silicate performed worse than either orthophosphate or zinc orthophosphate in mitigating lead release due to uniform (full LSL) corrosion (Figure 22; Appendix C, Figure 52). At 24 mg SiO_2/L, median lead in full LSL effluent was 398 µg/L (n=54). In the presence of orthophosphate or zinc orthophosphate (1 mg PO_4^{3-}/L), it was much lower: 67 µg/L (n=78) and 53 µg/L (n=78), respectively. Lead levels at 1 mg PO_4^{3-}/L were comparable to peak lead levels in homes with LSLs in the distribution system modeled,[37] and this system also maintains 1 mg PO_4^{3-}/L.

Sodium silicate did not protect against galvanic corrosion either, at least in comparison with the other two treatments. Here, galvanic effects were estimated as the difference in median lead release between full and partial LSLs receiving the same water type. Lead

release from partial LSLs treated with 24 mg SiO_2/L (median: 578 µg/L; n=54) was greater by 180 µg/L, while the effect of galvanic corrosion in the other two systems was relatively minor. Lead release from partial LSLs was greater by just 2 (median: 69 µg/L; n=78) and 15 µg/L (median: 68 µg/L; n=77) in the orthophosphate and zinc orthophosphate-treated systems, respectively. These effects are consistent with previous reports that, in galvanic systems, sodium silicate performs poorly in comparison with orthophosphate.[16,17]

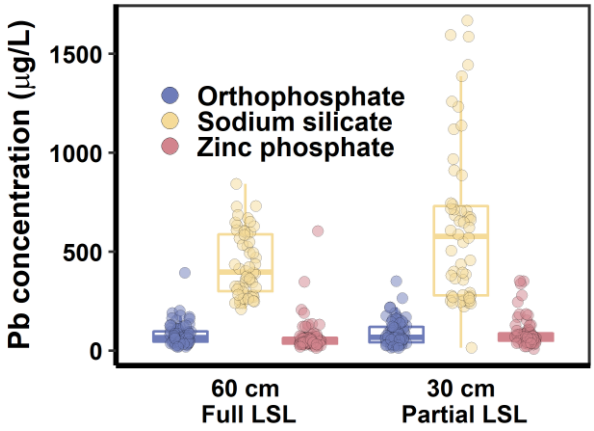

Figure 22 Lead concentration in LSL effluent grouped by corrosion inhibitor and LSL configuration (full or partial)(silicate dosage: 24 mg/L). Boxes span the interquartile range (IQR), medians divide the boxes in two, and whiskers extend from the upper and lower quartiles to the most extreme value within 1.5 times the IQR.

4.4.2 Galvanic corrosion and lead release

While sodium silicate was ineffective, relative to orthophosphate, in controlling lead release due to galvanic corrosion, orthophosphate did not inhibit charge transfer between copper and lead (Figure 23. Instead, it appeared to promote scale formation. In the presence of sodium silicate, each additional µA of current accompanied 94 µg Pb/L (r^2 = 0.89). In the presence of either orthophosphate or zinc orthophosphate, each additional µA accompanied much less: between 7.4 and 8.7 µg Pb/L (Figure 23. Moreover, the relationship between galvanic current and lead release in the presence of orthophosphate was generally weak, with r^2 ranging from 0.16 - 0.20. These findings are

consistent with previous work describing immobilization in scale of lead released due to galvanic corrosion.[16,53,80,81,157] The failure of sodium silicate, compared with orthophosphate, to immobilize lead is discussed mechanistically below.

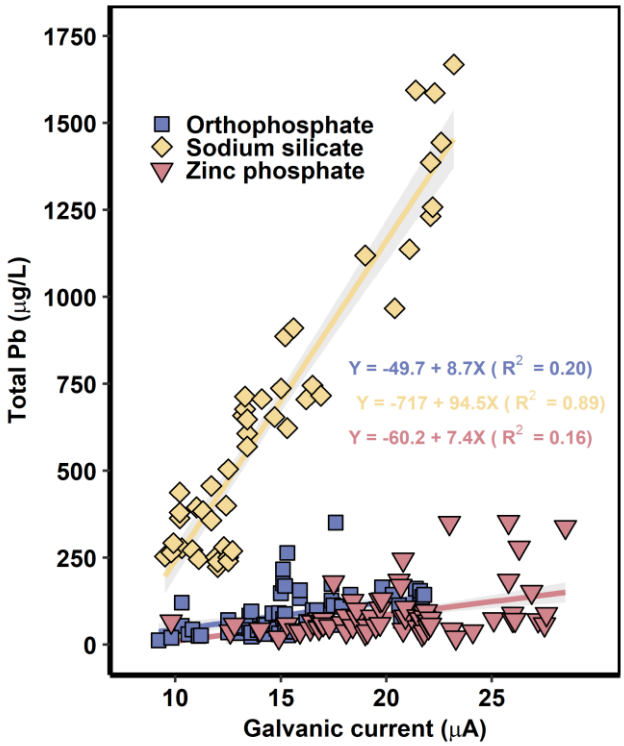

Figure 23 Lead release from partial LSLs, grouped by inhibitor and displayed as a function of galvanic current (silicate dosage: 24 mg/L). The shaded region defines a 95% confidence interval on the fitted values.

4.4.3 Role of iron release

In the presence of sodium silicate, LSLs supplied by unlined iron released much more lead than those supplied by PVC, with a median difference of 358 µg/L over the experiment. Given the strong prior evidence that iron is a driver for lead release,[46,48,137,158,159] observed lead mass loss was modeled as a smooth non-parametric function of iron concentration, where the relationship between the two variables was dictated by the data, not by a user-selected parameter (Table 2; Figure 24; Appendix C, Figure 54). The relationship between iron and lead was statistically

significant ($p << 0.001$), suggesting that iron particles represent a significant mobile sink for lead.

Table 2 Terms and their corresponding p-values in the additive model fit to lead level, expressed as mass release per unit length of lead pipe (µg Pb/cm). Estimates reflect the natural log transformation of the response, while percent increases are the result of back-transformation and are calculated relative to the reference state (full LSL or non-zinc orthophosphate for LSL type and inhibitor type predictors).

Term	Estimate	% increase	p-value
Partial LSL	0.7011	101.6	5.021e-15
Sodium silicate	2.103	719	3.871e-63
Zinc orthophosphate	0.3113	36.52	0.004416
Fe concentration (non-parametric smooth function)	NA	NA	1.635e-52

The other experimental factors—LSL type and inhibitor—were incorporated into the model as parametric effects. Partial LSLs released an estimated 102% more lead per unit length of lead pipe than full LSLs ($p << 0.001$), which is consistent with previous data[51,81,160] and the differences between lead release from full and parial LSLs summarized above.

Relative to orthophosphate, sodium silicate accompanied 719% more lead release ($p << 0.001$), which is also consistent with the differences summarized above. Zinc orthophosphate treatment resulted in 36% more lead ($p = 0.004$) (Figure 24; Table 2)). And while this difference is not apparent in Figure 22, the model controls for the positive effect of iron but the figure does not. Iron was higher in cast iron effluent treated with non-zinc orthophosphate, and excluding LSLs supplied by cast iron, zinc orthophosphate treatment resulted in a median of 23 µg/L more lead release than orthophosphate treatment.

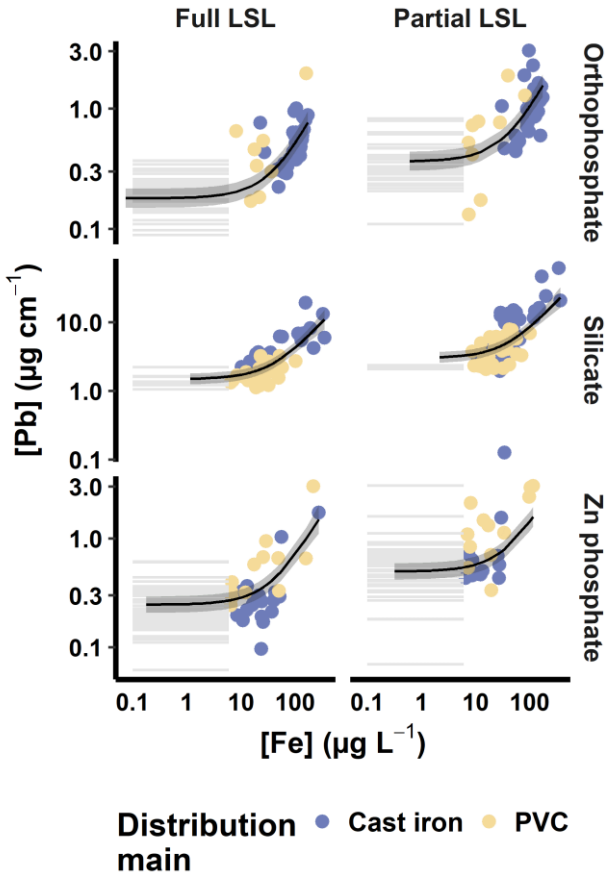

Figure 24 Lead release per unit lead pipe length as a function of iron concentration, grouped by inhibitor type and LSL configuration (silicate dosage: 24 and 48 mg/L). The additive model fit is superimposed, the shaded region denotes a point-wise 95% confidence interval on the fitted values, and horizontal grey lines represent iron concentrations below the reporting limit of 6 µg L^{-1}.

4.4.4 Dispersion of colloidal metals by sodium silicate

While the additive model describes variation in lead release as a function of inhibitor type, it does not account for variation in the dose of sodium silicate, except implicitly through covariation in iron concentrations. When the silicate dose was doubled from 24 to 48 mg SiO_2 in the final twelve weeks of the study (Figures 21b), lead and iron increased dramatically (Figure 25). This cannot be explained by effluent pH , which was maintained at 6.99 throughout the experiment. At 24 mg SiO_2/L, lead levels in full LSL effluent were relatively constant, with median values of 589 and 297 µg/L in cast iron

and PVC systems, respectively (Figure 25a). At 48 mg/L, median lead in full LSL effluent increased to 1234 and 425 µg/L, and partial LSL effluent exhibited a similar trend (Appendix C, Figure 52).

With the increase in silicate dose, median iron increased from 18 to 130 and 7 to 37 µg/L in cast iron and PVC distribution main effluent (that is, in the influent to LSL sections; Figures 25). Similar observations have been reported elsewhere:[10] in Hopkinton, MA, silicate addition (~25-55 mg SiO_2/L) without pH control accompanied an increase in iron, although seasonality and variable well use may have been factors in this case. Silicate treatment also accompanied a temporary increase in lead.[10]

Here, increases in iron and lead are likely due at least in part to colloidal dispersion of metals, originating either from corrosion scale or from iron deposits on PVC. The dispersive properties of sodium silicate have been highlighted in previous work, where silicate has been linked with formation of colloidal polymeric ferric iron[39] and dose-dependent dispersion of particulate/colloidal iron.[20] The negative surface charge imparted to iron oxide particles by sodium silicate[20,135] may play an important role in the elevated iron observed here, and silicate's negative effect on the rate of ferrous iron oxidation may also be relevant.[135,136]

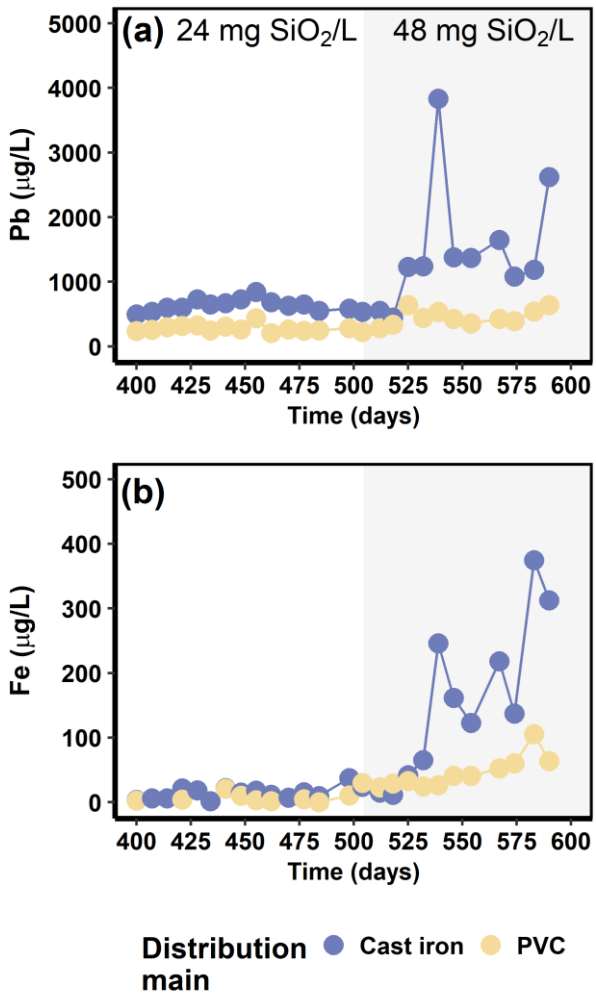

Figure 25 (a) Lead concentration in effluent from LSLs and (b) iron concentration in effluent from cast iron and PVC distribution mains, at sodium silicate doses of 24 (white background) and 48 mg SiO_2/L (grey background). Effluent pH in lead pipes was mantained at 6.99 at 24 and 48 mg SiO_2/L.

The dispersive effects of sodium silicate on iron and lead are apparent in the fractograms representing the “dissolved” (<0.45 µm) fraction of full and partial LSL effluent (Figure 26 and Appendix C, Figure 55, respectively). These element-specific size distributions show a substantial concentration of colloids in the presence of 48 mg SiO_2/L and a negligible concentration in the presence of zinc orthophosphate. Colloidal iron was much greater in LSLs supplied by cast iron compared with PVC, which is consistent with the higher levels of iron observed in cast iron pipe effluent (Figure 26).

The elevated lead levels in LSLs supplied by cast iron are probably explained by partitioning of lead to colloidal iron, which provides additional capacity—beyond the limits of equilibrium solubility—for water to transport lead.[138,152,161] Silicate addition may also disperse lead from LSL corrosion scale directly, but further study is needed to explore this possibility. A similar effect has been observed in the presence of excess orthophosphate or natural organic matter, which disperses particulate lead by imparting a negative surface charge.[107,128]

Colloidal iron and lead also occurred in LSLs supplied by PVC, albeit in a smaller size range: in the cast iron system, maximum colloid retention occurred at approximately 1 MDa, whereas in the PVC system it was closer to 100 kDa. The size distribution of UV_{254} absorbance tracked those of iron and lead closely. This is due largely to light scattering caused by colloid particles,[162] but may also represent absorbing species including natural organic matter. Colloids in LSL effluent also contained copper (due to low levels in source water or the copper pipe in partial LSLs (Appendix C, Figure 55), manganese (present at low levels in source water), and aluminum (due to alum coagulation). These metals have also been reported to co-occur with lead in previous work.[50,139,163,164]

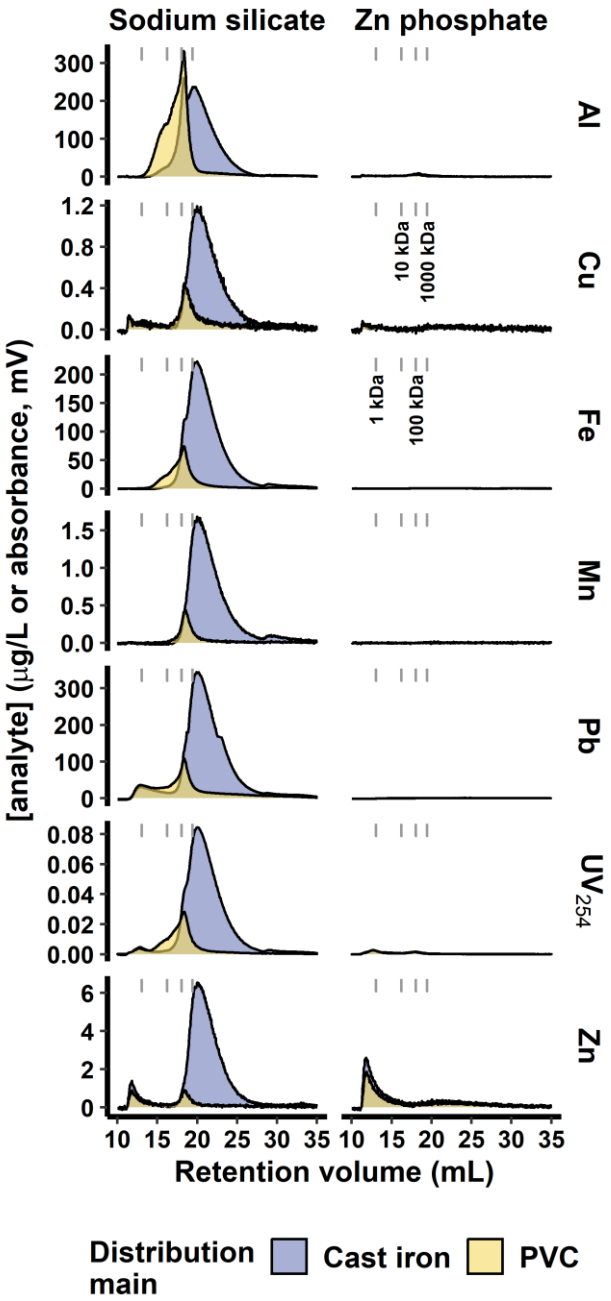

Figure 26 Fractograms representing 0.45 µm-filtered full LSL effluent, grouped by pipe loop material (PVC/cast iron), and inhibitor type (sodium silicate at 48 mg SiO_2 /L or zinc orthophosphate at 1 mg PO_4^{3-} /L). Each fractogram represents an average of duplicates.

4.4.5 Scale morphology, structure, and elemental composition

LSL corrosion scale formed in the presence of sodium silicate yielded an X-ray diffraction pattern dominated by hydrocerussite ($Pb_3(CO_3)_2(OH)_2$) (Figure 27a). Massicot (β-PbO), litharge (α-PbO), and metallic lead (Pb) were present as minor phases. Consistent with the diffraction data, corrosion scale in this system exhibited a platy crystalline morphology typical of hydrocerussite.[62,86,91] Quartz (SiO_2) was also identified by XRD, but crystalline lead silicate solids (e.g., $PbSiO_3$) were not. These findings are consistent with model predictions that a lead carbonate phase will dominate under the experimental conditions, regardless of the influence of silicate.[54,118]

In the presence of orthophosphate (with or without zinc), hyroxylpyromorphite ($Pb_5(PO_4)_3(OH)$) was the dominant crystalline phase (Figure 27b-c). Accordingly, scale exposed to orthophosphate exhibited a clustered, needle-like morphology characteristic of hydroxylpyromorphite.[91,92] Quartz, litharge, cerussite ($PbCO_3$), and metallic lead were identified as minor phases by XRD.

Sodium silicate did result in corrosion scale with greater silicon content (3.4 ± 0.1 % wt. by EDS) than orthophosphate (with or without zinc, Figure 28 and Appendix C, Figure 56). Lead was also relatively abundant (16.3 ± 0.9 % wt. by EDS) in the silicate-treated system, while calcium, chlorine, iron, and manganese were more abundant in the presence of orthophosphate and zinc orthophosphate. These findings are consistent with the strong dispersive action of sodium silicate. That is, colloidal dispersion by sodium silicate may have prevented these elements from accumulating on the surface of lead pipes, resulting in higher levels of suspended colloidal metals in the water phase.

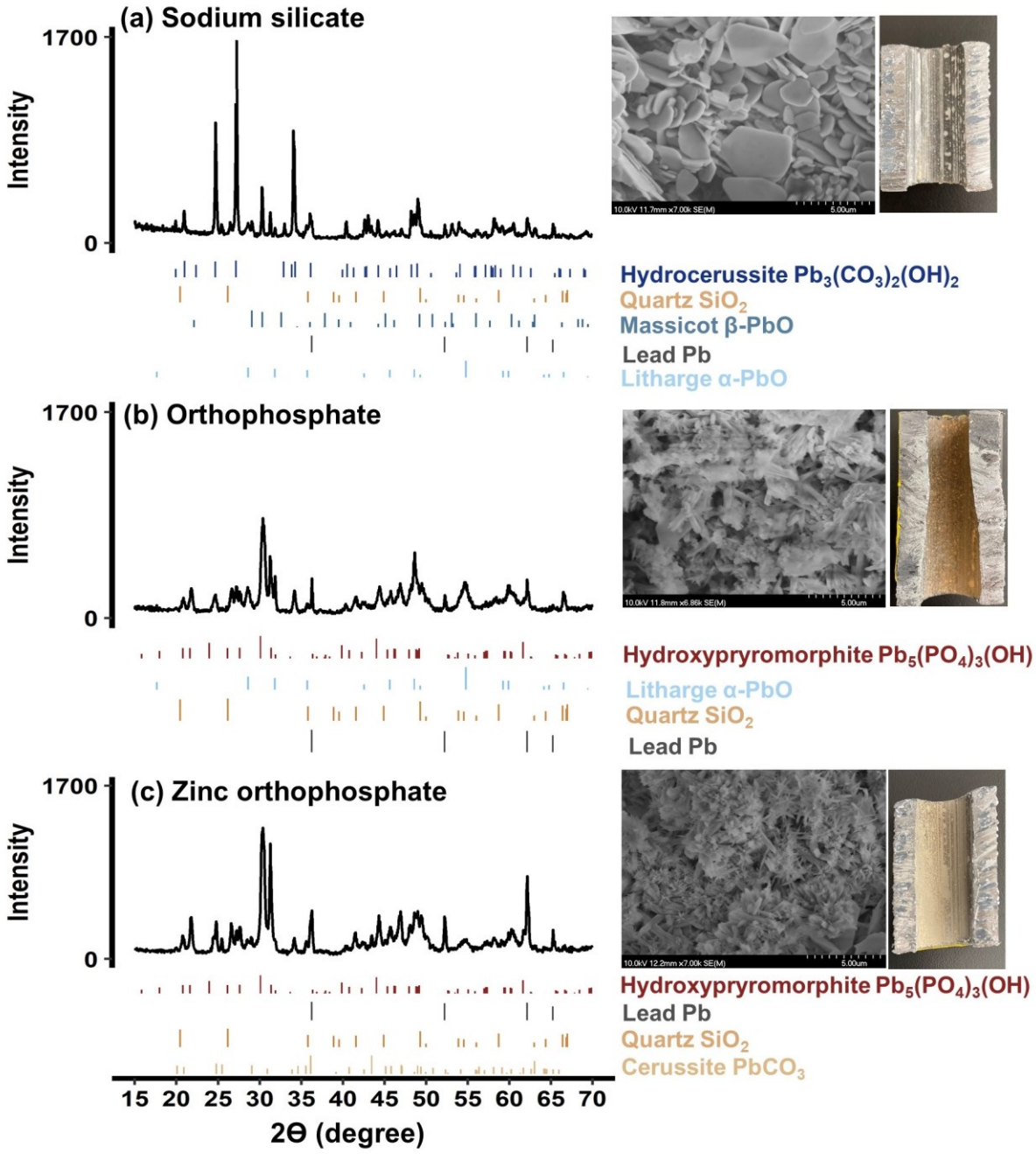

Figure 27 X-ray diffractograms (left), SEM micrographs (middle), and photographs (right) of corrosion scale representing full LSLs supplied by PVC and treated with (a) sodium silicate, (b) orthophosphate, or (c) zinc orthophosphate.

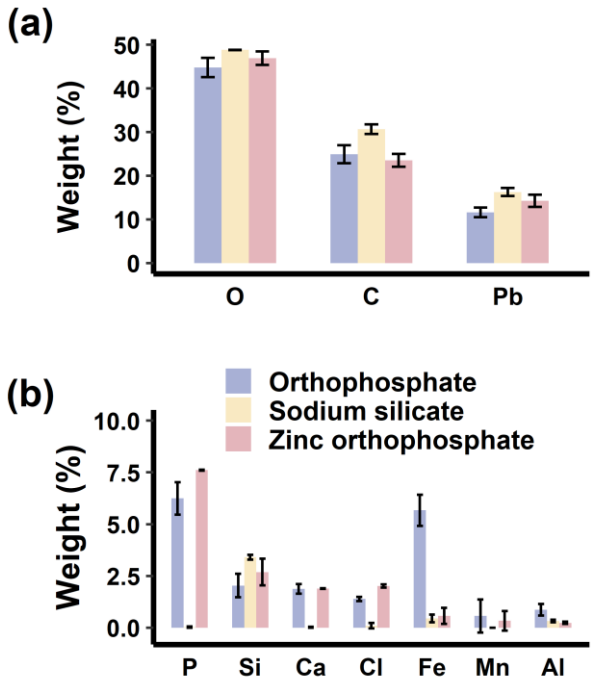

Figure 28 Elemental composition of LSL corrosion scale supplied by PVC, as determined by SEM-EDS.

4.4.6 XPS analysis of LSL surface chemistry

While silicate did not alter scale in any way that would clearly diminish lead release, the methods (XRD, SEM-EDS) provide information up to a depth of several micrometers.[93–95] However, a nanometer-thick silica coating has been proposed as a possible mechanism for corrosion control due to silicate in previous studies.[23,24] Since such a coating would be difficult to detect via XRD and SEM-EDS,[23] XPS was used to characterize the scale-water interface to a depth of several nanometers.[23,120,121]

Sodium silicate did promote formation of a thin silicon-rich layer at the surface: the silicon/lead ratio of atomic percentages was 42.6, 0.6, and 3.3 in the silicate-, orthophosphate-, and zinc orthophosphate-treated systems according to the XPS survey scan. Consistent with SEM-EDS results (Figure 28b), silicon (Si_{2p}) was observed in all systems, due either to naturally-occurring and added silicate (Figure 29d). The Pb_{4f} intensity was relatively low in the presence of sodium silicate (Figure

29a), and carbonate (~289 eV) was not detected at the scale surface. The C $_{1s}$ peak occurred instead at 285.0 eV. This peak is attributable to adventitious carbon from air exposure and was used to calibrate the other binding energies (Figure 29b).[98] As expected, phosphorus was not detected in scale exposed to added sodium silicate, whereas in the presence of orthophosphate it was relatively abundant (Figure 29c, P $_{2s}$).

Given the complex environment at the scale-water interface, there are many possible sources of oxygen (e.g., metal oxides, hydroxides or carbonate). In the presence of sodium silicate, the peak of O $_{1s}$ photoline occurred at 532.4 eV. Previous work suggests that O 1s due to metal oxides and hydroxides occurs between 530.9 and 531.5 eV,[165] while the non-bridging oxygen of silica compounds occurs at higher binding energies (e.g., O 1s due to SiO_2: 533.1-533.3 eV).[166,167] Thus, non-bridging oxygen (e.g., silica tetrahedra) appears to be relatively abundant in the sodium silicate treated system. In the presence of orthophosphate, the O $_{1s}$ peak occurred at a lower binding energy (531.5 eV) (Figure 29, O_{1s}), which may be due to the oxygen in phosphate and hydroxide from hydroxyprymorphite, reported elsewhere at ~531.3 eV.[168]

Together, the identification of lead carbonate (hydrocerussite, by XRD) as the dominant phase, the weak lead (Pb $_{4f}$) signal, the weak carbonate signal (C $_{1s}$ at 289 eV), the strong silica signal (Si $_{2p}$), and the high O $_{1s}$ binding energy suggest that the (lead carbonate) surface was covered by a thin silicate-rich layer. This agrees with previous results,[23] but no evidence was found that the nanometer-thick coating inhibited lead release, especially compared to orthophosphate treatment.

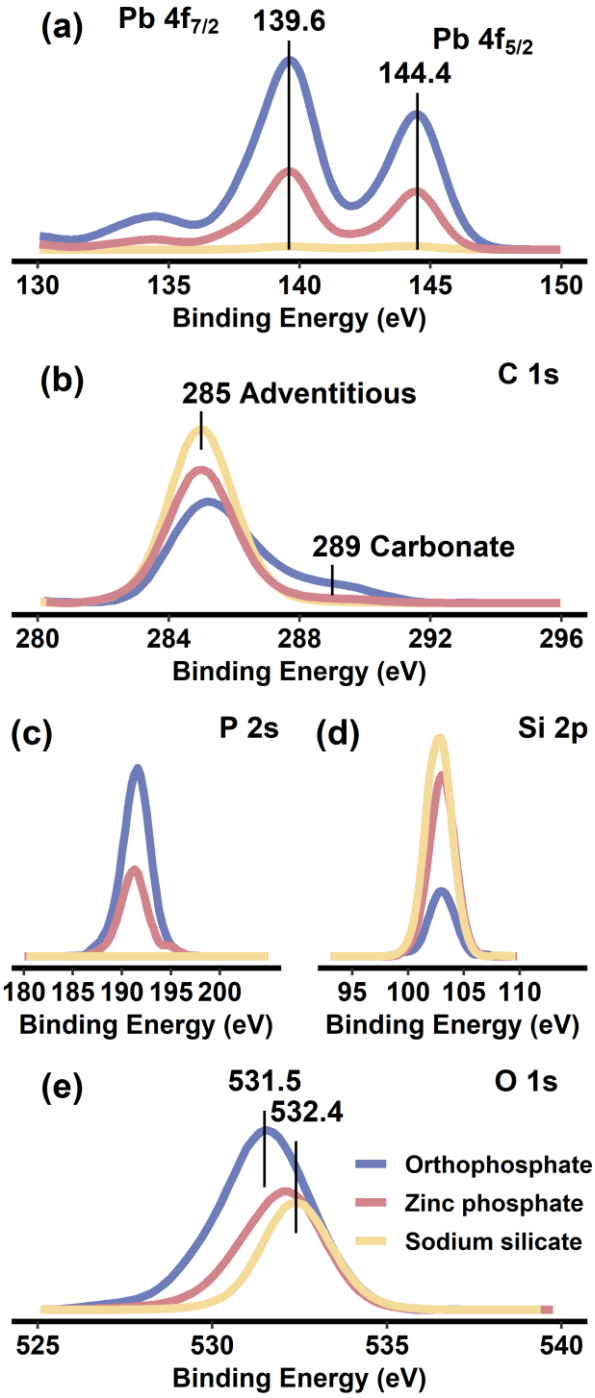

Figure 29 High-resolution XPS scans of the Pb 4f, C 1s, P 2s, Si 2p, and O 1s photolines.

4.5 Implications for corrosion control

This study eliminated the effect of pH that has confounded several previous studies on silicate corrosion control. And while silicate treatment might have reduced lead release relative to an inhibitor-free system, it fared poorly against even a moderate dose of orthophosphate, providing relatively little protection against either uniform or galvanic corrosion. Nevertheless, the benefit of sodium silicate as a pH control additive may be important: at low-to-moderate DIC, an increase in pH predicts a significant decrease in lead carbonate solubility[54] (Appendix C, Figure 57).

It is also possible that this study was not long enough to capture the benefits of silicate treatment. Here, the model system was operated for ~500 days at a low-to-moderate silicate dose (12 or 24 mg SiO_2/L) and ~90 days at a high dose (48 mg SiO_2/L). This time frame may not capture slow processes that eventually exert significant effects. But if the time to achieve the benefits of silicate addition is long relative to orthophosphate, silicate treatment is inherently less useful. And regardless of the potential long-term benefits, the short-term impacts identified here need to be carefully evaluated when silicate treatment is initiated.

Chief among them is the potential for sodium silicate to disperse metal-rich colloids. In this study, high levels of sodium silicate dispersed colloidal lead and iron, increasing the concentrations of these metals considerably. Dispersion may be especially important in LSLs supplied by iron distribution mains, and these LSLs are already at high risk for elevated lead release.[46,159] Moreover, point-of-use filters may be poorly suited to removing highly dispersed colloidal lead, although this might be less of an issue in systems with high hardness.[169]

4.6 Conclusions

Despite decades of use, significant knowledge gaps concerning sodium silicates remain, especially in the context of corrosion control. Sodium silicate was compared with orthophosphate at a constant pH, and our results suggest the following:

1. Relative to orthophosphate, sodium silicate did not control lead release due to either uniform (full LSL) or galvanic (partial LSL) corrosion. Hydrocerussite—a lead carbonate—dominated corrosion scale in the presence of sodium silicate, although a thin (~nm) silicon-rich coating did occur at the scale-water interface.
2. Sodium silicate dispersed colloidal iron and lead, highlighting a significant risk when silicate is used as a drinking water additive. Water systems with unlined iron or lead pipe should exercise particular care in dosing sodium silicate.
3. Corrosion inhibition due to direct lead-silicate interactions appears unlikely. But investigating the impact of silicate on recovered lead pipes with a complex, multi-layered corrosion scale may still be valuable. Future work should focus on silicate-based diffusion barriers that might form due to interaction with non-lead species (e.g., aluminosilicate, quartz, and other silicate minerals).

5 Chapter 5 Understanding the dispersing impact of sodium silicate on water quality and iron oxide particles

This chapter reproduced from Li, B., Trueman, B. F., Rahman, M. S., Gao, Y., Park, Y., & Gagnon, G. A. (2019). Understanding the impacts of sodium silicate on water quality and iron oxide particles. Environmental Science: Water Research & Technology, 5(8), 1360-1370. (20th reference) with permission from the Royal Society of Chemistry. https://doi.org/10.1039/C9EW00257J

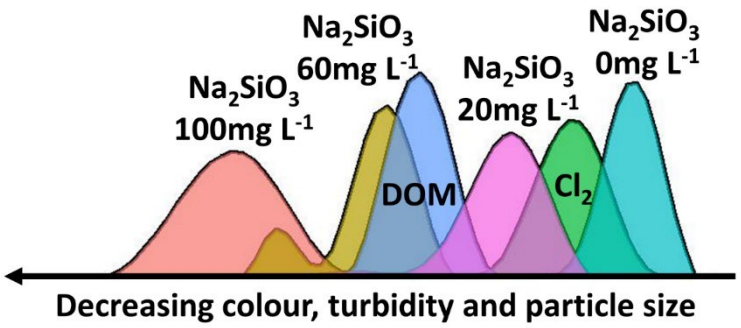

Figure 30 Artwork of effect of sodium silicate dosage on the colour, turbidity and iron particle size.

5.1 Abstract

Colloidal iron is strongly correlated with lead release in drinking water distribution system. Maintaining drinking water quality during distribution requires a range of tools to ensure chemical stability at the tap. Coloured water caused by iron release is a primary concern, and sodium silicates have been reported to reduce colour from iron. However, the impacts of water quality and the interactions between sodium silicate and iron oxides are not well characterized in this context. A better understanding about impact of sodium silicate on iron particles would also be helpful to avoid potential colloidal iron and lead release when sodium silicate is used as an sequestrant. Here, a bench-scale

factorial experiment (2^4) was used to evaluate the effect of sodium silicate on colour and turbidity with pH, humic acid, free chlorine, and sodium silicate as independent variables. Sodium silicate reduced colour and turbidity due to particulate iron by 113.3 Pt-Co and 4.0 NTU, respectively. Sodium silicate reduced the size of iron particles, as determined by dynamic light scattering and laser diffraction, and increased the apparent density, as assessed by electron microscopy. XRD and XPS data were consistent with increased amorphous and oxyhydroxide content in iron precipitates exposed to sodium silicate. Silicate also inhibited the adsorption of humic acid onto model iron oxides due to electrostatic repulsion: the zeta (ζ-) potentials of iron oxides in silicate-treated systems were substantially more negative.

5.2 Introduction

Previous chapters have indicated the dispersion of colloidal metals (e.g., iron and lead) in batch and pilot-scale experiments. Chapter 4 revealed the iron release considerably increased the lead release, along with the increased dosage of sodium silicate. Here, a better understanding of dispersion of iron oxide particles by sodium silicate would be helpful to prevent the potential colloidal iron and lead release when the silicate treatment is initiated.

“Red water” is a frequent consumer complaint received by water utilities.[170] Red water is caused by corrosion of iron pipes: soluble ferrous iron Fe (II) released due to corrosion is oxidized by dissolved oxygen and chlorine to ferric iron, forming insoluble iron oxides.[171,172] Phosphates (e.g., orthophosphate, hexametaphosphate, and their blends) are commonly used to sequester iron and control corrosion in drinking water systems,[36,58] but polyphosphate (e.g., hexametaphosphate) increases lead solubility.[36,58] This is a public health concern, as lead is strongly linked with cognitive deficits in children and cardiovascular disease mortality.[3,173] Phosphate is also a key nutrient for microorganisms and increases biomass regrowth at levels as low as 0.001 mg P/L[174] to 0.03 mg P/L.[175] Biomass regrowth is linked with taste and odor problems and increased risk of gastrointestinal illness.[176–178]

Sodium silicate is an alternative iron sequestrant[132,169,179] that does not increase lead solubility or biomass regrowth.[10,15,16,180] Early research supported its use for this purpose: Dart and Foley[179] suggested that silicate and ferric iron form a stable iron-silica complex, preventing aggregation of ferric iron; Browman et al. [39] proposed a mechanism involving formation of a colloidal or high molecular weight polymeric ferric iron phase; Robinson et al. [19] investigated five water facilities using sodium silicate and determined that the iron:silicate ratio is important for successful sequestration. The formation of particulate iron is also influenced by pH, chlorine, and dissolved organic matter (DOM): pH exerts a strong influence on the oxidation of ferrous iron,[181] chlorine reacts rapidly with ferrous iron in distribution systems,[182,183] and DOM from natural waters is correlated with both the oxidation rate of ferrous iron and the formation of colloidal Fe-DOM particles.[184,185] These factors affect the aesthetics of drinking water by altering the structural properties of iron oxide particles. However, the interactions between sodium silicate and iron oxides—and the influences of water quality—are not well characterized in this context.

The objectives of this study were (1) to evaluate the effect of sodium silicate—along with pH, free chlorine, and DOM— on aesthetic water quality in terms of colour (apparent colour) and turbidity, (2) to characterize the structural properties of iron oxides formed in a silicate-treated system, and (3) to investigate the effect of sodium silicate on the interaction between iron oxides and DOM. The findings will inform silicate use in water treatment applications and improve our understanding of iron oxide-DOM interactions.

5.3 Materials and methods

5.3.1 Bench-scale assessment of water quality parameters impacting iron-oxides

Sodium silicate-iron interactions were evaluated using a full factorial (2^4) design. The four independent variables (factors) were set at the following levels: sodium silicate at 0 and 100 mg as Na_2SiO_3 /L, chlorine at 0 and 2.5 mg/L, pH at 6.5 and 8.5, and DOM at 0 and 1.5 mg as TOC/L. A standard jar test was used to ensure mixing of chemical additives; tests were conducted in 1000 ml glass beaker mixed with magnetic stir bars.

A pH electrode, thermometer, and dissolved oxygen electrode were placed in the solution during the experiment. 1L of ultrapure water was added to each jar, and water quality was adjusted. $NaHCO_3$ was added to set dissolved inorganic carbon (DIC) at 5 mg C/L.[171,182] In the absence and the presence of chlorine, DOM and sodium silicate, the solution pH was adjusted to the target pH (6.5 or 8.5) using HCl (0.1 N/1N) and NaOH (0.1N) before adding ferrous iron. Water temperature was 21±1°C. Dissolved oxygen remained at approximately 8.5 mg/L during each test. $FeSO_4 \cdot 7H_2O$ was added to the solution to achieve a target concentration of 6 mg Fe(II)/L.[182] Samples were collected from each jar after 3.5 hours of reaction for analysis. The final pH was 6.12 ± 0.27 (mean ± SD, initial pH 6.5) and 7.44 ± 0.09 (initial pH 8.5), respectively (Appendix D, Figure 58).

Sodium silicate (Na_2SiO_3), goethite (α-FeOOH), magnetite (Fe_3O_4), and humic acid—as a model for DOM—were obtained from Sigma Corp., USA. Ferrous sulfate heptahydrate ($FeSO_4 \cdot 7H_2O$), sodium hydroxide (NaOH), hydrochloric acid (HCl), sodium hypochlorite (NaOCl), sodium chloride (NaCl) were obtained from Fisher Scientific, USA. Solutions and test waters were prepared using ultrapure water.

5.3.2 Iron oxide-DOM experiment

Iron oxide-DOM interactions were evaluated with sodium silicate in 250 ml conical flasks placed on a shaker table. The concentrations of goethite and magnetite were set at 0.3 g/L; these compounds were chosen to represent the major iron oxides in iron pipe corrosion scale.[186,187] A 150 mL DOM solution (3 mg TOC/L) was adjusted to 0.01 M ionic strength by NaCl and to pH 6.5 using HCl and NaOH. Sodium silicate was dosed in the range 0-90 mg/L. The mixed suspension was sonicated for 5 minutes to disperse the iron oxides and then shaken at 175 rpm at 21±1°C for 5 days to reach equilibrium.[186] Suspensions were then centrifuged for 15 min at 3000 rpm, and the supernatants were filtered using 0.45 μm cellulose nitrate membranes.

5.3.3 On-site analytical methods

Water temperature and pH were measured using an Accument XL50 meter (Fisher Scientific, USA). Dissolved oxygen was measured with a dissolved oxygen meter

(Thermo Orion, UK). Colour in this study was measured as apparent colour using the platinum-cobalt standard method and a DR 5000 UV-visible spectrophotometer (Hach, Loveland, Colorado). Turbidity was measured using a 2100AN turbidimeter (Hach, Loveland, Colorado).

5.3.4 Transmission electron microscope (TEM)

A transmission electron microscope (FEI Tecnai-12) with a MegaView II camera and AnalySIS software was used to capture images of iron particles. A 10 mL aliquot of aqueous suspension was vortexed for 1 min, and a droplet was evaporated on carbon film. After 24 hours the sample was placed in a holder and loaded into the instrument under vacuum for imaging.

5.3.5 Scanning Electron Microscopy - Energy Dispersive X-Ray Spectroscopy (SEM-EDS)

A Hitachi S-4700 scanning electron microscope was used for imaging and elemental analysis. A 250 mL aliquot of aqueous suspension was filtered through pre-conditioned 0.45 μm cellulose nitrate membranes; each membrane was then dried and coated in gold film (20 nm thickness). Samples were placed in a holder and loaded into the instrument for imaging.

5.3.6 X-ray powder diffraction (XRD)

A 50 mL aliquot of aqueous suspension was centrifuged for 5 min, and the pellet was dried in air for analysis. A Rigaku Ultima IV X-ray Diffractometer (XRD) with a copper Kα source coupled with a monochromator was used to identify crystalline phases. The X-ray tube was operated at 45 kV and 40 mA; samples were scanned from 10° to 80°/90° (2-theta) with a step size of 0.05° and a scan speed of 10 degree/min.

5.3.7 X-ray photoelectron spectroscopy (XPS)

A 50 mL aliquot of aqueous suspension was centrifuged for 5 min, and the pellet was evaporated on tin foil for analysis. A Thermo VG Scientific Multilab 2000 was used to examine the chemical states of elements. Measurements were performed using an

aluminum X-ray source (1486.6 eV) under high vacuum: 1 × 10-9 < P < 1 × 10-8 torr. The wide pressure range was due to degassing of the samples. Photoelectrons were analyzed using a CLAM4 Hemispherical Analyzer (r = 150mm) with a multichannel detector. High-resolution scans were made with a pass energy of 30 eV and an energy step of 0.1 eV.

5.3.8 Particle size distribution and Zeta potential

Particle size distributions were measured by dynamic light scattering (DLS) and laser diffraction using a Malvern Mastersizer 3000 and a Zetasizer-Nano-ZS (Malvern Instruments, Worcestershire, UK). Zeta potential was measured according to the electrophoretic light scattering method.[110,188]

5.3.9 SEC-HPLC

Size exclusion chromatography (SEC, Perkin-Elmer Series 200) with UV/Vis detection was used to determine the molecular weight (MW) distribution of DOM. Aqueous samples were filtered through pre-conditioned 0.45 µm cellulose nitrate membranes and collected headspace-free in pre-cleaned and baked 2 mL glass vials (100°C for 24 hours). Analysis was performed with a TSK G30000SW column (7.5 mm × 300 mm) and a TSKgel SW guard column (7.5 mm × 70 mm) connected to a Perkin Elmer Series 200 autosampler and Perkin UV/Vis detector. Sample absorbance was monitored at 254 nm with an injection volume of 100 µL, a flow rate of 0.7 mL/min, a 30-minute run time, and a mobile phase of 0.02M ammonium acetate.

5.3.10 Data analysis

Data were analyzed using R-studio (version 3.4.1).[189] The statistical analysis included graphical representation, Pearson's correlation coefficients, F-tests and an analysis of variance at the 95% confidence level. Effect sizes of experimental factors were calculated as described by Mac Berthouex and Brown.[190]

5.4 Results and discussion

5.4.1 Effect of sodium silicate on colour and turbidity

Addition of sodium silicate (100 mg Na_2SiO_3/L) reduced colour and turbidity by 113.3 Pt-Co (95% CI: -125.0 to -101.7) and 4.0 NTU (95% CI: -4.8 to -3.1), respectively (Figure 31; Appendix D, Figure 59; n = 4 replicates per treatment). These effects were dominant: they exceeded the effects of pH (-42.3 Pt-Co and 1.0 NTU), DOM (26.7 Pt-Co and -1.3 NTU), and free chlorine (-35 Pt-Co and -1.0 NTU). Sodium silicate moderated the effect of pH, as estimated by the interaction between the two factors (-23.0 Pt-Co and -1.65 NTU). That is, the increase in colour and turbidity at high pH was less pronounced in the presence of sodium silicate than would be expected based on the effect of each factor considered on its own. The interactions between silicate and free chlorine (54.9 Pt-Co and 3.7 NTU) were opposite in sign to the main effects, suggesting competitive interaction between these two factors. The same can be said of silicate and DOM with respect to turbidity but not colour: the decrease in turbidity due to silicate was diminished in the presence of DOM by 2.62 NTU (the interaction effect). The main effects of DOM and silicate on turbidity are probably due to adsorption of these species to the surface of iron oxide particles, limiting aggregation due to electrostatic and steric effects.[191,192] The interaction term might be explained by competitive adsorption: the effects are not additive because adsorption sites were limited. The main effect of silicate on colour (-113.3 Pt-Co) is probably also due to a reduction of iron particle size by silicate, while DOM represents a source of colour (30 Pt-Co on its own). Again, due to competitive adsorption, a higher concentration of DOM in the water phase was expected, but not confirmed, in the presence of silicate; this may explain the positive interaction (37.3 Pt-Co) between the two factors. Previous studies[135,136] have indicated that sodium silicate decreases the oxidation of ferrous iron, which would also result in less colour and turbidity, at least initially. Residual ferrous iron was observed at pH 6.5, but not at 8.5 (Appendix D, Figure 58). Given that the effects of sodium silicate on colour and turbidity were comparable when computed for the full dataset and at pH 8.5 alone, the physical nature of ferric iron precipitates appears to be the dominant mechanism.

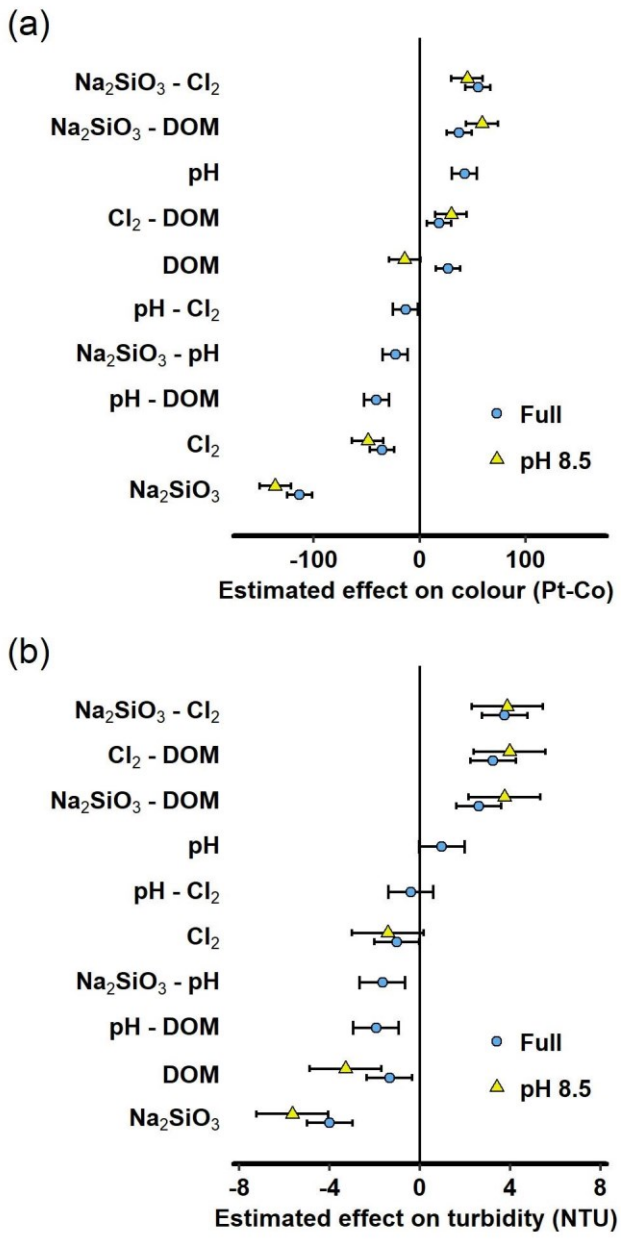

Figure 31 Estimated effects of sodium silicate, pH, free chlorine, and DOM on (a) colour and (b) turbidity in the full (2^4) design and at pH= 8.5 alone (i.e., no residual ferrous iron). Points indicate effect sizes and error bars span the 95% confidence intervals.

An extended study was conducted to evaluate the effect of sodium silicate dose (0-100 mg/L) on colour and turbidity in a $NaHCO_3$-buffered pure water system (Figure 32). Sodium silicate concentration was negatively correlated with colour (R^2 =0.988; $p<0.0001$; $\alpha=0.05$) and turbidity (R^2 = 0.826; $p <0.01$; $\alpha=0.05$), but at 20 mg/L, sodium

silicate increased turbidity. This result highlights a previous finding: the ratio between sodium silicate and iron concentration is critical for a successful sequestration.[19] Given the results of the factorial experiment, the primary explanatory mechanism for these trends appears to be particle characteristics. However, residual ferrous iron was slightly higher at 100 mg/L silicate compared with the control system (1.39 ± 0.1 mg/L vs. 1.7± 0.6 mg/L), and slowed ferrous iron oxidation due to silicate may also be important at pH 6.5.

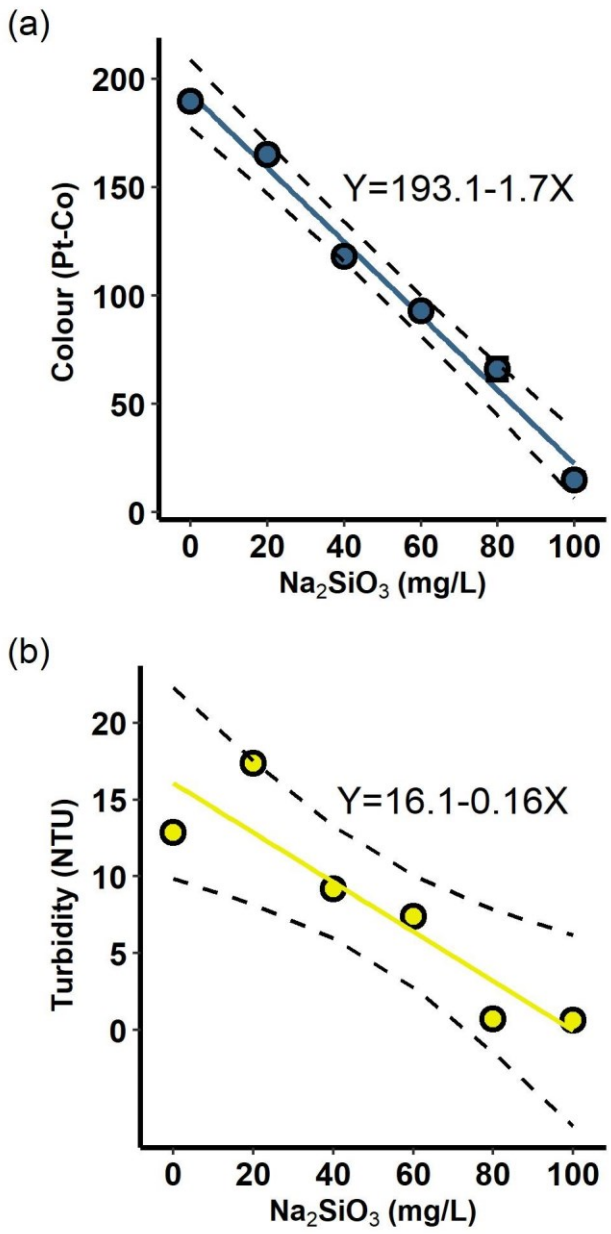

Figure 32 Effect of sodium silicate at doses of 0-100 mg/L on (a) colour and (b) turbidity in a $NaHCO_3$-buffered (5 mg C/L) pure water system at 21±1°C and pH 6.5. Dashed lines denote the 95% confidence interval on the fitted values.

5.4.2 Effect of sodium silicate on particle sizes, light-scattering and absorbance

Using dynamic light-scattering, the particle size distribution of colloidal iron was measured in the control system and in the presence of additives. Free chlorine (2.5 mg/L), DOM (1.5 mg TOC/L), and sodium silicate (0-100 mg/L) reduced median iron

particle size to 14.5 µm, 1.7 µm, and as low as 141 nm, respectively (Figure 33). Median particle size in the control system was estimated at 31.1 µm. The effect of DOM on particle size accords with previous work;[193] DOM enhances the stability (i.e., limits the aggregation) of iron oxide particles by increasing the negative surface charge.[192] The dose-dependent effect of sodium silicate in reducing particle size is also consistent with previous work: Rushing et al. [194] used membrane filtration to measure dissolved iron at 0-50 mg SiO_2/L, observing dispersed colloidal iron oxide particles in the presence of SiO_2.

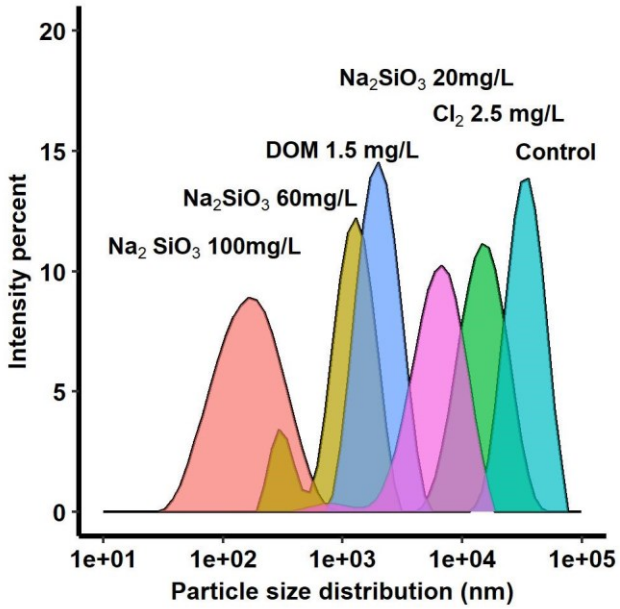

Figure 33 Particle size distribution of iron particles suspended in a $NaHCO_3$-buffered synthetic water system at pH 6.5 and 21±1°C.

In this study, the light scattering of particles across the measured size distribution can be explained by a combination of Mie and Rayleigh theory.[162] The turbidimeter used here measures the intensity of scattered light at 90° between λ= 400 nm and 900 nm.[195] The observed median particle size ranged from 31.1 µm to 141 nm. However, the wide particle size distribution and the limitations of DLS[196] and laser diffraction methods may lead to an underestimate of the percentage of small particles. Here, Rayleigh theory is applicable to the particle sizes observed at high sodium silicate doses (e.g., ~100 mg/L).[162] Under these conditions, light scattering would decrease with a decrease in

particle size, resulting in a decrease in turbidity. This explains the significant decrease in turbidity at relatively high silicate doses of 80-100 mg/L as shown in Figure 32. At medium and low doses (e.g., 20 mg/L), Mie theory is more applicable to explain variation in turbidity caused by sub-micrometer and micrometer particles: in this size range, smaller particles scatter more light, although the relationship is non-linear and non-monotonic.[162] Mie theory may explain the variation in turbidity at lower doses of sodium silicate: an increase was observed in turbidity and a decrease in particle size at 20 mg/L compared with the control (Figure 32). However, the relationship between sodium silicate and turbidity is probably complex, depending on particle number, morphology, fractal dimension, and polydispersity as well as size.[197,198] An increasing polydispersity was observed with increasing median particle size (Figure 33) and significant differences in morphology across treatments that complicate the application of scattering theory; in practice, the effect of sodium silicate on colour and turbidity due to iron should be evaluated on a case-by-case basis.

Apparent colour, determined by absorbance at 455 nm, decreased in the presence of sodium silicate (Figure 34) while ultraviolet absorbance increased. This may be due in part to morphology: for example, ferrihydrite, a possible oxidation product in the presence of sodium silicate, does not exhibit pronounced absorption lines in the visible range, while crystalline hematite does.[199] Scattering effects may be important, but the differences in particle size between the silicate and control systems complicate interpretation. Size-dependent changes in the optical band gap[200] and morphology-dependent changes (e.g., effective density[201]) in refractive index may also influence measured colour.

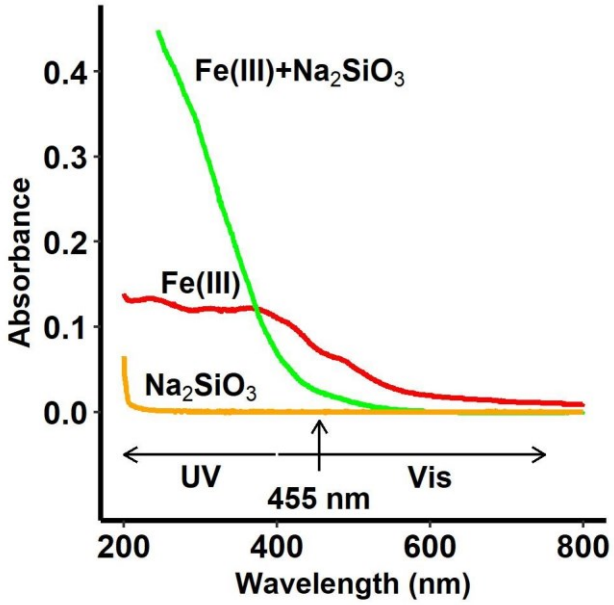

Figure 34 UV-Vis absorbance spectrum for Na_2SiO_3 (100 mg/L), an iron oxide suspension [6 mg Fe(III) /L], and an iron oxide suspension with added Na_2SiO_3 at pH 8.5 and 21±1°C.

5.4.3 Morphology changes and element analysis of iron oxide particles

Sodium silicate altered the morphology and elemental composition of iron oxide particles, as characterized by TEM, SEM-EDS, XRD, and XPS. Iron oxide particles formed in the control system appeared in TEM micrographs as dense masses with needlelike, poorly crystalline morphology (Figure 35). In the presence of sodium silicate, a clear change of shape to aggregates of spherical units was observed. This structure is consistent with observations from previous studies on SiO_2-coated iron nanoparticles.[202,203] In the presence of DOM and free chlorine (this study), a diffuse, distributed morphology was apparent. This finding is consistent with previous work examining the influence of DOM on the formation of particulate iron.[182,204] In a similar system, dense and opaque diffusely distributed nanoparticles were observed in the presence of DOM.[182] This may be due to complexation between carboxyl groups and metal oxide surfaces altering the surface charge, resulting in a highly stable colloid.[182,205] Addition of sodium silicate to the Fe-DOM-Cl_2 system yielded a

morphology similar to that of the Fe-Si system, with aggregates of spherical units apparent.

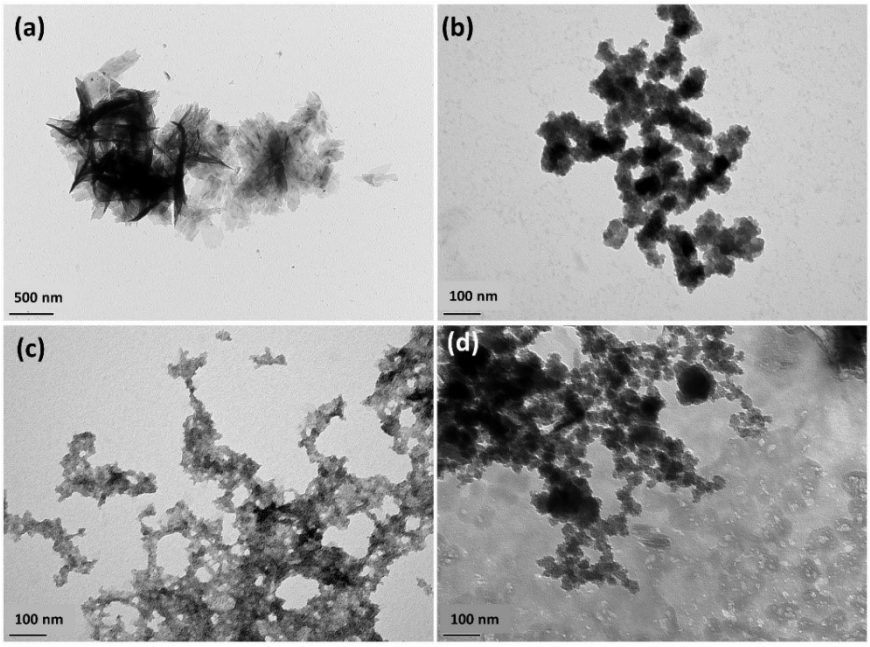

Figure 35 TEM micrographs of iron particles formed in a $NaHCO_3$-buffered pure water system at pH 6.5 and temperature 21±1°C: (a) the control system (Fe), (b) Na_2SiO_3 (60 mg/L) (Fe-Si), (c) DOM (3 mg TOC/L) and chlorine (2.5 mg/L) (Fe-DOM-Cl_2), (d) DOM, chlorine and Na_2SiO_3 (60 mg/L) (Fe-DOM-Cl_2-Si).

Consistent with TEM data, needlelike iron oxide particles were observed in the control and Fe-DOM-Cl_2 systems by SEM (Appendix D, Figure 60). In the presence of sodium silicate, small spherical particles with low apparent crystallinity were present in place of the needlelike particles; this is also consistent with TEM results. As expected, carbon, oxygen and iron were the most abundant elements as determined by SEM-EDS; these are typically the most abundant elements identified in cast iron pipe corrosion scales[29,186] (Table 3). In the presence of DOM and chlorine, the weight percentage of carbon (35.13%) was higher than that in the control system (18.75 %); this difference suggests the adsorption of DOM to iron oxide particles.[185,192] Aluminum (0.54 %) was also observed in these samples, likely originating from DOM as reported elsewhere.[206,207] Silicon was observed in the Fe-Si and Fe-DOM-Cl_2-Si systems at 5.06 % and 2.35 %, suggesting bond formation with iron oxides in these two systems.

Table 3 Elemental analysis (weight percentage %) by SEM-EDS

Element	Fe(II)	Fe(II)+Na_2SiO_3	Fe(II)+DOM+Cl_2	Fe(II)+DOM+Cl_2+Na2SiO_3
Si	ND	5.06	0.39	2.35
C	18.75	16.97	35.13	37.16
O	42.18	39.45	29.22	32.75
Fe	40.85	36.74	33.88	25.04
Al	ND	ND	0.54	0.6
Cl	ND	ND	0.87	1.26
Na	ND	ND	ND	0.86

The morphology changes in iron particles accorded with the results of XRD analysis (Appendix D, Figure 61): sodium silicate increased the X-ray amorphous content of iron oxides.[208] The control sample yielded an XRD trace with a low signal-to-noise ratio diffractogram—consistent with a large amorphous fraction—but the single identifiable peak did correspond to the principal peak in the lepidocrocite standard (γ-FeOOH). In the presence of sodium silicate, no peaks were identifiable; iron oxides were completely X-ray amorphous, although 2-line ferrihydrite is usually prepared by rapid oxidation of a Fe (II) solution[209–212] and was likely present here.

Similar trends have been reported elsewhere,[213] suggesting that silicate species inhibit the crystallization of iron oxides.[214,215] Specifically, silicate has been shown to inhibit lepidocrocite formation,[216] resulting in a higher amorphous ferrihydrite content and formation of silicate-ferrihydrite species.[135,136] Iron oxyhydroxide phases form due to dissolution of ferrihydrite followed by nucleation and crystal growth.[217,218] Sodium silicate inhibits the nucleation step, a precursor to lepidocrocite and goethite formation.[219] Zhao et al. [211] showed that silicate occupies the coordination unsaturated sites of iron ions on the surface of iron particles, blocking most of the crystal growth sites.

Sodium silicate appeared to alter the phase composition of iron oxide particles, as determined by high resolution XPS scans of the Fe $_{2p}^{3/2}$, O 1s and C 1s spectral regions (Figure 36). The binding energies of characteristic photoelectrons provide information on the chemical states of specific elements.[220] Previous studies have shown that iron oxide particles in aquatic samples are composed of lepidocrocite (Y-FeOOH), goethite (α-FeOOH), siderite ($FeCO_3$), magnetite (Fe_3O_4), hematite (Fe_2O_3) and

ferrihydrite.[170,182,194,214,217] Consistent with this work, our data suggest the occurrence of a mixture of iron oxides and oxyhydroxides. Fe $_{2p}^{3/2}$ peaks were observed at 711.4 eV-711.9 eV, and iron oxides generally yield Fe $_{2p}^{3/2}$ binding energies between 710.4 and 711.6 eV (Fe_2O_3: 710.40-711.60 eV; Fe_3O_4: 710.40- 711.40 eV).[221–225] Oxyhydroxides (FeOOH) yield energies between 711.0-711.9 eV.[225,226]

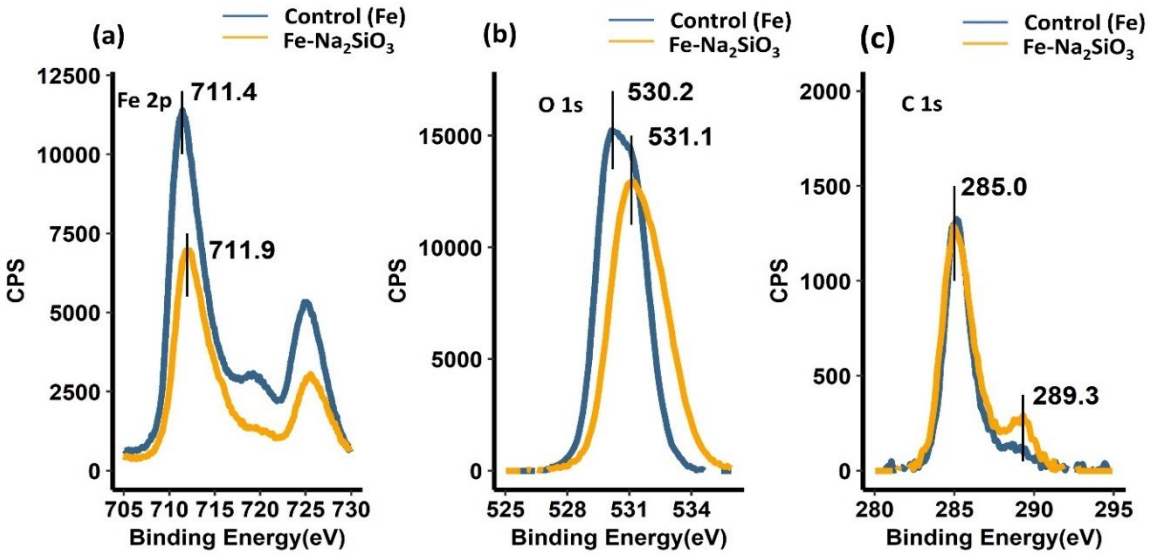

Figure 36 High resolution XPS scans of (a) Fe 2p, (b) O 1s, and (c) C1s in control (Fe) and Fe - Na_2SiO_3 (Na_2SiO_3 60 mg/L) systems.

In the presence of sodium silicate, the Fe $_{2p}^{3/2}$ peak increased from 711.4 to 711.9 eV, which may be explained by an increasing representation of hydroxyl groups in the samples. This interpretation is supported by a shift in the O 1s peak, from 530.2 eV with a prominent, higher energy shoulder in the control system to 531.1 eV in the present of sodium silicate. This finding is consistent with an increasing fraction of Fe-O-H bonds (531.1 eV) and a decreasing fraction of Fe-O bonds (530.0 eV).[227,228] Hence, sodium silicate may prevent the transformation of iron oxides from the internal dehydration and rearrangement of either ferrihydrite[214,222] or iron oxyhydroxide (e.g., lepidocrocite and goethite).[212,214]

In addition to iron (oxyhydr)oxides, siderite ($FeCO_3$)[187] may have occurred in our study as a minor phase, as indicated by a secondary C1s peak at 289.3 eV (289.4 eV in

Heuer and Stubbins' study).[229] The primary C_{1s} peak (adventitious carbon at 285.0 eV) was ascribed to carbon contamination during air exposure, as described elsewhere.[98]

5.4.4 Interactions among sodium silicate, DOM and iron oxides

The affinity of DOM for iron oxide and other mineral surfaces[185,193,230,231] has important implications for contaminant mobility in drinking water systems. Understanding the effect of sodium silicate on the interaction between iron oxides and DOM is important because DOM-coated iron oxide particles have been linked with transport of both organic and inorganic contaminants.[46,232–234] In this study, goethite (α-FeOOH) and magnetite (Fe_3O_4) were used to represent the corrosion scales of iron pipes that are released to water as iron oxide particles; goethite and magnetite are typically identified as major compounds in iron corrosion scale.[29,170]

Size exclusion chromatography (SEC) has been applied previously to characterize the molecular weight distribution (MW) of DOM.[235,236] Here, SEC was used to generate MW distributions for the residual DOM after reaction with goethite or magnetite (Appendix D, Figure 62). Increasing sodium silicate concentration within the range 0 - 90 mg/L reduced partitioning of DOM to the iron oxide surface, as indicated by the change in UV absorbance in the water phase (Figure 37). This approach does not capture DOM that absorbs poorly in the UV range, but previous studies[186,237] have indicated that aromatic and hydrophobic DOM is preferentially absorbed by iron oxides. Our analysis captures changes in highly adsorbable aromatic DOM due to silicate.

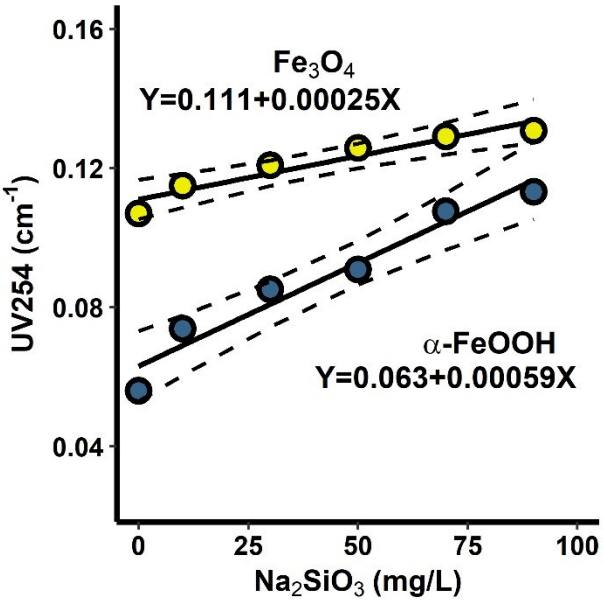

Figure 37 UV response of residual dissolved organic matter (DOM) in presence of 0.3 g/L of goethite or magnetite at pH 6.5 temperature 21±1°C. Dashed lines represent 95% confidence intervals on the fitted values.

The UV absorbance of residual DOM exhibited a linear dependence on sodium silicate dose. The MW distribution of DOM is an important factor in DOM adsorption to soil minerals[238,239] and Rahman and Gagnon[186] found that higher MW factions adsorbed preferentially to goethite and magnetite. Here, the weight-average MW (Appendix D, Figure 63) did not change significantly with sodium silicate dose in the range 0-90 mg/L. Weight-average MWs were 9416 – 10737 Da in the presence of goethite ($p = 0.95$; *F*-test on the compound-specific linear regression of weight-average MW on silicate dose) and 8918 – 9686 Da in the presence of magnetite ($p = 0.49$). That is, inhibition of solid phase partitioning by sodium silicate was independent of MW of DOM.

5.4.5 Zeta (ζ-) potential

Sodium silicate decreased the ζ- potential of model iron minerals ((Appendix D, Figure 64). In the goethite and magnetite control systems, solution pH values at the point of zero charge (pH_{pzc}) were approximately 8.5 and 7.2, respectively. These are similar to previously reported values.[240,241] In the presence of sodium silicate (20 mg/L), the pHpzc shifted to lower pH: 7.8 and 6.5 in the goethite and magnetite systems,

respectively. This trend is consistent with studies on the surface charge of magnetite in a solution of sodium silicate (1 mM)[242] and on the ζ- potential of goethite exposed to 0.1mM - 1.0 mM silicic acid.[243] This also explains the inhibiting effect of silicate on the adsorption of DOM to magnetite and goethite. Moreover, Alexandrino et al.[244] indicated that the sodium silicate increases the degree of dispersion and ζ- potential of hematite. Kinsela et al. [135] also observed the greater negative surface charge on lepidocrocite and silicate-ferrihydrite by adding sodium silicate. The higher negative surface charge imparted by sodium silicate explains our observation of colloidal particulate iron oxides at the highest silicate concentration (100 mg/L, Figure 33).

5.5 Conclusions

Compared with polyphosphates, sodium silicate has received little attention as a potential iron sequestrant. However, sodium silicates offer potential benefits in that they avoid the risks of polyphosphates: increased lead solubility and biofilm regrowth. Here, sodium silicate effectively reduced the colour and turbidity of iron oxide suspensions. Previous studies have indicated that sodium silicate inhibits the oxidation of ferrous iron, particular at relatively low pH: outer-sphere complexation of ferrous iron to silicate-ferrihydrite may retard the electron transfer rate compared with inner-sphere complexation to lepidocrocite. This may reduce color and turbidity in the short term. In the longer term, assuming complete oxidation of ferrous iron, the morphology, structure, and size of iron (oxyhydr)oxides and related compounds (e.g., silicate-ferrihydrite) has a greater influence on sequestration. TEM, SEM-EDS and XRD showed that iron oxides exhibited a poorly crystalline morphology and that sodium silicate altered this morphology by promoting formation of aggregates with spherical units. Sodium silicate also appeared to inhibit crystallization of iron (oxyhydr)oxides, resulting in X-ray amorphous precipitates with a higher hydroxyl group content. At the maximum sodium silicate dose, colloidal iron approached the nanoparticulate size range (1 - 100 nm); this was explained by the more negative surface charge of iron oxide in the presence of sodium silicate. The change in surface charge also explains the inhibition of DOM adsorption to magnetite and goethite, with potential implications for contaminant transport (e.g., microorganisms and heavy metals) in water distribution systems.

This is a preliminary study to investigate the effect of sodium silicate on sequestration and water quality. Besides those investigated here, other factors may also affect the application of sodium silicate. For example, according to the Schulze-Hardy rule, cations from water hardness may have an adverse effect on sequestration, inhibiting colloidal dispersion and increasing the sodium silicate requirement. DIC concentration may also affect the oxidation of ferrous iron. In engineering applications, bench-scale and field tests would be required to ensure successful sequestration without adverse consequences, such as precipitation and clogging or heavy metal mobilization. Further study is needed to the fully understand these factors and potential drawbacks.

In drinking distribution systems, the elevated colloidal iron release from sequestration by sodium silicate would elevate the lead release. The potential drawbacks of sodium silicate sequestration on other colloidal metals (e.g., lead) needs to be carefully evaluated when the silicate treatment is initiated.

6 Chapter 6 Conclusions and recommendations

6.1 Conclusions

This work investigated the effectiveness and impacts of sodium silicate on lead control and colloid size distributions.

A brief summary of key findings as follows:

a) Given that silicate-based inhibitors had a minimal impact on lead release control in drinking water—especially compared with the widely used orthophosphate-based inhibitors—elevated pH level appears to be the primary mechanism by which sodium silicate controls lead release. This was demonstrated in Chapters 2, 3 and 4. This work highlights the constraints on the conditions under which sodium silicate might be effective. Silicate-based inhibitors do not work in any way that is analogous to orthophosphate. If it works at all, it probably requires the rich aluminum or other metals of corroded lead pipes as described by Mishrra et al. [129]. But, this study revealed that having aluminum in the water is not sufficient, because the pilot-scale distribution system (Chapter 4) using real treated surface water (i.e., contains aluminum) did not show this mechanism.

b) Direct interaction between sodium silicate and lead appears unlikely. No passive corrosion scales (e.g., $PbSiO_3$) were observed in silicate-treated corrosion cells (Chapter 2), CSTRs (Chapter 3), and the pilot-scale distribution model (Chapter 4). Lead carbonates (e.g., cerussite or hydrocerussite) were the major corrosion scales of lead coupons and lead pipes treated in silicate-treated systems, which controls the chemical equilibrium of lead in water.

c) Silicate was adsorbed to the lead coupons in corrosion cells (Chapter 2) and lead carbonate solids in CSTRs (Chapter 3). This might work for the lead release mitigation at high pH (pH 9) and high DIC (50 mg C/L), but this finding was not confirmed by the corrosion cell experiment. A nanometer-thick coating was observed in the pilot-scale distribution system (Chapter 4), but the coating did not

maintain the lead concentration at an acceptable level and protect against galvanic corrosion.

d) Disperse property of sodium silicate resulted in the elevated colloidal lead and iron concentration at specific water quality conditions (e.g., overdose or certain pH and DIC level). As a sequestrant, sodium silicate contributed more negative surface charge (i.e., zeta potential). In the pilot-scale model (Chapter 4), colloidal metals (e.g., iron and lead) were dispersed at the high silicate level, which in turn considerably increased the total lead. This was consistent with the observation of the high total lead release in corrosion cells (Chapter 3) and the more nanoparticulate iron in the sequestration tests (Chapter 5). This finding represents a novel contribution that has not been demonstrated in the peer-reviewed literature to date.

6.2 Recommendations

First of all, despite decades of use, significant knowledge gaps concerning the role of sodium silicate remain in corrosion control of drinking water distribution systems. Previous studies often confounded with the increase in pH that accompanies with sodium silicate's use. This study, however, clearly indicates the benefits of sodium silicate alone are relatively negligible, except for the elevated pH with its use. Until proven otherwise, silicate-based corrosion inhibitors should be viewed as pH adjustment chemicals, like sodium hydroxide. This means water utilities need to carefully monitor and adjust the pH in raw water and treated water. For example, if raw water pH became lower (i.e., more corrosive), the protection from sodium silicate would disappear in a lead-water-carbonate system.

Secondly, the pH adjustment by sodium silicate may not be better than other pH adjustment methods due to its disperse property. In this study, the disperse property of sodium silicate for colloidal metals (e.g., iron and lead) has been observed. This indicates that the disperse property of sodium silicate could result in an extra colloidal lead and total lead release at the same pH level. A similar observation was reported in a pilot-study conducted by Aghasadeghi et al. [245]. Concerns raised about the disperse

property of orthophosphate[128] and polyphosphate in previous studies. Therefore, how to make a balance between chemical reagent dosage and the elevated disperse property (i.e., more negative zeta potentials) is a critical issue in corrosion control practices.

Thirdly, the long-term impact of sodium silicate is still worth investigating, but the low efficiency of sodium silicate would limit its use. Natural silicate minerals (e.g., aluminosilicate, quartz, etc…) are frequently observed in lead corrosion scales,[28,29] and a recent study using recovered lead pipe attributed declines in lead release with silicate addition to an aluminum-rich diffusion barrier.[129] These benefits seem to require a long-term silicate treatment to reach, especially compared with orthophosphate. For example, no evidence of silicate-related minerals (e.g.,aluminosilicate) and significant aluminum concentration (median in every pipe: 50 -166 μg/L) in the treated water of the pilot-scale model (Chapter 4) after ~600 days' operation while the passive lead-phosphate solids (i.e., hydroxylpyromorphite) formed in CSTRs (Chapter 3) within 40 hours. If the time to achieve the benefits of sodium silicate is long, however, the treatment is inherently less useful.

Fourth, in CSTRs, a decrease in lead release of lead carbonate at high pH and high DIC, but this finding was not confirmed by the corrosion cell experiment. It is possible that, at high pH and high DIC, the silicate adsorption may inhibit lead release (e.g., dissolution rate) in a dissolution rate (not equilibrium) control system. This will be a subject for future study.

Fifth, official drinking water guidelines published by national departments and agencies (i.e., Health Canada and USEPA)[9,26] regard sodium silicate as a legitimate lead control treatment. Unclarified mechanisms, however, in these documents may result in improper use. It is true that these documents pointed out the limited data, applications, and studies are available. But, the description in these documents about the unapproved passive film or diffusion barriers may result in a misunderstanding about the function of sodium silicate. This study indicates the sodium silicate may only play the role as a pH adjustment reagent. The research and regulatory community need to think about whether the word "inhibitor" is properly used to describe silicate-related reagent in lead control.

Sixth, the uncertainty of using sodium silicate needs to be carefully evaluated. This study did not investigate the hypothesis of diffusion barrier formation in recovered lead pipes which are rich in non-lead species (e.g., aluminum) as described elsewhere.[129] Even if this hypothesis is true, the various properties of corrosion scales in different distribution systems would result in uncertainties of efficiency and effectiveness. For example, two recent studies using recovered lead pipes showed the discrepancy in silicate treatment. Aghasadeghi et al. [245] found silicate treatment made lead control worse while Mishrra et al. [129] indicated silicate treatment was somewhat effective.

Finally, many current peer-reviewed papers cited the studies of iron corrosion control using sodium silicate. This may be due in part to the limited studies of lead corrosion control using sodium silicate. However, differences in chemical properties between iron and lead systems are considerable. Future work should include a comprehensive literature review of silicate's use in drinking water treatment and distribution. Such a review must carefully distinguish among the different metals in the distribution systems, and clearly differentiate the effect of pH and the protective film formation.

Literature and this study are unanimous that silicates are not as good as orthophosphate for lead release control. We still need to look for an alternative inhibitor in the future lead corrosion control.

Reference

(1) Watt, G.; Britton, A.; Gilmour, H.; Moore, M.; Murray, G.; Robertson, S. Public Health Implications of New Guidelines for Lead in Drinking Water: A Case Study in an Area with Historically High Water Lead Levels. *Food and Chemical Toxicology* **2000**, *38*, S73–S79.

(2) Watt, G. C.; Britton, A.; Gilmour, W. H.; Moore, M. R.; Murray, G. D.; Robertson, S. J.; Womersley, J. Is Lead in Tap Water Still a Public Health Problem? An Observational Study in Glasgow. *BMJ* **1996**, *313* (7063), 979–981.

(3) Lanphear, B. P.; Rauch, S.; Auinger, P.; Allen, R. W.; Hornung, R. W. Low-Level Lead Exposure and Mortality in Us Adults: A Population-Based Cohort Study. *The Lancet Public Health* **2018**, *3* (4), e177–e184.

(4) Navas-Acien, A.; Guallar, E.; Silbergeld, E. K.; Rothenberg, S. J. Lead Exposure and Cardiovascular Disease a Systematic Review. *Environmental Health Rerspectives* **2006**, *115* (3), 472–482.

(5) Loghman-Adham, M. Renal Effects of Environmental and Occupational Lead Exposure. *Environmental Health Perspectives* **1997**, *105* (9), 928–939.

(6) Canfield, R. L.; Henderson Jr, C. R.; Cory-Slechta, D. A.; Cox, C.; Jusko, T. A.; Lanphear, B. P. Intellectual Impairment in Children with Blood Lead Concentrations Below 10 μG Per Deciliter. *New England Journal of Medicine* **2003**, *348* (16), 1517–1526.

(7) Miranda, M. L.; Kim, D.; Galeano, M. A. O.; Paul, C. J.; Hull, A. P.; Morgan, S. P. The Relationship Between Early Childhood Blood Lead Levels and Performance on End-of-Grade Tests. *Environmental Health Perspectives* **2007**, *115* (8), 1242–1247.

(8) USEPA. Electronic Code of Federal Regulation. **2019**.

(9) Health Canada. *Guidance on Contorlling Corrosion in Drinking Water Distribution Systems*; Health Canada: Ottawa, Canada, 2019.

(10) Schock, M. R.; Lytle, D. A.; Sandvig, A. M.; Clement, J.; Harmon, S. M. Replacing Polyphosphate with Silicate to Solve Lead, Copper, and Source Water Iron Problems. *Journal-American Water Works Association* **2005**, *97* (11), 84–93.

(11) Noel, J. D.; Wang, Y.; Giammar, D. E. Effect of Water Chemistry on the Dissolution Rate of the Lead Corrosion Product Hydrocerussite. *Water Research* **2014**, *54*, 237–246.

(12) Koppelaar, R.; Weikard, H. Assessing Phosphate Rock Depletion and Phosphorus Recycling Options. *Global Environmental Change* **2013**, *23* (6), 1454–1466.

(13) Daneshgar, S.; Callegari, A.; Capodaglio, A. G.; Vaccari, D. The Potential Phosphorus Crisis: Resource Conservation and Possible Escape Technologies: A Review. *Resources* **2018**, *7* (2), 37.

(14) McGill, S. M. 'Peak'phosphorus? The Implications of Phosphate Scarcity for Sustainable Investors. *Journal of Sustainable Finance & Investment* **2012**, *2* (3-4), 222–239.

(15) Lintereur, P. A.; Duranceau, S. J.; Taylor, J. S.; Stone, E. D. Sodium Silicate Impacts on Lead Release in a Blended Potable Water Distribution System. *Desalination and Water Treatment* **2010**, *16* (1-3), 427–438.

(16) Kogo, A.; Payne, S. J.; Andrews, R. C. Comparison of Three Corrosion Inhibitors in Simulated Partial Lead Service Line Replacements. *Journal of Hazardous Materials* **2017**, *329*, 211–221.

(17) Woszczynski, M.; Bergese, J.; Payne, S. J.; Gagnon, G. A. Comparison of Sodium Silicate and Phosphate for Controlling Lead Release from Copper Pipe Rigs. *Canadian Journal of Civil Engineering* **2015**, *42* (11), 953–959.

(18) Pinto, J. A.; McAnally, A. S.; Flora, J. R. Evaluation of Lead and Copper Corrosion Control Techniques. *Journal of Environmental Science & Health Part A* **1997**, *32* (1), 31–53.

(19) Robinson, R. B.; Reed, G. D.; Frazier, B. Iron and Manganese Sequestration Facilities Using Sodium Silicate. *Journal-American Water Works Association* **1992**, *84* (2), 77–82.

(20) Li, B.; Trueman, B. F.; Rahman, M. S.; Gao, Y.; Park, Y.; Gagnon, G. Understanding the Impacts of Sodium Silicate on Water Quality and Iron Oxide Particles. *Environmental Science: Water Research & Technology* **2019**, 5(8), 1360-1370.

(21) Viglione, G. Water Treatment Failures Drove Newark's Lead Crisis. *Chemical & Engineering News* **2019**, *97* (35), 6–6.

(22) Corasaniti, N.; Kilgannon, C.; Schwartz, J. *Tainted Water, Ignored Warnings and a Boss with a Criminal Past*; The New York Times, 2019.

(23) Scheetz, B.; Thompson, J.; Delaney, P. J. XPS Characterization of Films Formed on Distribution Systems Using Additives to Control Pb/Cu Levels in Drinking Water. In *AWWA Water Quality Technology Conference*; American Water Works Association: Denver, CO, 1997.

(24) Thompson, J.; Scheetz, B.; Schock, M.; Lytle, D.; Delaney, P. Sodium Silicate Corrosion Inhibitors: Issues of Effectiveness and Mechanism. In *AWWA Water Quality Technology Conference*; American Water Works Association: Denver, CO, 1997.

(25) Hosseinibalajadeh, S. Lead Corrosion Inhibitors in Drinking Water. Master's thesis, University of Wisconsin-Milwaukee, 2018.

(26) USEPA. *Optimal Corrosion Control Treatment Evaluation Technical Recommendations for Primacy Agencies and Public Water Systems*; US Environmental Protection Agency; US Environmental Protection Agency, 2016.

(27) Tang, Z.; Hong, S.; Xiao, W.; Taylor, J. Impacts of Blending Ground, Surface, and Saline Waters on Lead Release in Drinking Water Distribution Systems. *Water Research* **2006**, *40* (5), 943–950.

(28) Kim, E. J.; Herrera, J. E. Characteristics of Lead Corrosion Scales Formed During Drinking Water Distribution and Their Potential Influence on the Release of Lead and Other Contaminants. *Environmental Science & Technology* **2010**, *44* (16), 6054–6061.

(29) Peng, C.-Y.; Korshin, G. V.; Valentine, R. L.; Hill, A. S.; Friedman, M. J.; Reiber, S. H. Characterization of Elemental and Structural Composition of Corrosion Scales and Deposits Formed in Drinking Water Distribution Systems. *Water Research* **2010**, *44* (15), 4570–4580.

(30) Svensson, U.; Dreybrodt, W. Dissolution Kinetics of Natural Calcite Minerals in CO_2-Water Systems Approaching Calcite Equilibrium. *Chemical Geology* **1992**, *100* (1-2), 129–145.

(31) McNeill, L. S.; Edwards, M. Phosphate Inhibitor Use at US Utilities. *Journal-American Water Works Association* **2002**, *94* (7), 57–63. https://doi.org/10.1002/j.1551-8833.2002.tb09506.x.

(32) Deshommes, E.; Trueman, B.; Douglas, I.; Huggins, D.; Laroche, L.; Swertfeger, J.; Spielmacher, A.; Gagnon, G. A.; Prévost, M. Lead Levels at the Tap and Consumer Exposure from Legacy and Recent Lead Service Line Replacements in Six Utilities. *Environmental Science & Technology* **2018**, *52* (16), 9451–9459.

(33) Zahran, S.; Mushinski, D.; McElmurry, S. P.; Keyes, C. Water Lead Exposure Risk in Flint, Michigan After Switchback in Water Source: Implications for Lead Service Line Replacement Policy. *Environmental Research* **2020**, *181*, 108928.

(34) Ng, D.-Q.; Chen, C.-Y.; Lin, Y.-P. A New Scenario of Lead Contamination in Potable Water Distribution Systems: Galvanic Corrosion Between Lead and Stainless Steel. *Science of The Total Environment* **2018**, *637*, 1423–1431.

(35) Schock, M. R. Understanding Corrosion Control Strategies for Lead. *Journal-American Water Works Association* **1989**, *81* (7), 88–100.

(36) Holm, T. R.; Shock, M. R. Potential Effects of Polyphosphate Products on Lead Solubility in Plumbing Systems. *Journal-American Water Works Association* **1991**, *83* (7), 76–82.

(37) Trueman, B. F.; Krkošek, W. H.; Gagnon, G. A. Effects of Ortho- and Polyphosphates on Lead Speciation in Drinking Water. *Environmental Science: Water Research & Technology* **2018**, *4* (4), 505–512. https://doi.org/10.1039/C7EW00521K.

(38) Trueman, B. F.; Locsin, J. A.; Krkošek, W. H.; Gagnon, G. A. Effects of Ortho- and Polyphosphates on Lead Speciation in Drinking Water. In *AWWA Water Quality Technology Conference*; American Water Works Association: Toronto, Canada, 2018.

(39) Browman, M. G.; Robinson, R. B.; Reed, G. D. Silica Polymerization and Other Factors in Iron Control by Sodium Silicate and Sodium Hypochlorite Additions. *Environmental Science & Technology* **1989**, *23* (5), 566–572.

(40) Trueman, B. F.; Camara, E.; Gagnon, G. A. Evaluating the Effects of Full and Partial Lead Service Line Replacement on Lead Levels in Drinking Water. *Environmental Science & Technology* **2016**, *50* (14), 7389–7396.

(41) Deshommes, E.; Laroche, L.; Deveau, D.; Nour, S.; Prévost, M. Short-and Long-Term Lead Release After Partial Lead Service Line Replacements in a Metropolitan Water Distribution System. *Environmental Science & Technology* **2017**, *51* (17), 9507–9515.

(42) Wang, Y.; Jing, H.; Mehta, V.; Welter, G. J.; Giammar, D. E. Impact of Galvanic Corrosion on Lead Release from Aged Lead Service Lines. *Water Research* **2012**, *46* (16), 5049–5060.

(43) St. Clair, J.; Cartier, C.; Triantafyllidou, S.; Clark, B.; Edwards, M. Long-Term Behavior of Simulated Partial Lead Service Line Replacements. *Environmental Engineering Science* **2016**, *33* (1), 53–64.

(44) Ma, X.; Armas, S. M.; Soliman, M.; Lytle, D. A.; Chumbimuni-Torres, K.; Tetard, L.; Lee, W. H. In Situ Monitoring of Pb^{2+} Leaching from the Galvanic Joint Surface in a Prepared Chlorinated Drinking Water. *Environmental Science & Technology* **2018**, *52* (4), 2126–2133.

(45) Ma, X.; Lytle, D. A.; Lee, W. H. Microelectrode Investigation on the Corrosion Initiation at Lead–Brass Galvanic Interfaces in Chlorinated Drinking Water. *Langmuir* **2019**, *35* (40), 12947–12954.

(46) Trueman, B. F.; Gagnon, G. A. Understanding the Role of Particulate Iron in Lead Release to Drinking Water. *Environmental Science & Technology* **2016**, *50* (17), 9053–9060.

(47) Cornwell, D. A.; Wagner, J. R. Coupon Procedures for Evaluating Lead and Copper Solubility. *Journal-American Water Works Association* **2019**, *111* (10), 12–24.

(48) Trueman, B. F.; Sweet, G. A.; Harding, M. D.; Estabrook, H.; Bishop, D. P.; Gagnon, G. A. Galvanic Corrosion of Lead by Iron (Oxyhydr) Oxides: Potential Impacts on Drinking Water Quality. *Environmental Science & Technology* **2017**, *51* (12), 6812–6820.

(49) Tibshirani, R.; Hastie, T. Local Likelihood Estimation. *Journal of the American Statistical Association* **1987**, *82* (398), 559–567.

(50) Trueman, B. F.; Gregory, B. S.; McCormick, N. E.; Gao, Y.; Gora, S.; Anaviapik-Soucie, T.; L'Hérault, V.; Gagnon, G. A. Manganese Increases Lead Release to Drinking Water. *Environmental Science & Technology* **2019**, *53* (9), 4803–4812.

(51) Hu, J.; Gan, F.; Triantafyllidou, S.; Nguyen, C.; Edwards, M. Copper-Induced Metal Release from Lead Pipe into Drinking Water. *Corrosion* **2012**, *68* (11), 1037–1048.

(52) Dudi, A. Reconsidering Lead Corrosion in Drinking Water: Product Testing, Direct Chloramine Attack and Galvanic Corrosion. PhD thesis, Virginia Tech, 2004.

(53) Nguyen, C. K.; Stone, K. R.; Dudi, A.; Edwards, M. A. Corrosive Microenvironments at Lead Solder Surfaces Arising from Galvanic Corrosion with Copper Pipe. *Environmental Science & Technology* **2010**, *44* (18), 7076–7081.

(54) Schock, M. R.; Wagner, I.; Oliphant, R. J. Corrosion and solubility of lead in drinking water. In *Internal corrosion of water distribution systems*; American Water Works Association Research Foundation: Denver, CO, 1996; pp 131–230.

(55) Yoshida, T.; Yamaguchi, T.; Iida, Y.; Nakayama, S. XPS Study of Pb (II) Adsorption on γ-Al_2O_3 Surface at High pH Conditions. *Journal of Nuclear Science and Technology* **2003**, *40* (9), 672–678.

(56) Krzywinski, M.; Altman, N. Points of Significance: Two-Factor Designs. *Nature methods* **2014**, *11* (12), 1187–1188.

(57) MacBerthouex, P.; Brown, L. C. *Statistics for Environmental Engineers*; Lewis Publishers, Washington, DC, 1996.

(58) Edwards, M.; McNeill, L. S. Effect of Phosphate Inhibitors on Lead Release from Pipes. *Journal-American Water Works Association* **2002**, *94* (1), 79–90.

(59) Suits, D. B. Use of Dummy Variables in Regression Equations. *Journal of the American Statistical Association* **1957**, *52* (280), 548–551.

(60) Berry, K. J.; Mielke Jr, P. W.; Iyer, H. K. Factorial Designs and Dummy Coding. *Perceptual and Motor Skills* **1998**, *87* (3), 919–927.

(61) Dermatas, D. Weathering of Lead in Fort Irwin Firing Range Soils. *Global Nest* **2004**, *6* (2), 167–175.

(62) Godelitsas, A.; Astilleros, J. M.; Hallam, K.; Harissopoulos, S.; Putnis, A. Interaction of Calcium Carbonates with Lead in Aqueous Solutions. *Environmental Science & Technology* **2003**, *37* (15), 3351–3360.

(63) R Core Team. *R: A Language and Environment for Statistical Computing*; R Foundation for Statistical Computing: Vienna, Austria, 2019.

(64) Wickham, H.; Averick, M.; Bryan, J.; Chang, W.; McGowan, L. D.; François, R.; Grolemund, G.; Hayes, A.; Henry, L.; Hester, J.; Kuhn, M.; Pedersen, T. L.; Miller, E.; Bache, S. M.; Müller, K.; Ooms, J.; Robinson, D.; Seidel, D. P.; Spinu, V.; Takahashi, K.; Vaughan, D.; Wilke, C.; Woo, K.; Yutani, H. Welcome to the tidyverse. *Journal of Open Source Software* **2019**, *4* (43), 1686. https://doi.org/10.21105/joss.01686.

(65) Wickham, H. *ggplot2: Elegant Graphics for Data Analysis*; Springer-Verlag New York, 2016.

(66) Wilke, C. O. *cowplot: Streamlined Plot Theme and Plot Annotations for 'ggplot2'*; 2019.

(67) Lawlor, J. *PNWColors: A Pacific Northwest Color Palette Package*; 2019.

(68) Ooms, J. *Pdftools: Text Extraction, Rendering and Converting of Pdf Documents*; 2020.

(69) Urbanek, S. *Png: Read and Write Png Images*; 2013.

(70) Pedersen, T. L. *Patchwork: The Composer of Plots*; 2019.

(71) Zhu, H. *KableExtra: Construct Complex Table with 'Kable' and Pipe Syntax*; 2019.

(72) Daróczi, G.; Tsegelskyi, R. *Pander: An R 'Pandoc' Writer*; 2018.

(73) Schauberger, P.; Walker, A. *Openxlsx: Read, Write and Edit Xlsx Files*; 2019.

(74) Bae, Y.; Pasteris, J. D.; Giammar, D. E. Impact of Orthophosphate on Lead Release from Pipe Scale in High pH, Low Alkalinity Water. *Water Research* **2020**, *177*, 115764. https://doi.org/10.1016/j.watres.2020.115764.

(75) Bae, Y.; Pasteris, J. D.; Giammar, D. E. The Ability of Phosphate to Prevent Lead Release from Pipe Scale When Switching from Free Chlorine to Monochloramine. *Environmental Science & Technology* **2020**, *54* (2), 879–888. https://doi.org/10.1021/acs.est.9b06019.

(76) Masten, S. J.; Davies, S. H.; McElmurry, S. P. Flint Water Crisis: What Happened and Why? *Journal-American Water Works Association* **2016**, *108* (12), 22–34.

(77) Schock, M. R. Response of Lead Solubility to Dissolved Carbonate in Drinking Water. *Journal-American Water Works Association* **1980**, *72* (12), 695–704.

(78) Stanforth, R.; Qiu, J. Effect of Phosphate Treatment on the Solubility of Lead in Contaminated Soil. *Environmental Geology* **2001**, *41* (1-2), 1–10.

(79) Cartier, C.; Doré, E.; Laroche, L.; Nour, S.; Edwards, M.; Prévost, M. Impact of Treatment on Pb Release from Full and Partially Replaced Harvested Lead Service Lines (LSLs). *Water Research* **2013**, *47* (2), 661–671. https://doi.org/10.1016/j.watres.2012.10.033.

(80) Zhou, E.; Payne, S. J. O.; Hofmann, R.; Andrews, R. C. Factors Affecting Lead Release in Sodium Silicate-Treated Partial Lead Service Line Replacements. *Journal of Environmental Science and Health Part A* **2015**, *50* (9), 922–930.

(81) Cartier, C.; Arnold Jr, R. B.; Triantafyllidou, S.; Prévost, M.; Edwards, M. Effect of Flow Rate and Lead/Copper Pipe Sequence on Lead Release from Service Lines. *Water Research* **2012**, *46* (13), 4142–4152.

(82) Venkateswarlu, K.; Sandhyarani, M.; Nellaippan, T.; Rameshbabu, N. Estimation of Crystallite Size, Lattice Strain and Dislocation Density of Nanocrystalline Carbonate Substituted Hydroxyapatite by X-Ray Peak Variance Analysis. *Procedia Materials Science* **2014**, *5*, 212–221.

(83) Londoño-Restrepo, S. M.; Jeronimo-Cruz, R.; Millán-Malo, B. M.; Rivera-Muñoz, E. M.; Rodriguez-García, M. E. Effect of the Nano Crystal Size on the X-Ray Diffraction Patterns of Biogenic Hydroxyapatite from Human, Bovine, and Porcine Bones. *Scientific Reports* **2019**, *9* (1), 5915.

(84) Martens, W. N.; Rintoul, L.; Kloprogge, J. T.; Frost, R. L. Single Crystal Raman Spectroscopy of Cerussite. *American Mineralogist* **2004**, *89* (2-3), 352–358.

(85) Liu, H.; Korshin, G. V.; Ferguson, J. F. Investigation of the Kinetics and Mechanisms of the Oxidation of Cerussite and Hydrocerussite by Chlorine. *Environmental Science & Technology* **2008**, *42* (9), 3241–3247.

(86) Korshin, G. V.; Ferguson, J. F.; Lancaster, A. N. Influence of Natural Organic Matter on the Morphology of Corroding Lead Surfaces and Behavior of Lead-Containing Particles. *Water Research* **2005**, *39* (5), 811–818.

(87) Bucca, M.; Dietzel, M.; Tang, J.; Leis, A.; Köhler, S. J. Nucleation and Crystallization of Otavite, Witherite, Calcite, Strontianite, Hydrozincite, and Hydrocerussite by CO_2 Membrane Diffusion Technique. *Chemical Geology* **2009**, *266* (3-4), 143–156.

(88) Wasserstrom, L. W.; Miller, S. A.; Triantafyllidou, S.; Desantis, M. K.; Schock, M. R. Scale Formation Under Blended Phosphate Treatment for a Utility with Lead Pipes. *Journal-American Water Works Association* **2017**, *109* (11), E464–E478.

(89) Hopwood, J. D.; Davey, R. J.; Jones, M. O.; Pritchard, R. G.; Cardew, P. T.; Booth, A. Development of Chloropyromorphite Coatings for Lead Water Pipes. *Journal of Materials Chemistry* **2002**, *12* (6), 1717–1723.

(90) Holm, T. R.; Edwards, M. Metaphosphate Reversion in Laboratory and Pipe-Rig Experiments. *Journal-American Water Works Association* **2003**, *95* (4), 172–178.

(91) Lower, S. K.; Maurice, P. A.; Traina, S. J.; Carlson, E. H. Aqueous Pb Sorption by Hydroxylapatite: Applications of Atomic Force Microscopy to Dissolution, Nucleation, and Growth Studies. *American Mineralogist* **1998**, *83* (1), 147–158.

(92) Kwaśniak-Kominek, M.; Manecki, M.; Matusik, J.; Lempart, M. Carbonate Substitution in Lead Hydroxyapatite $Pb_5(PO_4)_3OH$. *Journal of Molecular Structure* **2017**, *1147*, 594–602.

(93) Krost, A.; Bläsing, J. Fast, Micrometer Scale Characterization of Group-III Nitrides with Laboratory X-Ray Diffraction. *Materials Science and Engineering: A* **2009**, *524* (1-2), 82–88.

(94) Onoue, F.; Tsuji, K. X-Ray Elemental Imaging in Depth by Combination of Fe-Sem-Eds and Glow Discharge Sputtering. *ISIJ international* **2013**, *53* (11), 1939–1942.

(95) Rades, S.; Hodoroaba, V.-D.; Salge, T.; Wirth, T.; Lobera, M. P.; Labrador, R. H.; Natte, K.; Behnke, T.; Gross, T.; Unger, W. E. High-Resolution Imaging with SEM/T-SEM, EDX and SAM as a Combined Methodical Approach for Morphological and Elemental Analyses of Single Engineered Nanoparticles. *RSC Advances* **2014**, *4* (91), 49577–49587.

(96) Feng, Q.; Wen, S.; Cao, Q.; Deng, J.; Zhao, W. The Effect of Chloride Ions on the Activity of Cerussite Surfaces. *Minerals* **2016**, *6* (3), 92.

(97) Feng, Q.; Wen, S.; Zhao, W.; Deng, J.; Xian, Y. Adsorption of Sulfide Ions on Cerussite Surfaces and Implications for Flotation. *Applied Surface Science* **2016**, *360*, 365–372.

(98) Greczynski, G.; Hultman, L. C 1s Peak of Adventitious Carbon Aligns to the Vacuum Level: Dire Consequences for Material's Bonding Assignment by Photoelectron Spectroscopy. *ChemPhysChem* **2017**, *18* (12), 1507–1512.

(99) Shi, Z.; Stone, A. T. PbO_2 (S, Plattnerite) Reductive Dissolution by Aqueous Manganous and Ferrous Ions. *Environmental Science & Technology* **2009**, *43* (10), 3596–3603.

(100) Xie, Y.; Wang, Y.; Giammar, D. E. Impact of Chlorine Disinfectants on Dissolution of the Lead Corrosion Product Pbo2. *Environmental Science & Technology* **2010**, *44* (18), 7082–7088.

(101) Kraal, P.; Genuchten, C. M. van; Behrends, T.; Rose, A. L. Sorption of Phosphate and Silicate Alters Dissolution Kinetics of Poorly Crystalline Iron (Oxyhydr) Oxide. *Chemosphere* **2019**, *234*, 690–701.

(102) Trueman, B. F.; Krkošek, W. H.; Gagnon, G. A. Effects of Ortho-and Polyphosphates on Lead Speciation in Drinking Water. *Environmental Science: Water Research & Technology* **2018**, *4* (4), 505–512.

(103) Health Canada. *Guidelines for Canadian Drinking Water Quality: Guideline Technical Document, Lead.*; 2019.

(104) Hoekstra, E.; Hayes, C.; Aertgeerts, R.; Becker, A.; Jung, M.; Postawa, A.; Russell, L.; Witczak, S. Guidance on Sampling and Monitoring for Lead in Drinking Water. *JRC Scientific and Technical Reports* **2009**.

(105) Xie, L.; Giammar, D. E. Equilibrium Solubility and Dissolution Rate of the Lead Phosphate Chloropyromorphite. *Environmental Science & Technology* **2007**, *41* (23), 8050–8055.

(106) Xie, Y.; Wang, Y.; Singhal, V.; Giammar, D. E. Effects of pH and Carbonate Concentration on Dissolution Rates of the Lead Corrosion Product PbO2. *Environmental science & technology* **2010**, *44* (3), 1093–1099.

(107) Korshin, G.; Liu, H. Preventing the Colloidal Dispersion of Pb (IV) Corrosion Scales and Lead Release in Drinking Water Distribution Systems. *Environmental Science: Water Research & Technology* **2019**, *5* (7), 1262–1269.

(108) Wang, Y.; Wu, J.; Giammar, D. E. Kinetics of the Reductive Dissolution of Lead (IV) Oxide by Iodide. *Environmental Science & Technology* **2012**, *46* (11), 5859–5866.

(109) Dunnington, D. *Tidyphreeqc: Tidy Geochemical Modeling Using Phreeqc*; 2020.

(110) Gittings, M.; Saville, D. The Determination of Hydrodynamic Size and Zeta Potential from Electrophoretic Mobility and Light Scattering Measurements. *Colloids and Surfaces A: Physicochemical and Engineering Aspects* **1998**, *141* (1), 111–117.

(111) Wickham, H. *Tidyverse: Easily Install and Load the 'Tidyverse'*; 2017.

(112) Wickham, H. *Ggplot2: Elegant Graphics for Data Analysis*; Springer-Verlag New York, 2016.

(113) Wickham, H.; François, R.; Henry, L.; Müller, K. *Dplyr: A Grammar of Data Manipulation*; 2019.

(114) Allaire, J.; Xie, Y.; McPherson, J.; Luraschi, J.; Ushey, K.; Atkins, A.; Wickham, H.; Cheng, J.; Chang, W.; Iannone, R. *Rmarkdown: Dynamic Documents for R*; 2019.

(115) Lawlor, J. *PNWColors: A Pacific Northwest Color Palette Package*; 2019.

(116) Parkhurst, D. L.; Appelo, C. A. J. *Description of Input and Examples for Phreeqc Version 3–a Computer Program for Speciation, Batch-Reaction, One-Dimensional Transport, and Inverse Geochemical Calculations*; Techniques and methods; U.S. Geological Survey, 2013; Vol. book 6, p 497.

(117) Parkhurst, D. L.; Appelo, C.; others. User's Guide to Phreeqc (Version 2): A Computer Program for Speciation, Batch-Reaction, One-Dimensional Transport, and Inverse Geochemical Calculations. *Water-resources investigations report* **1999**, *99* (4259), 312.

(118) Weaver, C. L. Lead Silicate Solubility and the Control of Lead Contamination in Drinking Water. PhD thesis, Virginia Tech, 1994.

(119) Li, Y.; Zhu, Y.; Zhao, S.; Liu, X. The Weathering and Transformation Process of Lead in China's Shooting Ranges. *Environmental Science: Processes & Impacts* **2015**, *17* (9), 1620–1633.

(120) Hajati, S.; Coultas, S.; Blomfield, C.; Tougaard, S. Nondestructive Quantitative XPS Imaging of Depth Distribution of Atoms on the Nanoscale. *Surface and Interface Analysis* **2008**, *40* (3-4), 688–691.

(121) Tougaard, S. Quantitative XPS: Non-Destructive Analysis of Surface Nano-Structures. *Applied Surface Science* **1996**, *100*, 1–10.

(122) Stanley, C.; Jones, G.; Hart, A.; Keller, P.; Lloyd, D. Barstowite, $3PbCl_2.PbCO_3.H_2O$, a New Mineral from Bounds Cliff, St Endellion, Cornwall. *Mineralogical Magazine* **1991**, *55* (378), 121–125.

(123) Durman, R.; Jayasooriya, U. A.; Kettle, S. F. Is Cerussite an Aragonite? Longitudinal Optical–Transverse Optical Splitting in the Single-Crystal Raman Spectra. *Journal of the Chemical Society, Chemical Communications* **1985**, No. 13, 916–917.

(124) Siidra, O.; Nekrasova, D.; Depmeier, W.; Chukanov, N.; Zaitsev, A.; Turner, R. Hydrocerussite-Related Minerals and Materials: Structural Principles, Chemical Variations and Infrared Spectroscopy. *Acta Crystallographica Section B: Structural Science, Crystal Engineering and Materials* **2018**, *74* (2), 182–195.

(125) Frost, R. L.; Martens, W.; Kloprogge, J. T.; Ding, Z. Raman Spectroscopy of Selected Lead Minerals of Environmental Significance. *Spectrochimica Acta Part A: Molecular and Biomolecular Spectroscopy* **2003**, *59* (12), 2705–2711.

(126) Vidal, L.; Joussein, E.; Colas, M.; Cornette, J.; Sanz, J.; Sobrados, I.; Gelet, J.; Absi, J.; Rossignol, S. Controlling the Reactivity of Silicate Solutions: A Ftir, Raman and Nmr Study. *Colloids and Surfaces A: Physicochemical and Engineering Aspects* **2016**, *503*, 101–109.

(127) Awonusi, A.; Morris, M. D.; Tecklenburg, M. M. Carbonate Assignment and Calibration in the Raman Spectrum of Apatite. *Calcified tissue international* **2007**, *81* (1), 46–52.

(128) Zhao, J.; Giammar, D. E.; Pasteris, J. D.; Dai, C.; Bae, Y.; Hu, Y. Formation and Aggregation of Lead Phosphate Particles: Implications for Lead Immobilization in Water Supply Systems. *Environmental Science & Technology* **2018**, *52* (21), 12612–12623.

(129) Mishrra, A.; Giammar, D. Effects of Sodium Silicate Corrosion Inhibitors on Lead Release from Pipe Materials. In *AWWA Water Quality Technology Conference*; American Water Works Association: Dallas, TX, 2019.

(130) Brandhuber, P. Manage Water Quality to Control Lead in Drinking Water. *Opflow* **2018**, *44* (1), 16–19.

(131) NSF. *NSF/ANSI/CAN 60 Drinking Water Treatment Chemicals - Health Effects*; NSF International, 2020.

(132) McNeill, L. S.; Edwards, M. Iron Pipe Corrosion in Distribution Systems. *Journal-American Water Works Association* **2001**, *93* (7), 88–100.

(133) Dart, F. J.; Foley, P. D. Silicate as Fe, Mn Deposition Preventative in Distribution Systems. *Journal-American Water Works Association* **1972**, *64* (4), 244–249.

(134) Cantor, A. F.; Denig-Chakroff, D.; Vela, R. R.; Oleinik, M. G.; Lynch, D. L. Use of Polyphosphate in Corrosion Control. *Journal-American Water Works Association* **2000**, *92* (2), 95–102.

(135) Kinsela, A. S.; Jones, A. M.; Bligh, M. W.; Pham, A. N.; Collins, R. N.; Harrison, J. J.; Wilsher, K. L.; Payne, T. E.; Waite, T. D. Influence of Dissolved Silicate on Rates of Fe (II) Oxidation. *Environmental Science & Technology* **2016**, *50* (21), 11663–11671.

(136) Jones, A. M.; Griffin, P. J.; Collins, R. N.; Waite, T. D. Ferrous Iron Oxidation Under Acidic Conditions–the Effect of Ferric Oxide Surfaces. *Geochimica et Cosmochimica Acta* **2014**, *145*, 1–12.

(137) Masters, S.; Edwards, M. Increased Lead in Water Associated with Iron Corrosion. *Environmental Engineering Science* **2015**, *32* (5), 361–369.

(138) Trueman, B. F.; Anaviapik-Soucie, T.; L'Hérault, V.; Gagnon, G. A. Characterizing Colloidal Metals in Drinking Water by Field Flow Fractionation. *Environmental Science: Water Research & Technology* **2019**, *5* (12), 2202–2209.

(139) Knowles, A. D.; Nguyen, C. K.; Edwards, M. A.; Stoddart, A.; McIlwain, B.; Gagnon, G. A. Role of Iron and Aluminum Coagulant Metal Residuals and Lead Release from Drinking Water Pipe Materials. *Journal of Environmental Science and Health Part A* **2015**, *50* (4), 414–423.

(140) Lytle, D. A.; Schock, M. R.; Scheckel, K. The Inhibition of Pb (IV) Oxide Formation in Chlorinated Water by Orthophosphate. *Environmental Science & Technology* **2009**, *43* (17), 6624–6631.

(141) Gagnon, G. A.; Doubrough, J. D. Lead Release from Premise Plumbing: A Profile of Sample Collection and Pilot Studies from a Small System. *Canadian Journal of Civil Engineering* **2011**, *38* (7), 741–750.

(142) Woszczynski, M.; Bergese, J.; Gagnon, G. A. Comparison of Chlorine and Chloramines on Lead Release from Copper Pipe Rigs. *Journal of Environmental Engineering* **2013**, *139* (8), 1099–1107. https://doi.org/10.1061/(ASCE)EE.1943-7870.0000712.

(143) Kuch, A.; Wagner, I. A Mass Transfer Model to Describe Lead Concentrations in Drinking Water. *Water Research* **1983**, *17* (10), 1303–1307. https://doi.org/10.1016/0043-1354(83)90256-7.

(144) Stoddart, A. K.; Gagnon, G. A. Full-Scale Prechlorine Removal: Impact on Filter Performance and Water Quality. *Journal-American Water Works Association* **2015**, *107* (12), E638–E647.

(145) Brown, L. C.; Mac Berthouex, P. *Statistics for Environmental Engineers*; CRC press, 2002.

(146) APHA. *Standard Methods for the Examination of Water and Wastewater*, 22nd ed.; American Public Health Association, American Waterworks Association, Water Pollution Control Federation. American Public Heath Association: Washington,DC, 2012.

(147) APHA. 3125 Metals by Inductively Coupled Plasma—Mass Spectrometry (2017). In *Standard methods for the examination of water and wastewater*; American Public Heath Associationr: Washington,DC, 2012. https://doi.org/10.2105/SMWW.2882.048.

(148) Poda, A.; Bednar, A.; Kennedy, A.; Harmon, A.; Hull, M.; Mitrano, D.; Ranville, J.; Steevens, J. Characterization of Silver Nanoparticles Using Flow-Field Flow Fractionation Interfaced to Inductively Coupled Plasma Mass Spectrometry. *Journal of Chromatography A* **2011**, *1218* (27), 4219–4225.

(149) Cuss, C. W.; Grant-Weaver, I.; Shotyk, W. AF4-ICPMS with the 300 Da Membrane to Resolve Metal-Bearing “Colloids”< 1 kDa: Optimization, Fractogram Deconvolution, and Advanced Quality Control. *Analytical chemistry* **2017**, *89* (15), 8027–8035.

(150) Podzimek, S. *Light Scattering, Size Exclusion Chromatography and Asymmetric Flow Field Flow Fractionation: Powerful Tools for the Characterization of Polymers, Proteins and Nanoparticles*; John Wiley & Sons, 2011.

(151) Lesher, E. K.; Ranville, J. F.; Honeyman, B. D. Analysis of pH Dependent Uranium (Vi) Sorption to Nanoparticulate Hematite by Flow Field-Flow Fractionation-Inductively Coupled Plasma Mass Spectrometry. *Environmental Science & Technology* **2009**, *43* (14), 5403–5409.

(152) Gora, S. L.; Trueman, B. F.; Anaviapik-Soucie, T.; Gavin, M. K.; Ontiveros, C. C.; Campbell, J.; L’Hérault, V.; Stoddart, A. K.; Gagnon, G. A. Source Water Characteristics and Building-Specific Factors Influence Corrosion and Point of Use Water Quality in a Decentralized Arctic Drinking Water System. *Environmental Science & Technology* **2020**, *54* (4), 2192–2201.

(153) Wood, S. N. *Generalized Additive Models: An Introduction with R*, 2nd ed.; Chapman; Hall/CRC, 2017.

(154) Simpson, G. L. Modelling Palaeoecological Time Series Using Generalised Additive Models. *Frontiers in Ecology and Evolution* **2018**, *6*, 149. https://doi.org/10.3389/fevo.2018.00149.

(155) Pinheiro, J.; Bates, D. *Mixed-Effects Models in S and S-Plus*; Springer Science & Business Media, 2006.

(156) Pedersen, E. J.; Miller, D. L.; Simpson, G. L.; Ross, N. Hierarchical Generalized Additive Models in Ecology: An Introduction with Mgcv. *PeerJ* **2019**, *7*, e6876. https://doi.org/10.7717/peerj.6876.

(157) Triantafyllidou, S.; Edwards, M. Galvanic Corrosion After Simulated Small-Scale Partial Lead Service Line Replacements. *Journal-American Water Works Association* **2011**, *103* (9), 85–99.

(158) Deshommes, E.; Laroche, L.; Nour, S.; Cartier, C.; Prévost, M. Source and Occurrence of Particulate Lead in Tap Water. *Water Research* **2010**, *44* (12), 3734–3744.

(159) Camara, E.; Montreuil, K. R.; Knowles, A. K.; Gagnon, G. A. Role of the Water Main in Lead Service Line Replacement: A Utility Case Study. *Journal-American Water Works Association* **2013**, *105* (8), E423–E431.

(160) Doré, E.; Deshommes, E.; Laroche, L.; Nour, S.; Prévost, M. Study of the Long-Term Impacts of Treatments on Lead Release from Full and Partially Replaced Harvested Lead Service Lines. *Water Research* **2019**, *149*, 566–577.

(161) Trueman, B. F.; Gagnon, G. A. A New Analytical Approach to Understanding Nanoscale Lead-Iron Interactions in Drinking Water Distribution Systems. *Journal of Hazardous Materials* **2016**, *311*, 151–157. https://doi.org/10.1016/j.jhazmat.2016.03.001.

(162) Latimer, P.; Pyle, B. Light Scattering at Various Angles: Theoretical Predictions of the Effects of Particle Volume Changes. *Biophysical journal* **1972**, *12* (7), 764–773.

(163) Pan, W.; Pan, C.; Bae, Y.; Giammar, D. Role of Manganese in Accelerating the Oxidation of Pb (II) Carbonate Solids to Pb (IV) Oxide at Drinking Water Conditions. *Environmental Science & Technology* **2019**, *53* (12), 6699–6707.

(164) Schock, M. R.; Cantor, A. F.; Triantafyllidou, S.; Desantis, M. K.; Scheckel, K. G. Importance of Pipe Deposits to Lead and Copper Rule Compliance. *Journal-American Water Works Association* **2014**, *106* (7), E336–E349.

(165) Dupin, J.-C.; Gonbeau, D.; Vinatier, P.; Levasseur, A. Systematic XPS Studies of Metal Oxides, Hydroxides and Peroxides. *Physical Chemistry Chemical Physics* **2000**, *2* (6), 1319–1324.

(166) Guittet, M.; Crocombette, J.; Gautier-Soyer, M. Bonding and XPS Chemical Shifts in ZrSiO4 Versus SiO2 and ZrO2: Charge Transfer and Electrostatic Effects. *Physical Review B: Condensed Matter* **2001**, *63* (12), 125117.

(167) Hochella Jr, M. F.; Brown Jr, G. E. Aspects of Silicate Surface and Bulk Structure Analysis Using X-Ray Photoelectron Spectroscopy (XPS). *Geochimica et Cosmochimica Acta* **1988**, *52* (6), 1641–1648.

(168) Mallet, M.; Barthélémy, K.; Ruby, C.; Renard, A.; Naille, S. Investigation of Phosphate Adsorption onto Ferrihydrite by X-Ray Photoelectron Spectroscopy. *Journal of Colloid and Interface Science* **2013**, *407*, 95–101.

(169) Robinson, R. B.; Minear, R. A.; Holden, J. M. Effects of Several Ions on Iron Treatment by Sodium Silicate and Hypochlorite. *Journal-American Water Works Association* **1987**, *79* (7), 116–125.

(170) Sarin, P.; Snoeyink, V.; Bebee, J.; Jim, K.; Beckett, M.; Kriven, W. M.; Clement, J. Iron Release from Corroded Iron Pipes in Drinking Water Distribution Systems: Effect of Dissolved Oxygen. *Water Research* **2004**, *38* (5), 1259–1269.

(171) Lytle, D. A.; Magnuson, M. L.; Snoeyink, V. L. Effect of Oxidants on the Properties of Fe (III) Particles and Suspensions Formed from the Oxidation of Fe (II). *Journal-American Water Works Association* **2004**, *96* (8), 112–124.

(172) McNeill, L. S.; Edwards, M. Phosphate Inhibitors and Red Water in Stagnant Iron Pipes. *Journal of Environmental Engineering* **2000**, *126* (12), 1096–1102.

(173) Pocock, S. J.; Smith, M.; Baghurst, P. Environmental Lead and Children's Intelligence: A Systematic Review of the Epidemiological Evidence. *Bmj* **1994**, *309* (6963), 1189–1197.

(174) Lehtola, M. J.; Miettinen, I. T.; Vartiainen, T.; Martikainen, P. J. Changes in Content of Microbially Available Phosphorus, Assimilable Organic Carbon and Microbial Growth Potential During Drinking Water Treatment Processes. *Water Research* **2002**, *36* (15), 3681–3690.

(175) Fang, W.; Hu, J.; Ong, S. Influence of Phosphorus on Biofilm Formation in Model Drinking Water Distribution Systems. *Journal of applied microbiology* **2009**, *106* (4), 1328–1335.

(176) Prévost, M.; Rompré, A.; Coallier, J.; Servais, P.; Laurent, P.; Clément, B.; Lafrance, P. Suspended Bacterial Biomass and Activity in Full-Scale Drinking Water Distribution Systems: Impact of Water Treatment. *Water Research* **1998**, *32* (5), 1393–1406.

(177) Payment, P.; Franco, E.; Siemiatycki, J. Absence of Relationship Between Health Effects Due to Tap Water Consumption and Drinking Water Quality Parameters. *Water Science and Technology* **1993**, *27* (3-4), 137–143.

(178) LeChevallier, M. W.; McFeters, G. A. Interactions Between Heterotrophic Plate Count Bacteria and Coliform Organisms. *Appl. Environ. Microbiol.* **1985**, *49* (5), 1338–1341.

(179) Dart, F. J.; Foley, P. D. Preventing Iron Deposition with Sodium Silicate. *Journal-American Water Works Association* **1970**, *62* (10), 663–668.

(180) Kogo, A.; Payne, S. J.; Andrews, R. C. Impact of Corrosion Control on Biofilm Development in Simulated Partial Lead Service Line Replacements. *Environmental Engineering Science* **2017**, *34* (10), 711–720.

(181) Stumm, W.; Lee, G. F. Oxygenation of Ferrous Iron. *Industrial & Engineering Chemistry* **1961**, *53* (2), 143–146.

(182) Rahman, M. S.; Gagnon, G. A. Bench-Scale Evaluation of Drinking Water Treatment Parameters on Iron Particles and Water Quality. *Water Research* **2014**, *48*, 137–147.

(183) Eisnor, J. D.; Gagnon, G. A. Impact of Secondary Disinfection on Corrosion in a Model Water Distribution System. *Journal of Water Supply: Research and Technology—AQUA* **2004**, *53* (7), 441–452.

(184) Pullin, M. J.; Cabaniss, S. E. The Effects of pH, Ionic Strength, and Iron–Fulvic Acid Interactions on the Kinetics of Non-Photochemical Iron Transformations. I. Iron (II) Oxidation and Iron (III) Colloid Formation. *Geochimica et Cosmochimica Acta* **2003**, *67* (21), 4067–4077.

(185) Gu, B.; Schmitt, J.; Chen, Z.; Liang, L.; McCarthy, J. F. Adsorption and Desorption of Natural Organic Matter on Iron Oxide: Mechanisms and Models. *Environmental Science & Technology* **1994**, *28* (1), 38–46.

(186) Rahman, M. S.; Whalen, M.; Gagnon, G. A. Adsorption of Dissolved Organic Matter (DOM) onto the Synthetic Iron Pipe Corrosion Scales (Goethite and Magnetite): Effect of pH. *Chemical Engineering Journal* **2013**, *234*, 149–157.

(187) Sarin, P.; Snoeyink, V.; Bebee, J.; Kriven, W. M.; Clement, J. Physico-Chemical Characteristics of Corrosion Scales in Old Iron Pipes. *Water Research* **2001**, *35* (12), 2961–2969.

(188) Kaszuba, M.; Corbett, J.; Watson, F. M.; Jones, A. High-Concentration Zeta Potential Measurements Using Light-Scattering Techniques. *Philosophical Transactions of the Royal Society A: Mathematical, Physical and Engineering Sciences* **2010**, *368* (1927), 4439–4451.

(189) Team, R. RStudio: Integrated Development for R [Computer Software]. *URL http://www. rstudio. com/. Boston, MA: RStudio, Inc* **2016**.

(190) McCuen, R. H. Statistics for Environmental Engineers. *Journal of the American Water Resources Association* **2002**, *38* (6), 1775.

(191) Carlson, J.; Kawatra, S. Factors Affecting Zeta Potential of Iron Oxides. *Mineral Processing and Extractive Metallurgy Review* **2013**, *34* (5), 269–303.

(192) Baalousha, M. Aggregation and Disaggregation of Iron Oxide Nanoparticles: Influence of Particle Concentration, pH and Natural Organic Matter. *Science of the total Environment* **2009**, *407* (6), 2093–2101.

(193) Pédrot, M.; Le Boudec, A.; Davranche, M.; Dia, A.; Henin, O. How Does Organic Matter Constrain the Nature, Size and Availability of Fe Nanoparticles for Biological Reduction? *Journal of Colloid and Interface Science* **2011**, *359* (1), 75–85.

(194) Rushing, J. C.; McNeill, L. S.; Edwards, M. Some Effects of Aqueous Silica on the Corrosion of Iron. *Water Research* **2003**, *37* (5), 1080–1090.

(195) Lytle, D. A.; Snoeyink, V. L. Effect of Ortho-and Polyphosphates on the Properties of Iron Particles and Suspensions. *Journal-American Water Works Association* **2002**, *94* (10), 87–99.

(196) Hassellöv, M.; Readman, J. W.; Ranville, J. F.; Tiede, K. Nanoparticle Analysis and Characterization Methodologies in Environmental Risk Assessment of Engineered Nanoparticles. *Ecotoxicology* **2008**, *17* (5), 344–361.

(197) Yao, M.; Nan, J.; Chen, T. Effect of Particle Size Distribution on Turbidity Under Various Water Quality Levels During Flocculation Processes. *Desalination* **2014**, *354*, 116–124.

(198) Kleizen, H.; De Putter, A.; Van der Beek, M.; Huynink, S. Particle Concentration, Size and Turbidity. *Filtration & Separation* **1995**, *32* (9), 897–901.

(199) Schwaminger, S. P.; Surya, R.; Filser, S.; Wimmer, A.; Weigl, F.; Fraga-García, P.; Berensmeier, S. Formation of Iron Oxide Nanoparticles for the Photooxidation of Water: Alteration of Finite Size Effects from Ferrihydrite to Hematite. *Scientific Reports* **2017**, *7* (1), 1–9.

(200) Lassoued, A.; Dkhil, B.; Gadri, A.; Ammar, S. Control of the Shape and Size of Iron Oxide (α-Fe_2O_3) Nanoparticles Synthesized Through the Chemical Precipitation Method. *Results in Physics* **2017**, *7*, 3007–3015.

(201) Gregory, J. Optical Monitoring of Particle Aggregates. *Journal of Environmental Sciences* **2009**, *21* (1), 2–7.

(202) Rastogi, S.; Jabal, J.; Zhang, H.; Gibson, C.; Haler, K.; Qiang, Y.; Aston, D.; Branen, A. Antibody@ Silica Coated Iron Oxide Nanoparticles: Synthesis, Capture of E. Coli and Sers Titration of Biomolecules with Antibacterial Silver Colloid. *J. Nanomedic Nanotechnol* **2011**, *2* (7), 1–8.

(203) Jiang, W.; Mashayekhi, H.; Xing, B. Bacterial Toxicity Comparison Between Nano- and Micro-Scaled Oxide Particles. *Environmental Pollution* **2009**, *157* (5), 1619–1625.

(204) Baalousha, M.; Manciulea, A.; Cumberland, S.; Kendall, K.; Lead, J. R. Aggregation and Surface Properties of Iron Oxide Nanoparticles: Influence of pH and Natural Organic Matter. *Environmental Toxicology and Chemistry: An International Journal* **2008**, *27* (9), 1875–1882.

(205) Tombácz, E.; Libor, Z.; Illes, E.; Majzik, A.; Klumpp, E. The Role of Reactive Surface Sites and Complexation by Humic Acids in the Interaction of Clay Mineral and Iron Oxide Particles. *Organic Geochemistry* **2004**, *35* (3), 257–267.

(206) Luster, J.; Lloyd, T.; Sposito, G.; Fry, I. V. Multi-Wavelength Molecular Fluorescence Spectrometry for Quantitative Characterization of Copper (II) and Aluminum (III) Complexation by Dissolved Organic Matter. *Environmental Science & Technology* **1996**, *30* (5), 1565–1574.

(207) Shuman, M. S. Dissociation Pathways and Species Distribution of Aluminum Bound to an Aquatic Fulvic Acid. *Environmental Science & Technology* **1992**, *26* (3), 593–598.

(208) Deng, Y. Formation of Iron (III) Hydroxides from Homogeneous Solutions. *Water Research* **1997**, *31* (6), 1347–1354.

(209) Cudennec, Y.; Lecerf, A. The Transformation of Ferrihydrite into Goethite or Hematite, Revisited. *Journal of Solid State Chemistry* **2006**, *179* (3), 716–722.

(210) Jambor, J. L.; Dutrizac, J. E. Occurrence and Constitution of Natural and Synthetic Ferrihydrite, a Widespread Iron Oxyhydroxide. *Chemical Reviews* **1998**, *98* (7), 2549–2586.

(211) Zhao, J.; Huggins, F. E.; Feng, Z.; Huffman, G. P. Ferrihydrite: Surface Structure and Its Effects on Phase Transformation. *Clays and Clay Minerals* **1994**, *42* (6), 737–746.

(212) Drits, V.; Sakharov, B.; Salyn, A.; Manceau, A. Structural Model for Ferrihydrite. *Clay Minerals* **1993**, *28* (2), 185–207.

(213) Zeng, L. A Method for Preparing Silica-Containing Iron (III) Oxide Adsorbents for Arsenic Removal. *Water Research* **2003**, *37* (18), 4351–4358.

(214) Cornell, R.; Giovanoli, R.; Schindler, P. Effect of Silicate Species on the Transformation of Ferrihydrite into Goethite and Hematite in Alkaline Media. *Clays and Clay Minerals* **1987**, *35* (1), 21–28.

(215) Anderson, P. R.; Benjamin, M. M. Effect of Silicon on the Crystallization and Adsorption Properties of Ferric Oxides. *Environmental Science & Technology* **1985**, *19* (11), 1048–1053.

(216) Schwertmann, U.; Thalmann, H. The Influence of [Fe (II)],[Si], and pH on the Formation of Lepidocrocite and Ferrihydrite During Oxidation of Aqueous FeCl2 Solutions. *Clay Minerals* **1976**, *11* (3), 189–200.

(217) Benali, O.; Abdelmoula, M.; Refait, P.; Génin, J.-M. R. Effect of Orthophosphate on the Oxidation Products of Fe (II)-Fe (III) Hydroxycarbonate: The Transformation of Green Rust to Ferrihydrite. *Geochimica et Cosmochimica Acta* **2001**, *65* (11), 1715–1726.

(218) Schwertmann, U.; Murad, E. Effect of pH on the Formation of Goethite and Hematite from Ferrihydrite. *Clays and Clay Minerals* **1983**, *31* (4), 277–284.

(219) Wang, X.; Zhu, M.; Lan, S.; Ginder-Vogel, M.; Liu, F.; Feng, X. Formation and Secondary Mineralization of Ferrihydrite in the Presence of Silicate and Mn (II). *Chemical Geology* **2015**, *415*, 37–46.

(220) Biesinger, M. C.; Payne, B. P.; Grosvenor, A. P.; Lau, L. W.; Gerson, A. R.; Smart, R. S. C. Resolving Surface Chemical States in XPS Analysis of First Row Transition Metals, Oxides and Hydroxides: Cr, Mn, Fe, Co and Ni. *Applied Surface Science* **2011**, *257* (7), 2717–2730.

(221) Allen, G. C.; Curtis, M. T.; Hooper, A. J.; Tucker, P. M. X-Ray Photoelectron Spectroscopy of Iron–Oxygen Systems. *Journal of the Chemical Society, Dalton Transactions* **1974**, No. 14, 1525–1530.

(222) Nefedov, V.; Salyn, Y. V.; Leonhardt, G.; Scheibe, R. A Comparison of Different Spectrometers and Charge Corrections Used in X-Ray Photoelectron Spectroscopy. *Journal of Electron Spectroscopy and Related Phenomena* **1977**, *10* (2), 121–124.

(223) Oscarson, D.; Huang, P.; Defosse, C.; Herbillon, A. Oxidative Power of Mn (IV) and Fe (III) Oxides with Respect to as (III) in Terrestrial and Aquatic Environments. *Nature* **1981**, *291* (5810), 50–51.

(224) Mills, P.; Sullivan, J. A Study of the Core Level Electrons in Iron and Its Three Oxides by Means of X-Ray Photoelectron Spectroscopy. *Journal of Physics D: Applied Physics* **1983**, *16* (5), 723.

(225) Oku, M.; Hirokawa, K. The Effect of the Next Nearest Neighbor Ion on the X-Ray Photoelectron Spectra of 2p Levels for $Co^{2+,}$ Ni^{2+} and Cu^{2+} in Mgo. *Journal of Electron Spectroscopy and Related Phenomena* **1977**, *10* (2), 103–110.

(226) McIntyre, N.; Zetaruk, D. X-Ray Photoelectron Spectroscopic Studies of Iron Oxides. *Analytical Chemistry* **1977**, *49* (11), 1521–1529.

(227) Xu, Z.; Yu, J.; Xiao, W. Microemulsion-Assisted Preparation of a Mesoporous Ferrihydrite/SiO2 Composite for the Efficient Removal of Formaldehyde from Air. *Chemistry–A European Journal* **2013**, *19* (29), 9592–9598.

(228) Martinez, L.; Leinen, D.; Martin, F.; Gabas, M.; Ramos-Barrado, J.; Quagliata, E.; Dalchiele, E. Electrochemical Growth of Diverse Iron Oxide (Fe_3O_4, α-FeOOH, and γ-FeOOH) Thin Films by Electrodeposition Potential Tuning. *Journal of the Electrochemical Society* **2007**, *154* (3), D126–D133.

(229) Heuer, J.; Stubbins, J. F. An Xps Characterization of $FeCO_3$ Films from CO_2 Corrosion. *Corrosion Science* **1999**, *41* (7), 1231–1243.

(230) Barber, A.; Brandes, J.; Leri, A.; Lalonde, K.; Balind, K.; Wirick, S.; Wang, J.; Gélinas, Y. Preservation of Organic Matter in Marine Sediments by Inner-Sphere Interactions with Reactive Iron. *Scientific Reports* **2017**, *7* (1), 1–10.

(231) Lv, J.; Zhang, S.; Wang, S.; Luo, L.; Cao, D.; Christie, P. Molecular-Scale Investigation with ESI-FT-ICR-MS on Fractionation of Dissolved Organic Matter Induced by Adsorption on Iron Oxyhydroxides. *Environmental Science & Technology* **2016**, *50* (5), 2328–2336.

(232) Aiken, G. R.; Hsu-Kim, H.; Ryan, J. N. Influence of Dissolved Organic Matter on the Environmental Fate of Metals, Nanoparticles, and Colloids, 2011.

(233) Kalbitz, K.; Wennrich, R. Mobilization of Heavy Metals and Arsenic in Polluted Wetland Soils and Its Dependence on Dissolved Organic Matter. *Science of the Total Environment* **1998**, *209* (1), 27–39.

(234) Tang, M.; Nystrom, V.; Pieper, K.; Parks, J.; Little, B.; Guilliams, R.; Esqueda, T.; Edwards, M. The Relationship Between Discolored Water from Corrosion of Old Iron Pipe and Source Water Conditions. *Environmental Engineering Science* **2018**, *35* (9), 943–952.

(235) Gaulier, F.; Gibert, A.; Walls, D.; Langford, M.; Baker, S.; Baudot, A.; Porcheron, F.; Lienemann, C.-P. Mercury Speciation in Liquid Petroleum Products: Comparison Between on-Site Approach and Lab Measurement Using Size Exclusion Chromatography with High Resolution Inductively Coupled Plasma Mass Spectrometric Detection (SEC-ICP-HR MS). *Fuel Processing Technology* **2015**, *131*, 254–261.

(236) Park, J.-H. Spectroscopic Characterization of Dissolved Organic Matter and Its Interactions with Metals in Surface Waters Using Size Exclusion Chromatography. *Chemosphere* **2009**, *77* (4), 485–494.

(237) McKnight, D. M.; Bencala, K. E.; Zellweger, G. W.; Aiken, G. R.; Feder, G. L.; Thorn, K. A. Sorption of Dissolved Organic Carbon by Hydrous Aluminum and Iron Oxides Occurring at the Confluence of Deer Creek with the Snake River, Summit County, Colorado. *Environmental Science & Technology* **1992**, *26* (7), 1388–1396.

(238) Ohno, T.; Chorover, J.; Omoike, A.; Hunt, J. Molecular Weight and Humification Index as Predictors of Adsorption for Plant-and Manure-Derived Dissolved Organic Matter to Goethite. *European Journal of Soil Science* **2007**, *58* (1), 125–132.

(239) Guo, M.; Chorover, J. Transport and Fractionation of Dissolved Organic Matter in Soil Columns. *Soil Science* **2003**, *168* (2), 108–118.

(240) Aredes, S.; Klein, B.; Pawlik, M. The Removal of Arsenic from Water Using Natural Iron Oxide Minerals. *Journal of Cleaner Production* **2013**, *60*, 71–76.

(241) Anastassakis, G. N. A Study on the Separation of Magnesite Fines by Magnetic Carrier Methods. *Colloids and Surfaces A: Physicochemical and Engineering Aspects* **1999**, *149* (1-3), 585–593.

(242) Potapova, E.; Yang, X.; Grahn, M.; Holmgren, A.; Forsmo, S.; Fredriksson, A.; Hedlund, J. The Effect of Calcium Ions, Sodium Silicate and Surfactant on Charge and Wettability of Magnetite. *Colloids and Surfaces A: Physicochemical and Engineering Aspects* **2011**, *386* (1-3), 79–86.

(243) Waltham, C. A.; Eick, M. J. Kinetics of Arsenic Adsorption on Goethite in the Presence of Sorbed Silicic Acid. *Soil Science Society of America Journal* **2002**, *66* (3), 818–825.

(244) Alexandrino, J. S.; Peres, A. E. C.; Lopes, G. M.; Rodrigues, O. M. S. Dispersion Degree and Zeta Potential of Hematite. *Rem: Revista Escola de Minas* **2016**, *69* (2), 193–198.

(245) Aghasadeghi, K.; Trueman, B.; Peldszus, S.; Jakovljevic, A.; Beaulieu, P.; Gagnon, G. Revisiting Sodium Silicates as a Corrosion Control Treatment for Lead: A Pilot Study. In *AWWA Water Quality Technology Conference*; American Water Works Association: Dallas, Texas, 2019.

Appendix A: Supporting Data for Chapter 2

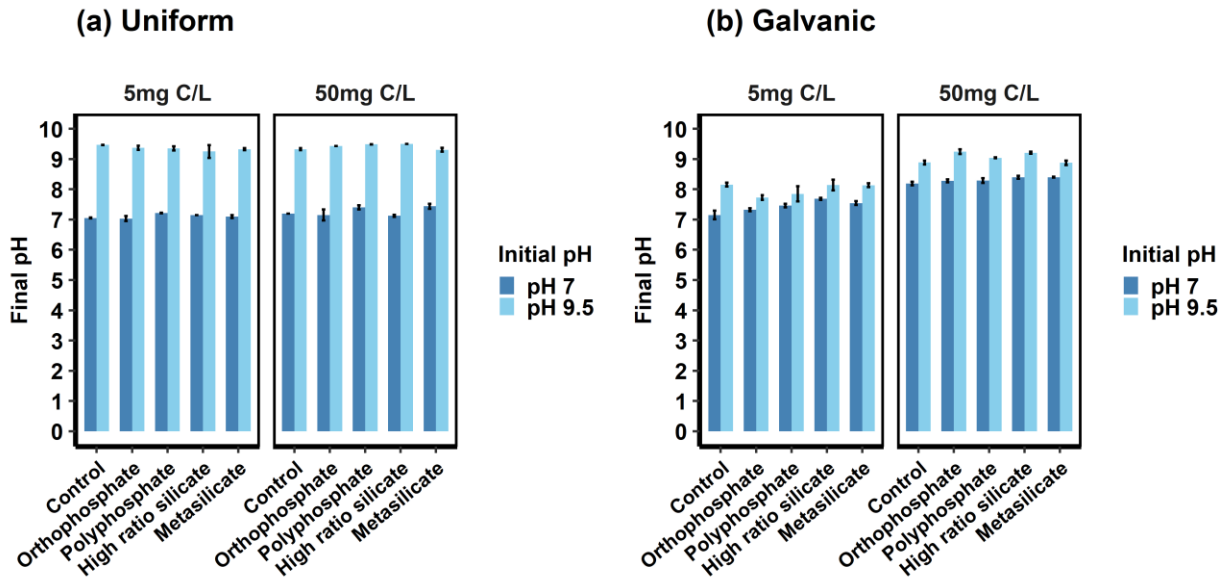

Figure 38 Final pH, at stable-state, of electrolyte solution after 48 hours of (a) uniform or (b) galvanic corrosion.

Factorial designs

Factorial designs are widely used to study the synergies among factors when probing complex systems.[56] This is useful in the present context: in lead corrosion studies, pH and DIC have important effects on the performance of corrosion inhibitors. For example, increasing DIC decreases lead solubility at circumneutral pH, but it has the opposite effect in the presence of orthophosphate.[11]

Figure 39a illustrates the outcomes in a 2 × 2 factorial experiment fit to hypothetical control system data (no corrosion inhibitor). The main effect of DIC is equal to the difference in Pb concentration between the low (5 mg C/L) and high levels (50 mg C/L). The main effect of pH is equal to the difference between the dashed and solid lines (pH 7 + 5 or 50 mg C/L). At pH 9.5 and DIC 50 mg C/L, the observed Pb concentration is higher than the sum of the main effects of pH and DIC; this is due to the (two-way) interaction between DIC and pH.

In the presence of an inhibitor (Figure 39b), the main effects of the inhibitor can be evaluated the same way. In an extended factorial design of 2 pH levels × 2 DIC levels × 2 inhibitor levels (absence/presence) = 8 treatments, Pb concentrations can be used to investigate the three-way interaction (inhibitor-pH-DIC).

Lead release under the conditions these experiments represent is estimated by adding the relevant main effects and interactions. For instance, lead release at pH 9 and DIC 5 mg C/L in the presence of the inhibitor (Figure 39b) is the sum of three numbers: the main effects of the inhibitor, pH, and the inhibitor × pH interaction. In our study, effects were estimated after log transformation, so the re-transformed estimates are multiplicative. 0/1 coding was used for the model matrix so that all effects are calculated relative to a reference condition (here, the pH 7 + 5 mg C/L control).

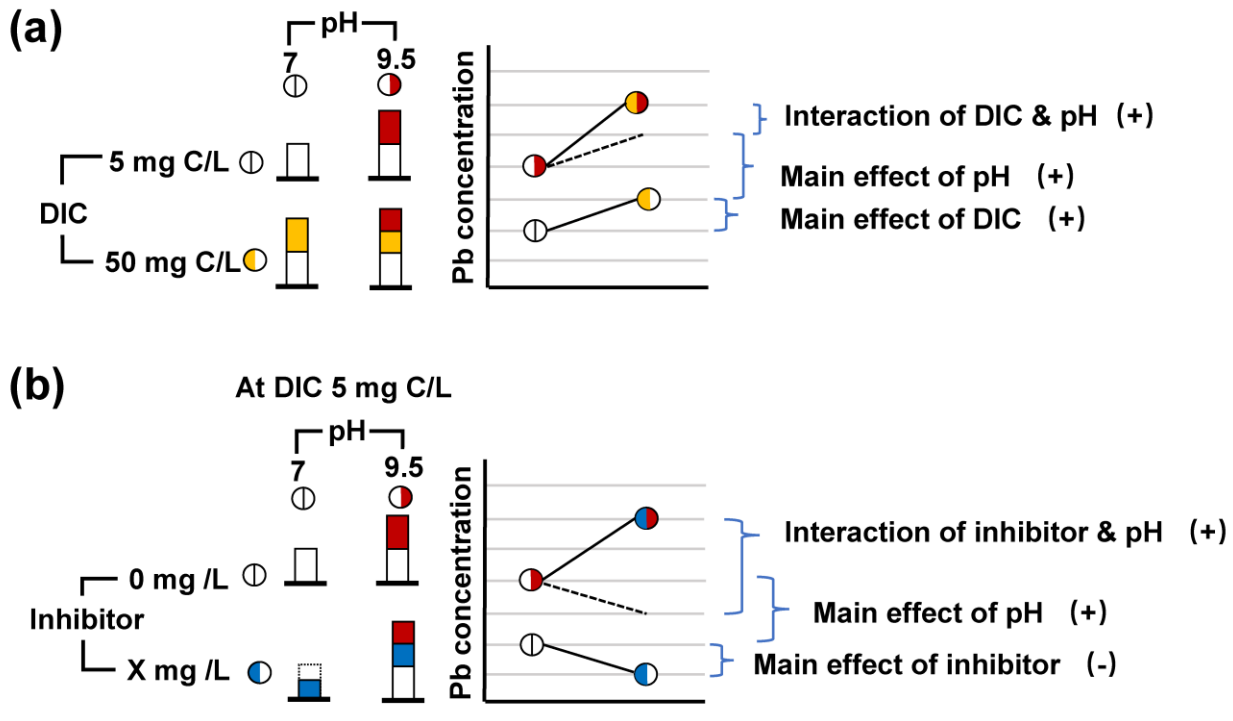

Figure 39 Conceptual diagram of the factorial design (artwork is not scientifically accurate). (a) Main effects of DIC and pH and the two-way interaction in the inhibitor-free system. (b) Main effects of an inhibitor, pH and the two-way interaction; + indicates an increase in lead concentration; - indicates a decrease.

Experimental design for evaluating lead corrosion control

Here, a factorial design was used to evaluate the effect of corrosion control on lead release (Figure 40). Treatments at two pH (7 and 9.5) and two DIC levels (5 and 50 mg C/L) were used to evaluate the main effects and interactions in the inhibitor-free control group (i.e., 0 mg P/L). These levels were selected based on a well-established solubility model incorporating cerussite, hydrocerussite, and hydroxylpyromorphite.[54] In the presence of orthophosphate (2 mg P/L), the main effect of orthophosphate and the orthophosphate × DIC interaction can be evaluated by comparing lead release at pH 7 with or without orthophosphate. The evaluation of high ratio silicate, metasilicate, and polyphosphate were evaluated following the same pattern.

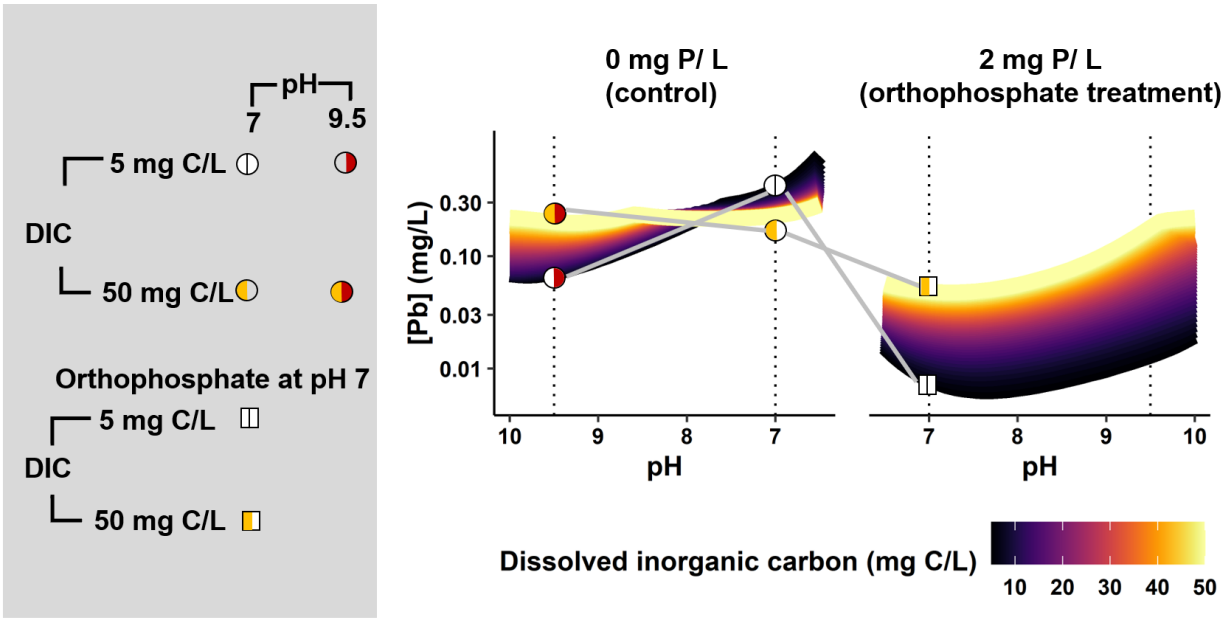

Figure 40 Solubility equilibrium of lead with cerussite, hydrocerussite, or hydroxylpyromorphite as a function of pH, dissolved inorganic carbon concentration (5 - 50 mg C/L), and orthophosphate concentration (0 or 2 mg P/L). The pH settings used in this study (7 and 9.5) are indicated by vertical dotted lines. Thermodynamic data are due to Schock et al.[54] and solubility calculations were made with tidyphreeqc.[109]

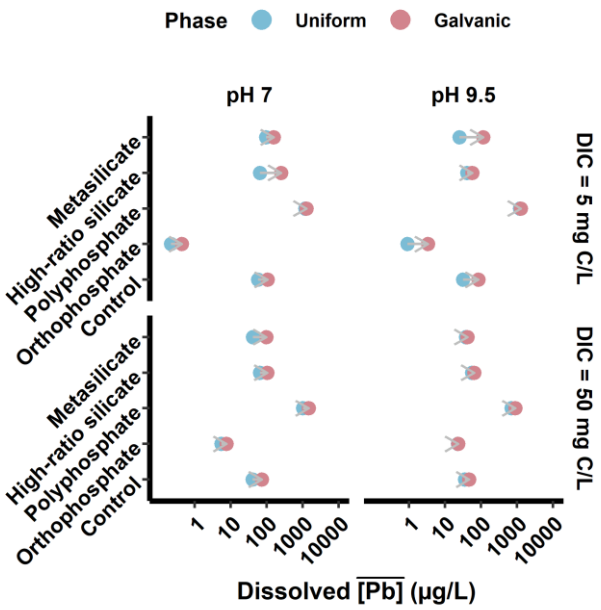

Figure 41(a) Geometric mean dissolved lead release (<0.45 µm) due to uniform (stable phase) and galvanic corrosion (initial phase) at two pH and DIC levels. Arrows indicate the increase in lead release due to coupling lead and copper.

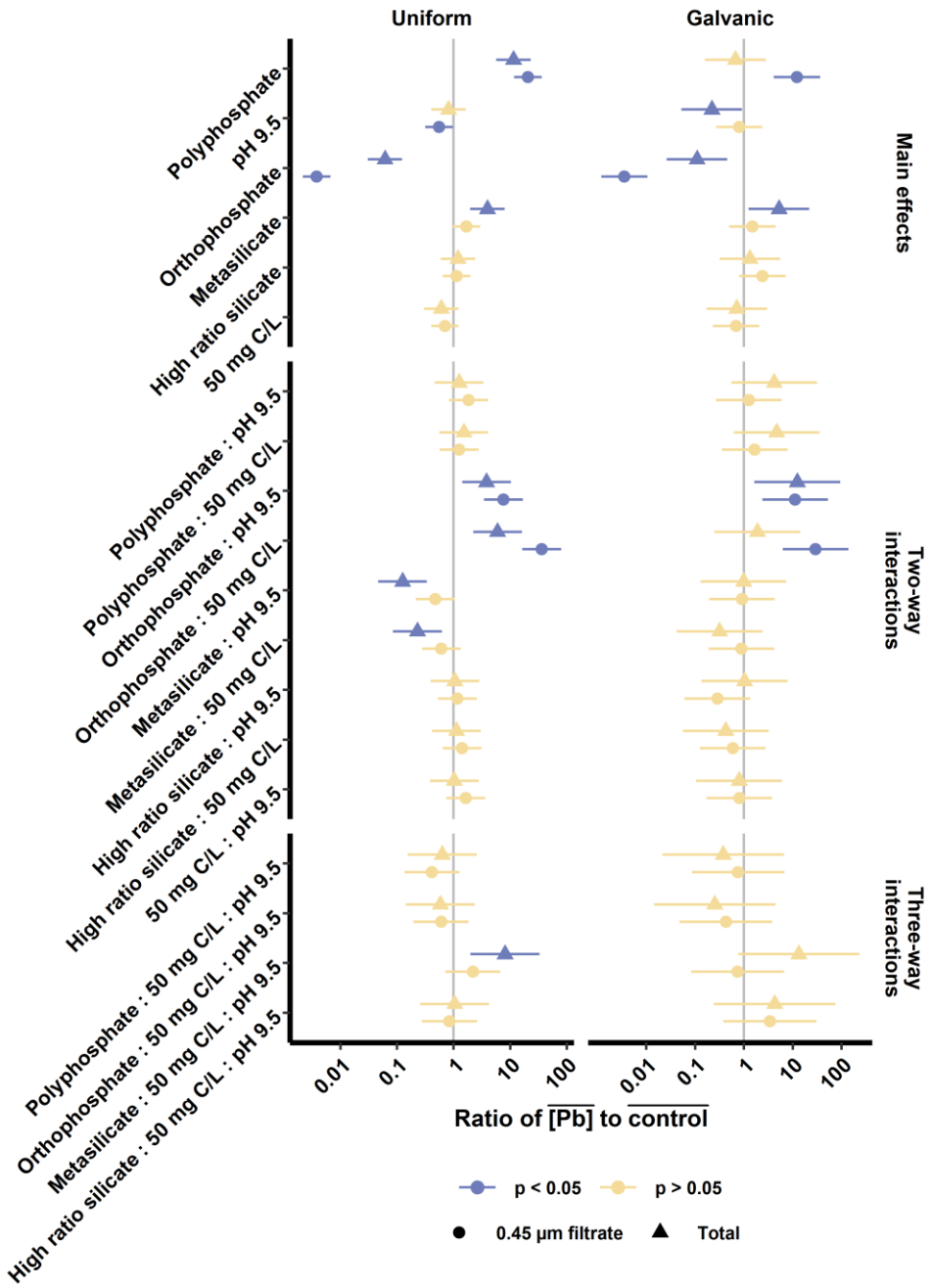

Figure 42 Linear model coefficients estimate the ratio of geometric mean lead in each treatment group (e.g., pH, DIC, or orthophosphate) to that of the reference group (pH 7, DIC 5 mg C/L, no inhibitor) with uniform corrosion (stable phase) and galvanic corrosion (initial phase). Points represent coefficient magnitudes and error bars span the 95% confidence intervals; a ratio greater than 1 indicates an increase in mean lead release in the associated treatment group.

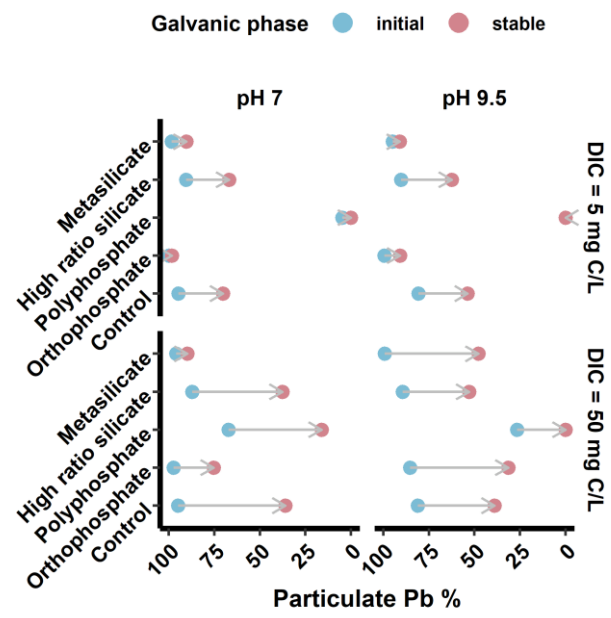

Figure 43 Particulate lead (>0.45 µm) as a percentage of total lead during the initial and stable galvanic phases of the experiment.

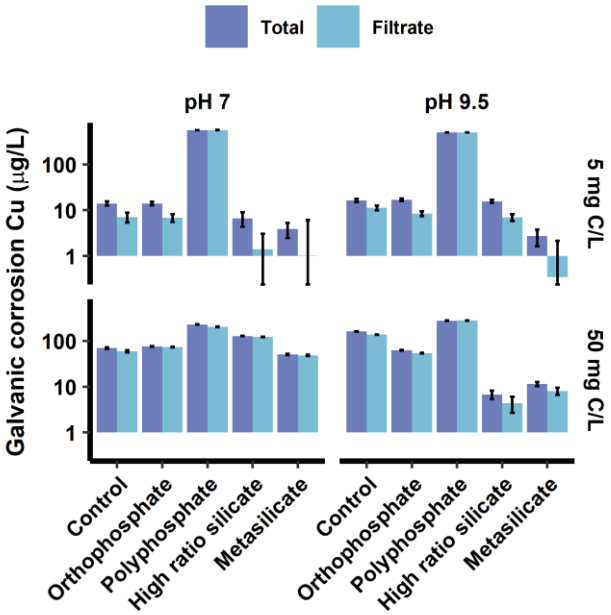

Figure 44 Geometric mean of total and filtrate (<0.45 µm) copper after 48-hr stagnation during the stable phase. Error bars span one geometric standard deviation about the mean.

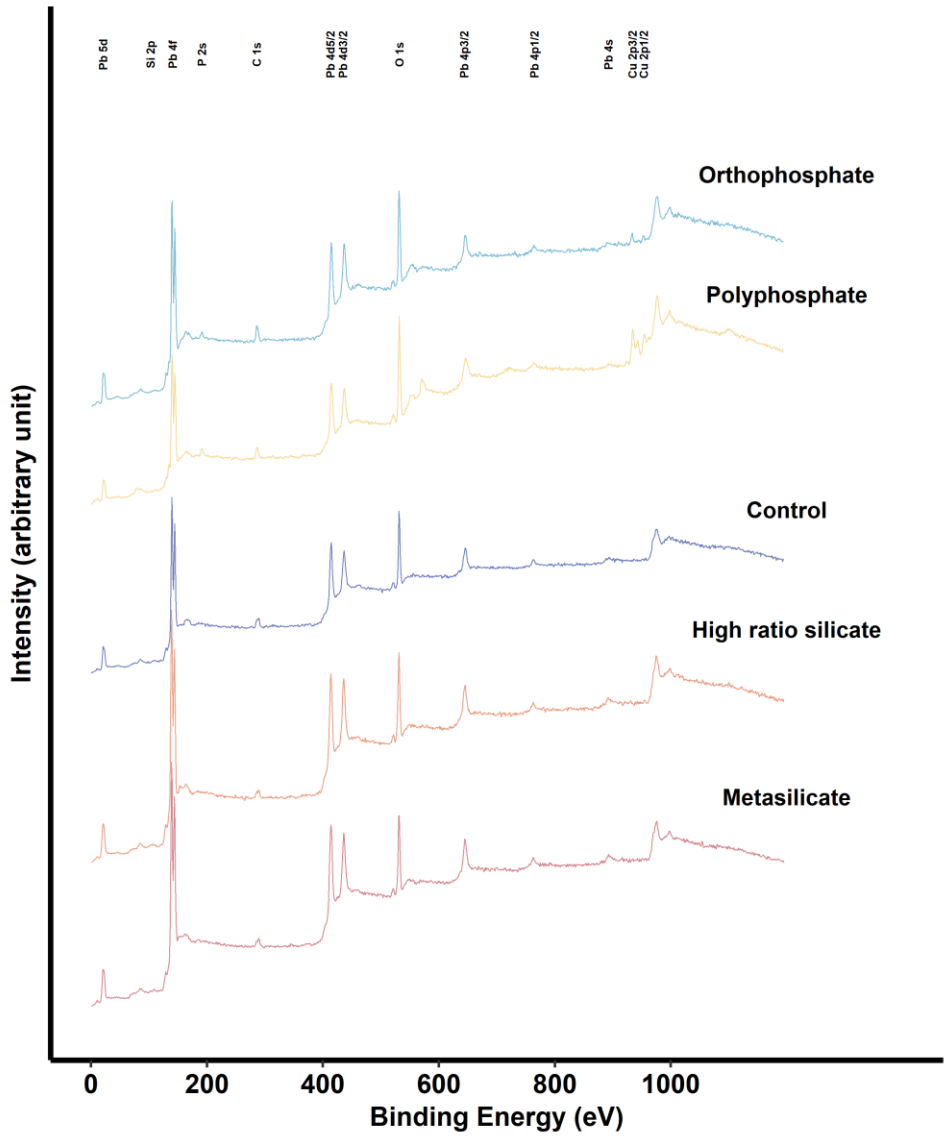

Figure 45 XPS survey of lead coupons at pH 7 and DIC 5 mg C/L.

Appendix B: Supporting Data for Chapter 3

Table 4 Summary of thermodynamic data used in equilibrium solubility modeling.[54]

Phase	Equation	log K
-	$Pb^{+2} + H_2O = PbOH^+ + H^+$	-7.22
-	$Pb^{+2} + 3H_2O = Pb(OH)_3^- + 3H^+$	-28.08
-	$Pb^{+2} + 4H_2O = Pb(OH)_4^{-2} + 4H^+$	-39.72
-	$Pb^{+2} + 2H_2O = Pb(OH)_2 + 2H^+$	-16.91
-	$2Pb^{+2} + H_2O = Pb_2OH^{+3} + H^+$	-6.36
-	$3Pb^{+2} + 4H_2O = Pb_3(OH)_4^{+2} + 4H^+$	-23.86
-	$4Pb^{+2} + 4H_2O = Pb_4(OH)_4^{+4} + 4H^+$	-20.88
-	$6Pb^{+2} + 8H_2O = Pb_6(OH)_8^{+4} + 8H^+$	-43.62
-	$Pb^{+2} + CO_3^{-2} = PbCO_3$	7.10
-	$Pb^{+2} + 2CO_3^{-2} = Pb(CO_3)_2^{-2}$	10.33
-	$Pb^{+2} + CO_3^{-2} + H^+ = PbHCO_3^+$	12.59
-	$Pb^{+2} + PO_4^{-3} + H^+ = PbHPO_4$	15.41
-	$Pb^{+2} + PO_4^{-3} + 2H^+ = PbH_2PO_4^+$	21.05
-	$Pb^{+2} + SO_4^{-2} = PbSO_4$	2.73
-	$Pb^{+2} + 2SO_4^{-2} = Pb(SO_4)_2^{-2}$	3.50
-	$Pb^{+2} + Cl^- = PbCl^+$	1.59
-	$Pb^{+2} + 2Cl^- = PbCl_2$	1.80
-	$Pb^{+2} + 3Cl^- = PbCl_3^-$	1.71
-	$Pb^{+2} + 4Cl^- = PbCl_4^{-2}$	1.43
Cerussite	$PbCO_3 = Pb^{+2} + CO_3^{-2}$	-13.11
Hydrocerussite	$Pb(OH)_2{:}2PbCO_3 + 2H^+ = 3Pb^{+2} + 2CO_3^{-2} + 2H_2O$	-18.00
Hydroxylpyromorphite	$Pb_5(PO_4)_3OH + H^+ = 5Pb^{+2} + 3PO_4^{-3} + H_2O$	-62.83

Table 5 Linear model coefficients, p-values, and 95% confidence intervals (lower and upper bounds).

Filter pore size (μm)	Term	Coefficient	p-value	Lower bound	Upper bound
0.2	(Intercept)	78.78	0.00	65.86	94.23
0.2	Polyphosphate	23.49	0.00	17.23	32.03
0.2	Orthophosphate	0.03	0.00	0.02	0.05
0.2	Silicate	1.23	0.08	0.98	1.55
0.2	50 mg C/L	0.62	0.00	0.45	0.84
0.2	pH 9	0.49	0.00	0.36	0.67
0.2	Polyphosphate : 50 mg C/L	1.60	0.05	1.00	2.58
0.2	Orthophosphate : 50 mg C/L	14.11	0.00	8.79	22.66
0.2	Silicate : 50 mg C/L	0.82	0.34	0.53	1.25
0.2	Polyphosphate : pH 9	1.90	0.01	1.18	3.05
0.2	Orthophosphate : pH 9	6.23	0.00	3.88	10.00
0.2	Silicate : pH 9	1.33	0.18	0.87	2.04
0.2	50 mg C/L : pH 9	5.73	0.00	3.57	9.20
0.2	Polyphosphate : 50 mg C/L : pH 9	0.06	0.00	0.03	0.13
0.2	Orthophosphate : 50 mg C/L : pH 9	0.22	0.00	0.11	0.43
0.2	Silicate : 50 mg C/L : pH 9	0.49	0.04	0.25	0.95
0.45	(Intercept)	122.93	0.00	102.81	147.00
0.45	Polyphosphate	15.92	0.00	11.68	21.70
0.45	Orthophosphate	0.04	0.00	0.03	0.05
0.45	Silicate	1.00	0.99	0.80	1.26
0.45	50 mg C/L	0.47	0.00	0.34	0.64
0.45	pH 9	0.40	0.00	0.31	0.53
0.45	Polyphosphate : 50 mg C/L	2.07	0.00	1.29	3.32
0.45	Orthophosphate : 50 mg C/L	18.27	0.00	11.38	29.32
0.45	Silicate : 50 mg C/L	1.21	0.36	0.79	1.86
0.45	Polyphosphate : pH 9	2.28	0.00	1.46	3.58
0.45	Orthophosphate : pH 9	6.38	0.00	4.07	10.01
0.45	Silicate : pH 9	1.58	0.03	1.06	2.36
0.45	50 mg C/L : pH 9	6.66	0.00	4.25	10.45
0.45	Polyphosphate : 50 mg C/L : pH 9	0.07	0.00	0.04	0.14
0.45	Orthophosphate : 50 mg C/L : pH 9	0.14	0.00	0.07	0.28
0.45	Silicate : 50 mg C/L : pH 9	0.41	0.01	0.22	0.79

Table 6 Ratio of geometric mean lead release in the inhibitor group to the corresponding control group.

Filter pore size (µm)	Inhibitor	pH	DIC (mg C/L)	Ratio (inhibitor:control)
0.2	Polyphosphate	7.5	5	23.49
0.2	Polyphosphate	7.5	50	37.68
0.2	Polyphosphate	9	5	44.65
0.2	Polyphosphate	9	50	4.60
0.2	Orthophosphate	7.5	5	0.03
0.2	Orthophosphate	7.5	50	0.47
0.2	Orthophosphate	9	5	0.21
0.2	Orthophosphate	9	50	0.63
0.2	Sodium silicate	7.5	5	1.23
0.2	Sodium silicate	7.5	50	1.01
0.2	Sodium silicate	9	5	1.64
0.2	Sodium silicate	9	50	0.66
0.45	Polyphosphate	7.5	5	15.92
0.45	Polyphosphate	7.5	50	32.96
0.45	Polyphosphate	9	5	36.36
0.45	Polyphosphate	9	50	5.39
0.45	Orthophosphate	7.5	5	0.04
0.45	Orthophosphate	7.5	50	0.67
0.45	Orthophosphate	9	5	0.24
0.45	Orthophosphate	9	50	0.62
0.45	Sodium silicate	7.5	5	1.00
0.45	Sodium silicate	7.5	50	1.21
0.45	Sodium silicate	9	5	1.58
0.45	Sodium silicate	9	50	0.79

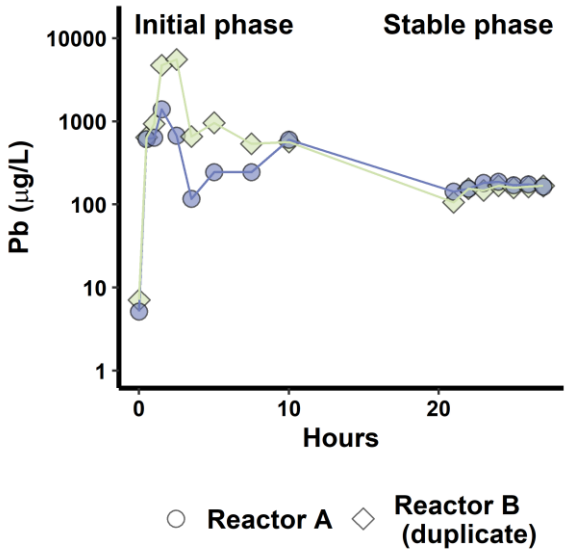

Figure 46 Lead in effluent from CSTRs with 1 g/L cerussite as a function of operational times. Hydraulic residence time of 30 min at pH 7.5 and dissolved inorganic carbon of 5 mg C/L

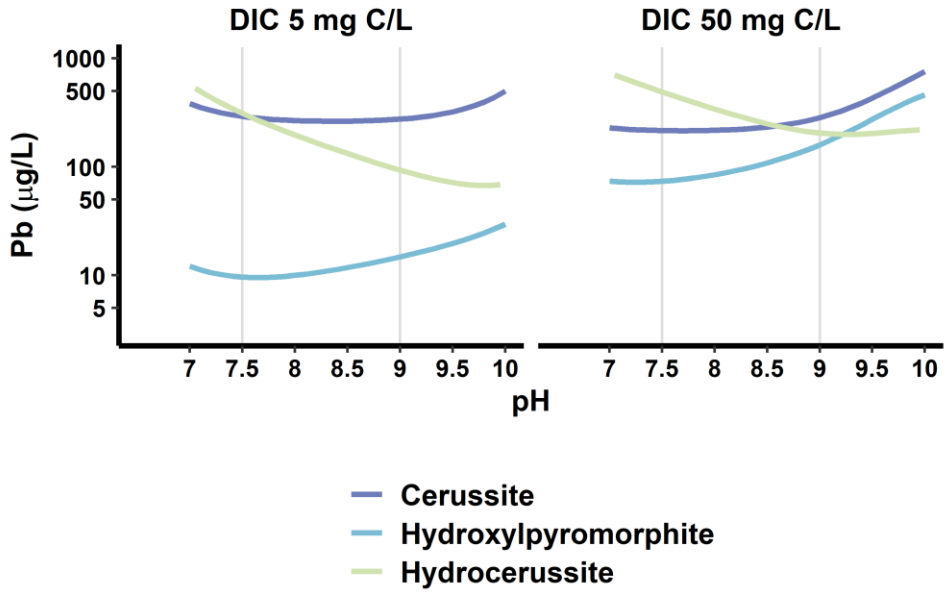

Figure 47 Equlibirium solubility of cerussite, hydrocerussite, and hydroxylpyromorphite at DIC 5 and 50 mg C/L. Grey lines indicated experimental pH condition (7.5 or 9) in this study. Thermodynamic data are due to Schock et al. [54] and solubility calculations were made with tidyphreeqc.[109]

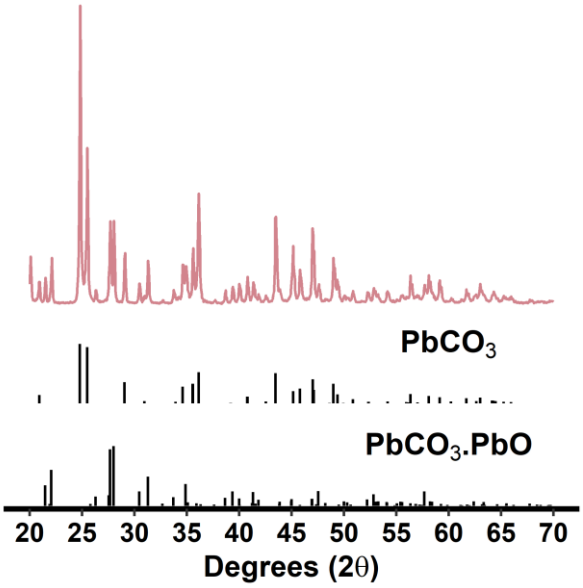

Figure 48 X-ray diffraction (XRD) patterns representing the lead carbon solids before reaction.

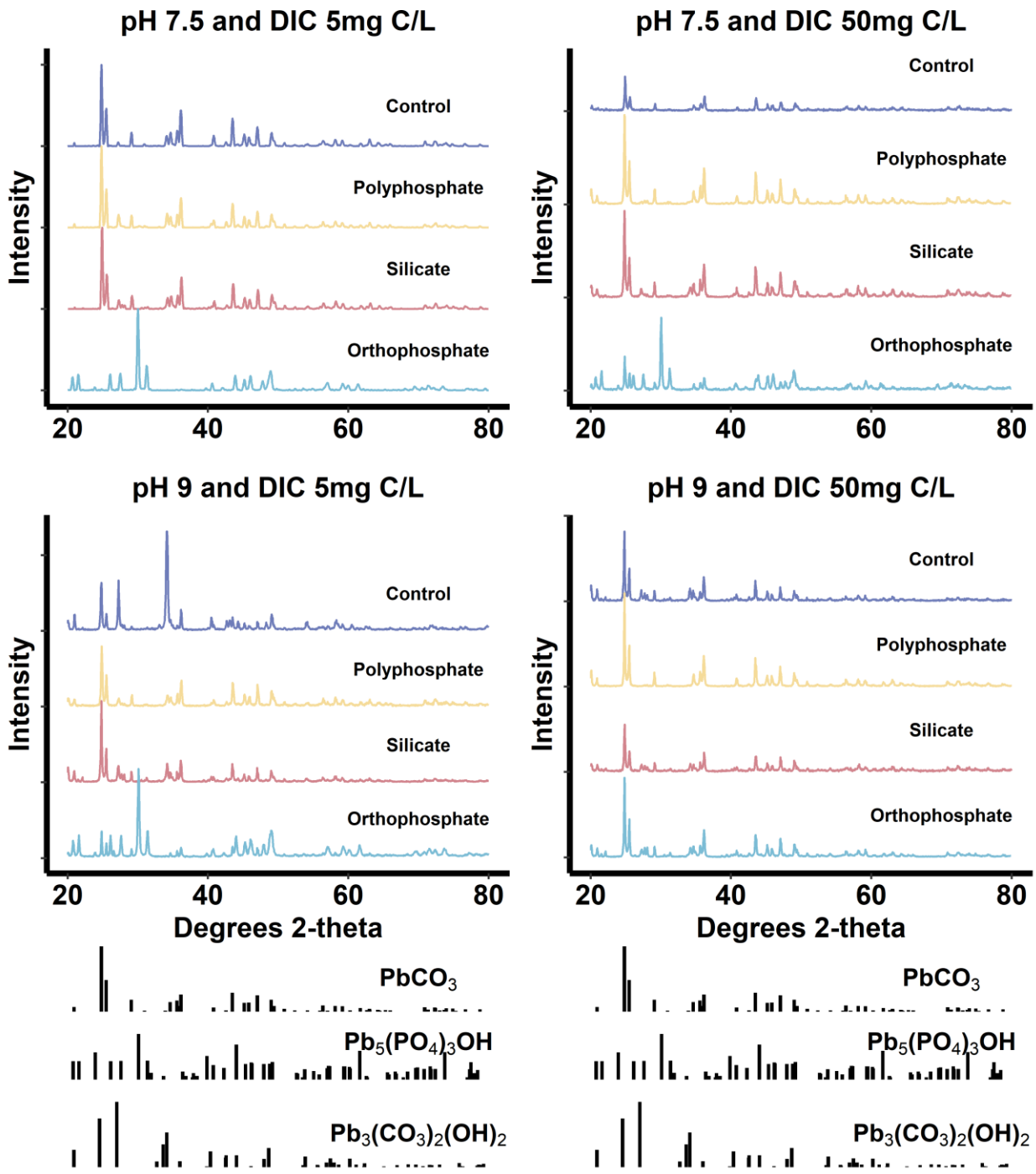

Figure 49 X-ray diffraction (XRD) patterns characterizing cerrusite particles after reaction with orthophosphate, polyphosphate, or sodium silicate at two pH (7.5 and 9) and DIC levels (5 and 50 mg C/ L^{-1}).

Appendix C: Supporting Data for Chapter 4

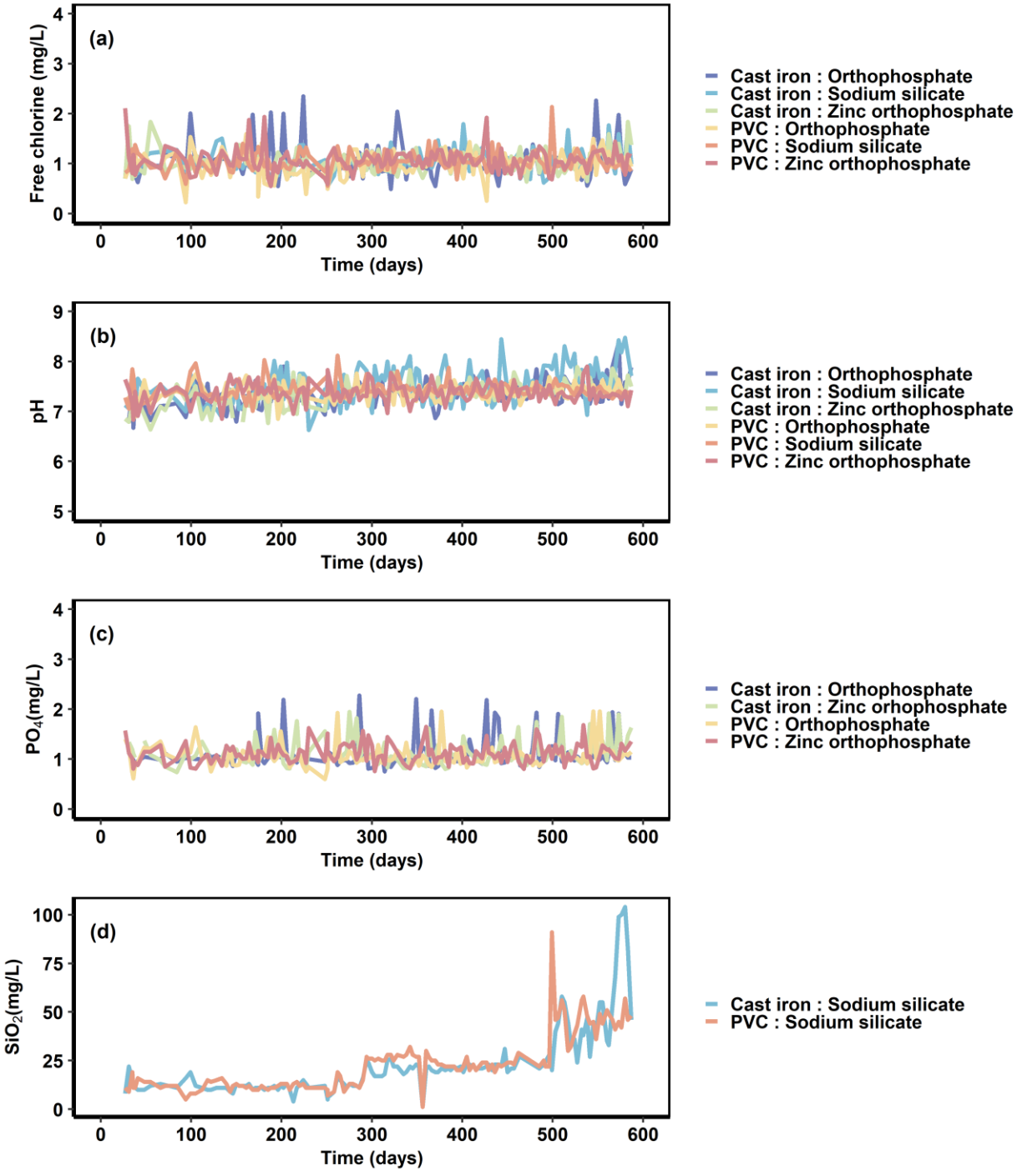

Figure 50 Free chlorine (a), pH (b), orthophosphate (c), silicate (d) in the influent to LSLs (full/partial). The free chlorine, pH, and orthophosphate series were smoothed using a four-point moving average.

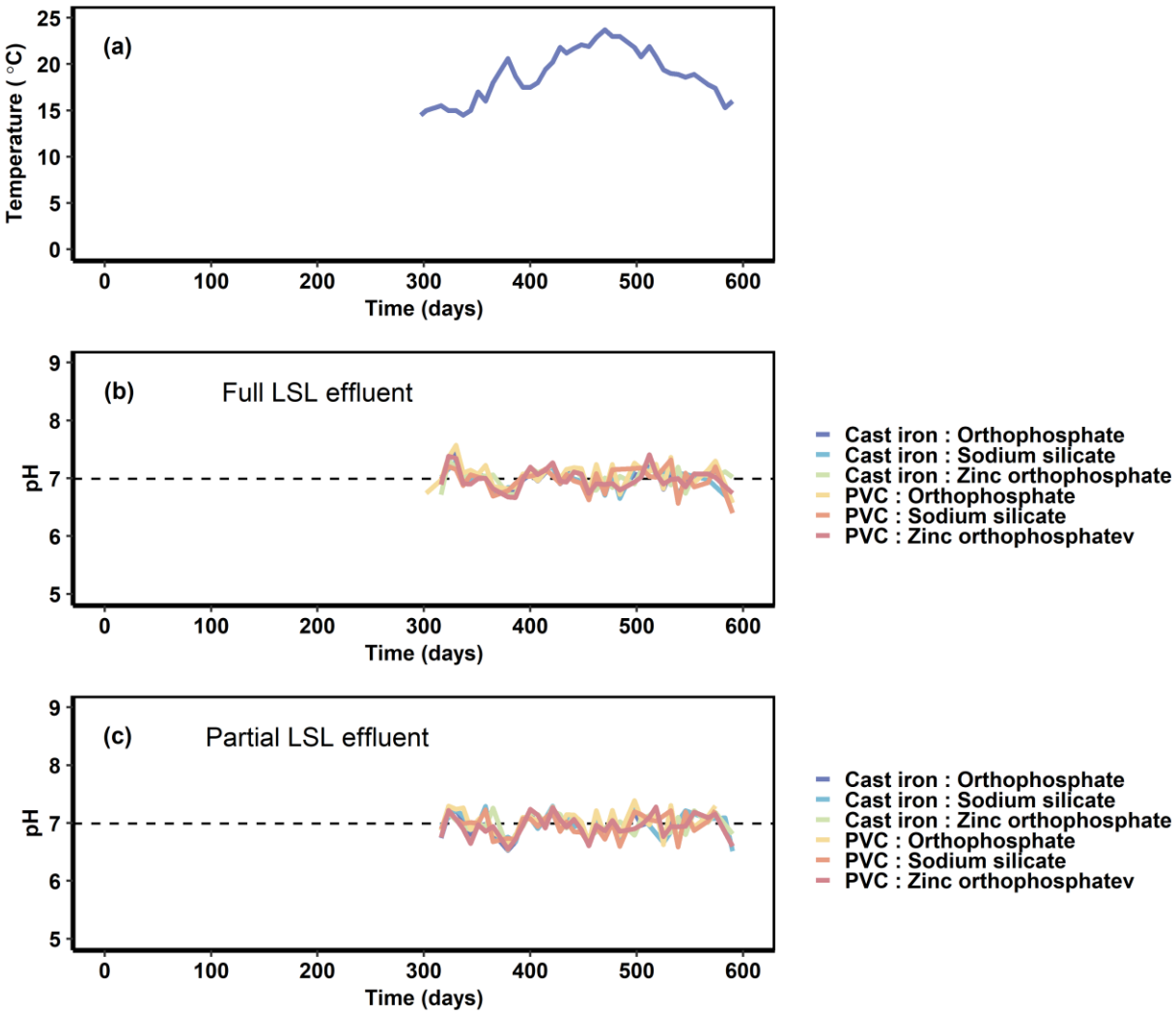

Figure 51 (a) water temperature in LSL (full/partial) effluent, (b) pH in full LSL effluent, (c) pH in partial LSL effluent. The pH series were smoothed using a four-point moving average.

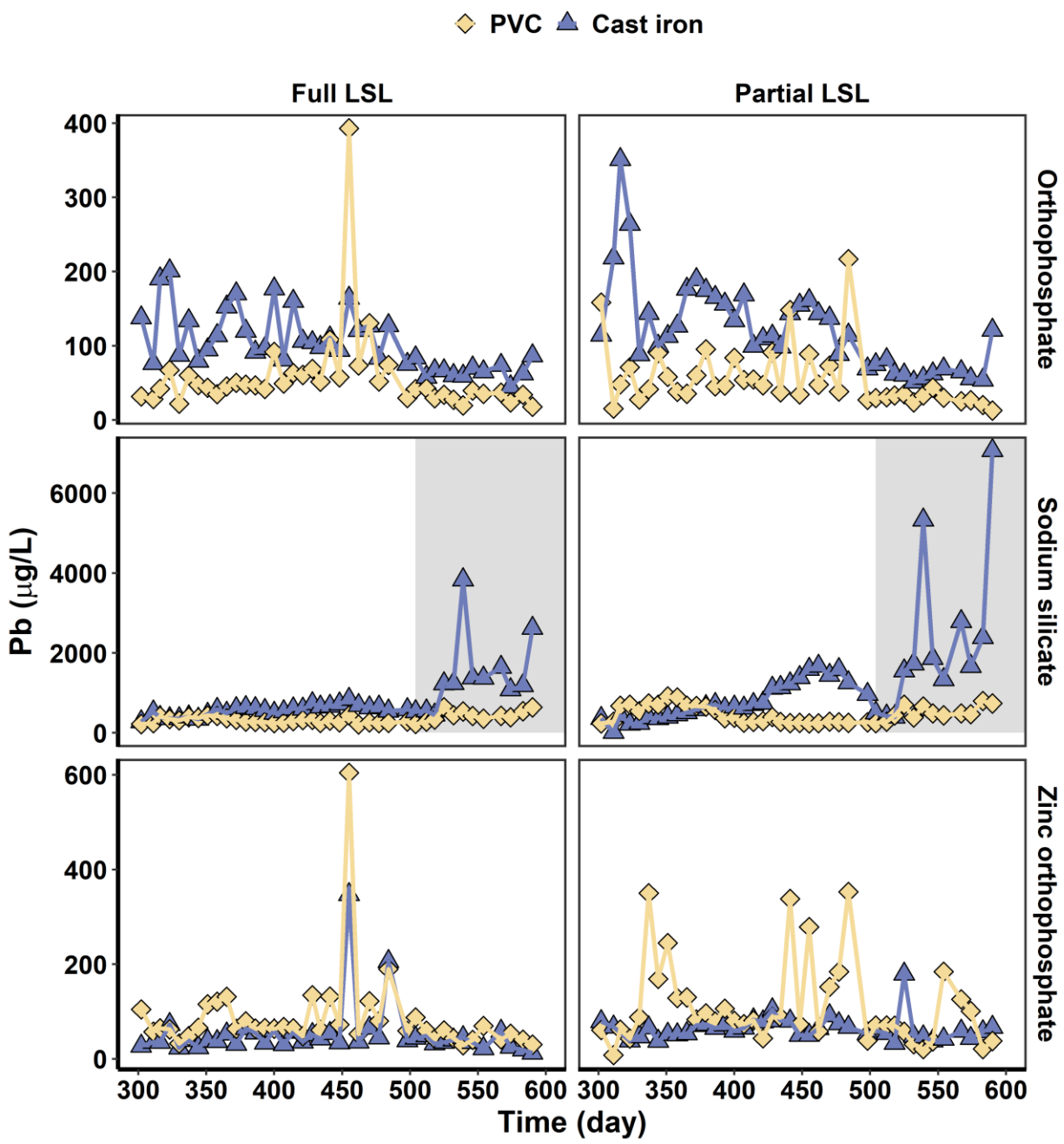

Figure 52 Lead in LSL (full/partial) effluent at an orthophosphate concentration of 1 mg PO_4^{3-} or a sodium silicate concentration of 24 (white background) or 48 mg SiO_2 mg/L (grey background).

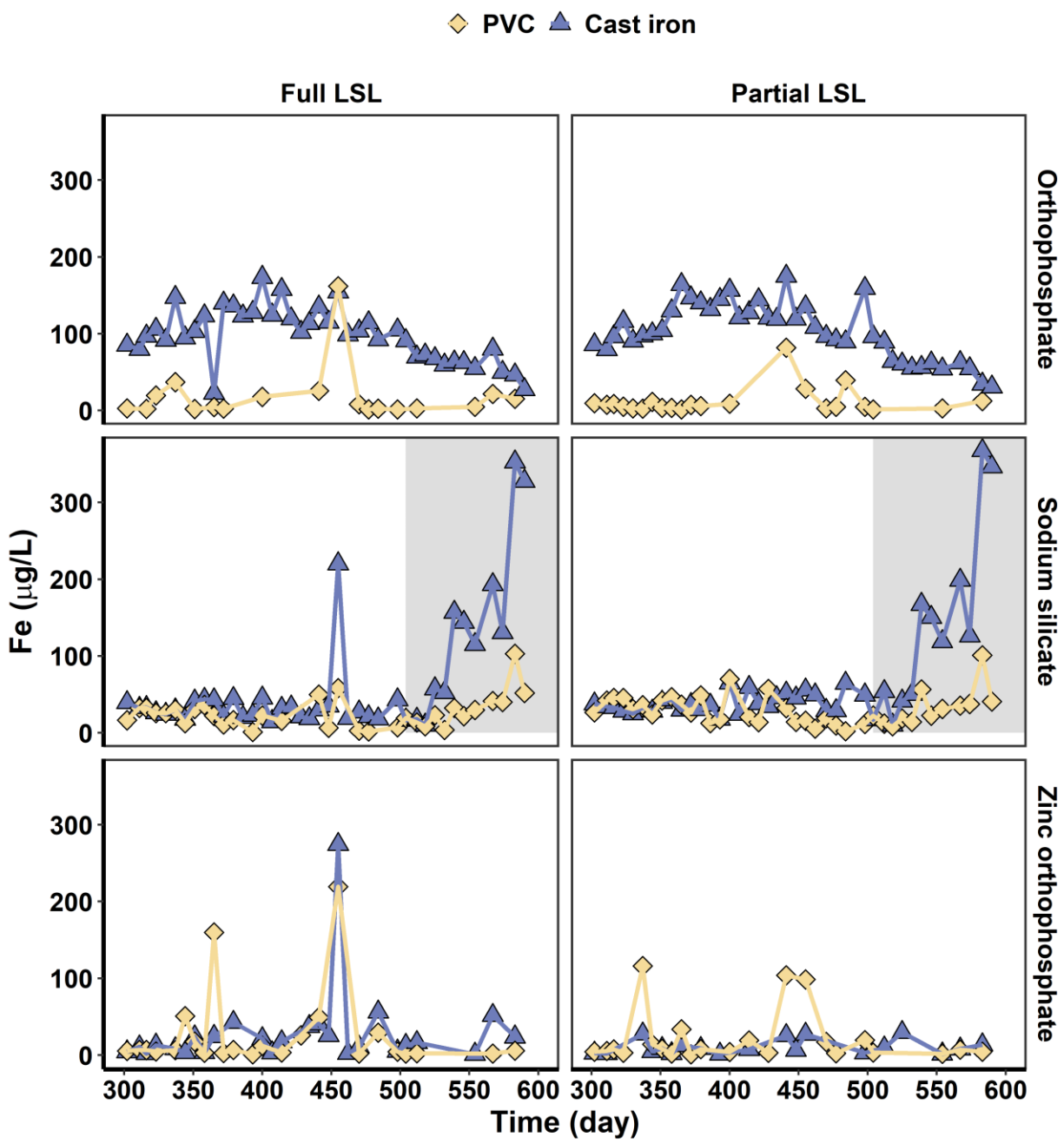

Figure 53 Iron in LSL (full/partial) effluent at an orthophosphate concentration of 1 mg PO_4^{3-} or a sodium silicate concentration of 24 (white background) or 48 mg SiO_2 mg/L (grey background).

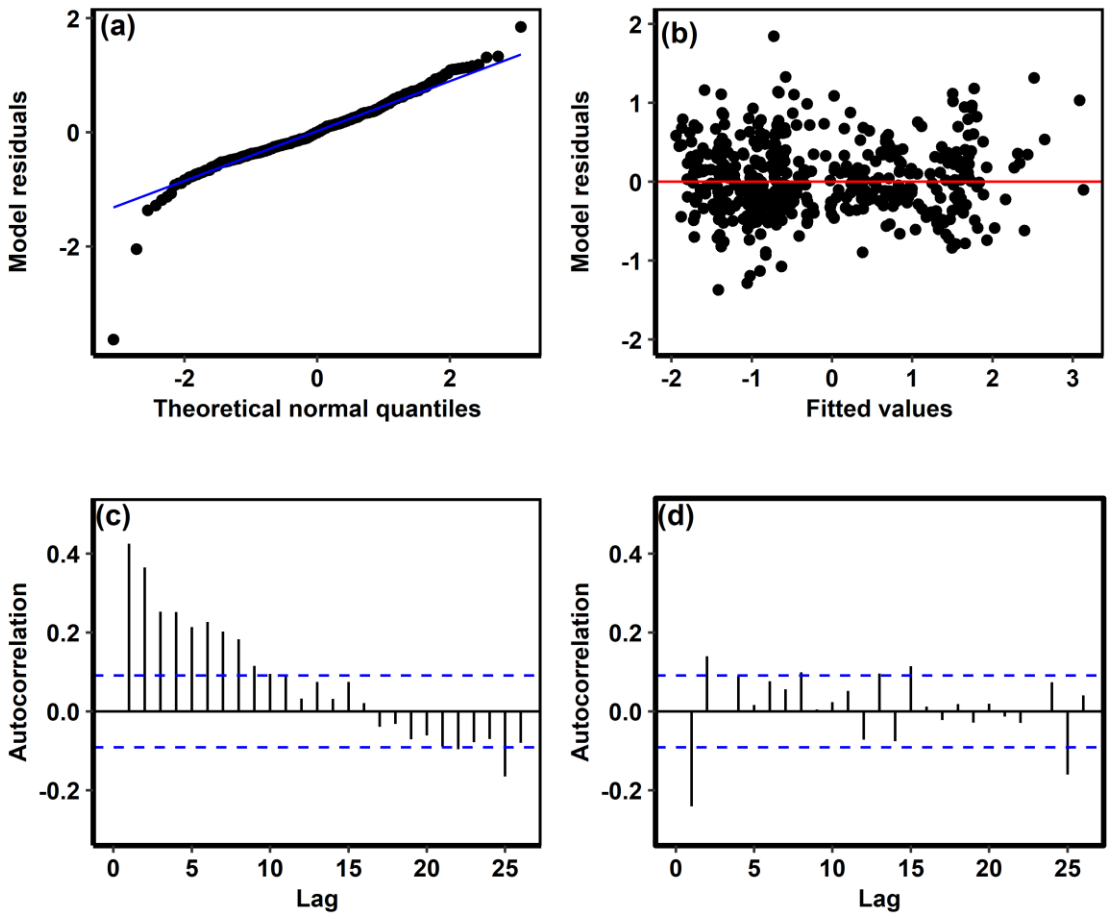

Figure 54 (a) Model residuals (data minus fitted values) were approximately Gaussian, as shown here plotted against the quantiles of the standard normal distribution. (b) The variance of the model residuals was approximately constant accross the range of fitted values. (c) The autocorrelation function of the raw model residuals (difference between data and fitted values). (d) The autocorrelation function of the normalized residuals, transformed according to the CAR(1) error model (nlme::corCAR1()). This model accounts for the majority of residual autocorrelation.

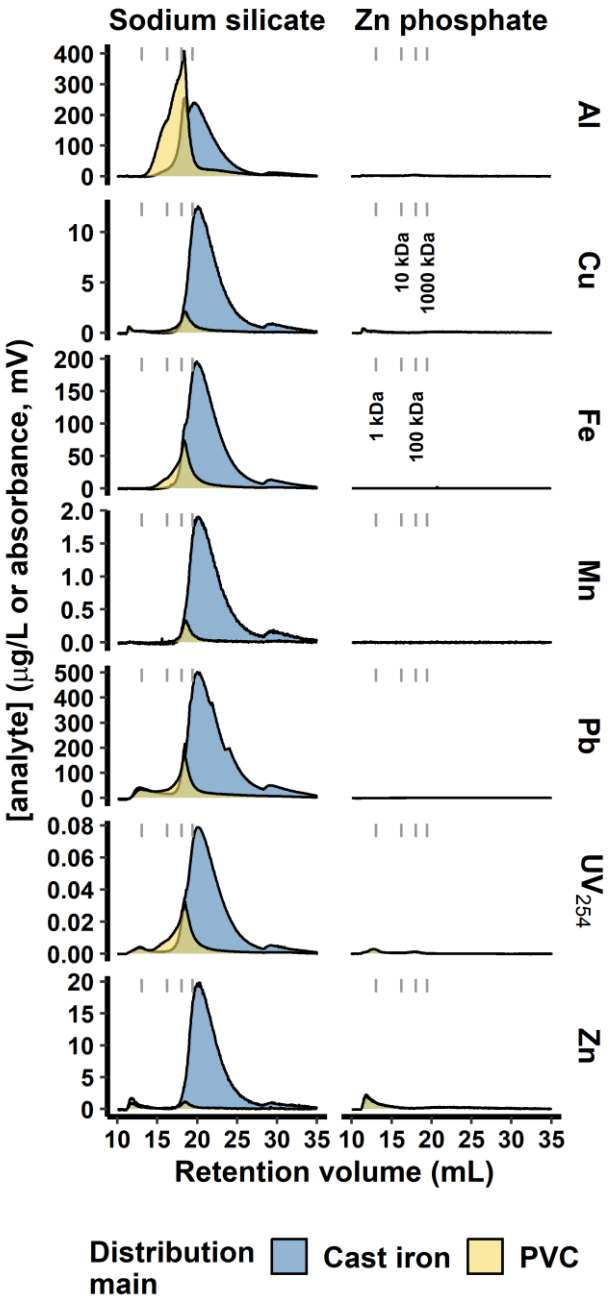

Figure 55 Fractograms representing 0.45 µm-filtered partial LSL effluent, grouped by pipe loop material (PVC/cast iron), and inhibitor type (sodium silicate at 48 mg SiO_2 /L or zinc orthophosphate at 1 mg PO_4^{3-} /L). Each fractogram represents an average of duplicates.

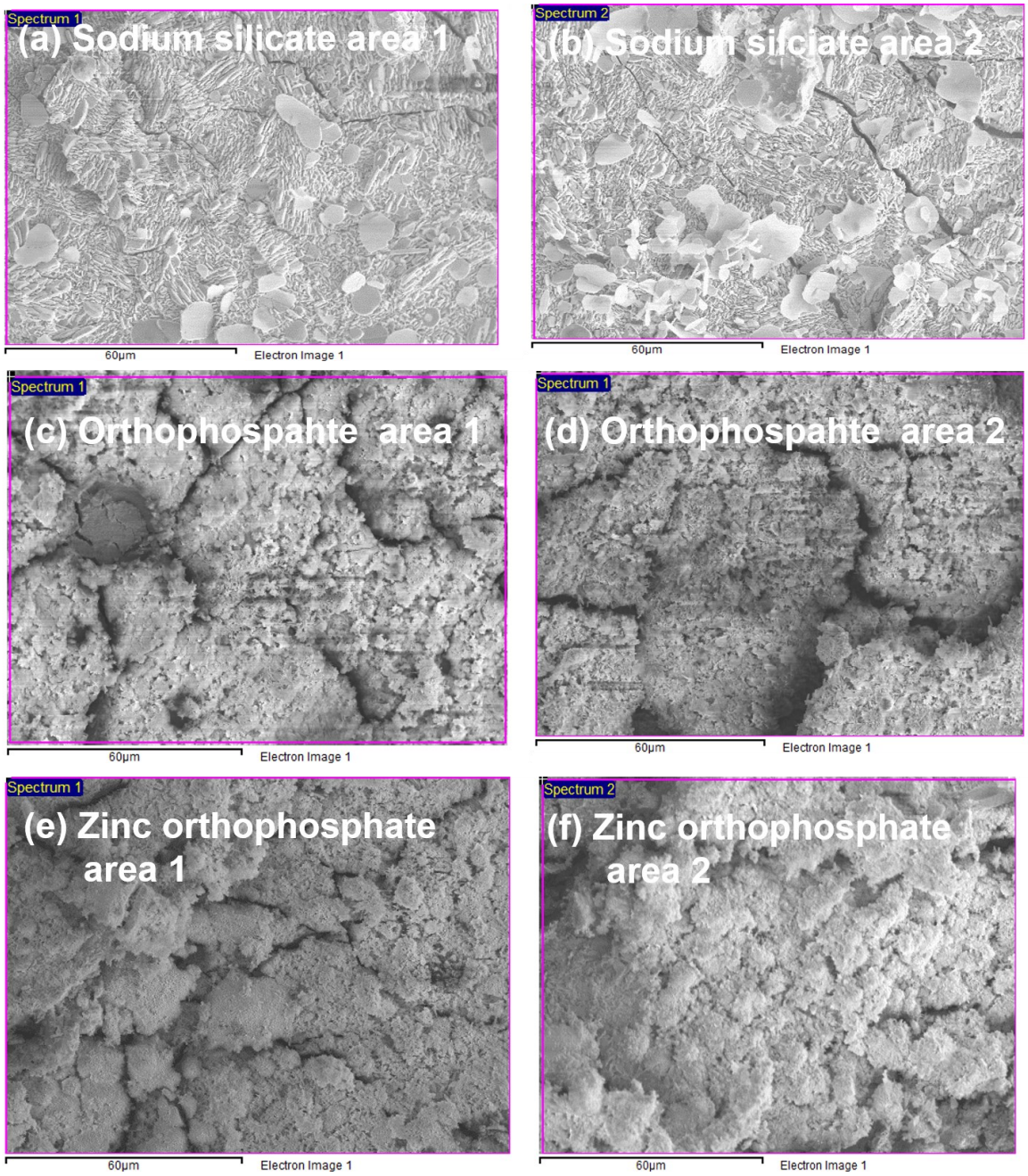

Figure 56 Scan area (duplicate) used for element analysis by SEM-EDS.

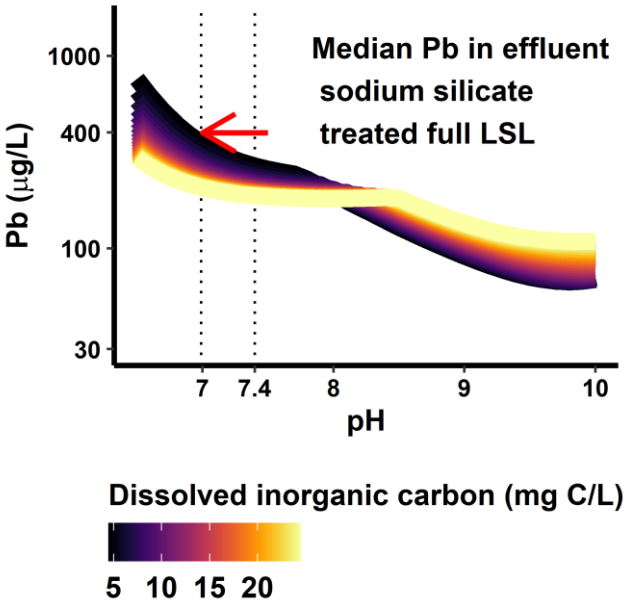

Figure 57 Solubility equilibrium of lead with cerussite and hydrocerussite as a function of pH, dissolved inorganic carbon concentration (4.5 - 25 mg C/L) at 17.9 °C (median water temperature in this study). The water pH range of 6.99 to 7.4 observed in this study are indicated by vertical dotted lines. Thermodynamic data are due to Schock et al. [54] and solubility calculations were made with tidyphreeqc.[109]

Appendix D: Supporting Data for Chapter 5

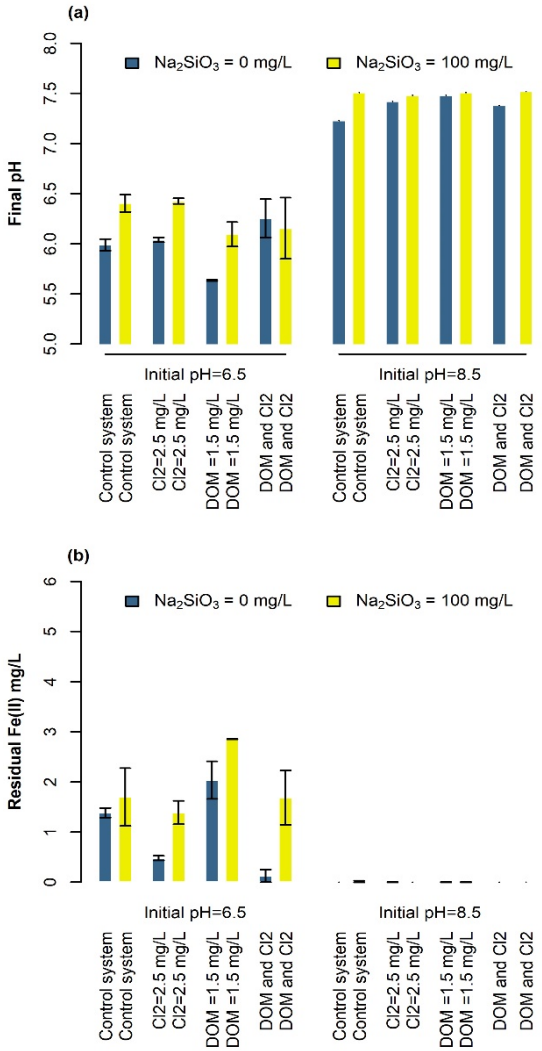

Figure 58 Final pH and residual Fe (II) after 3.5 hour of reaction.

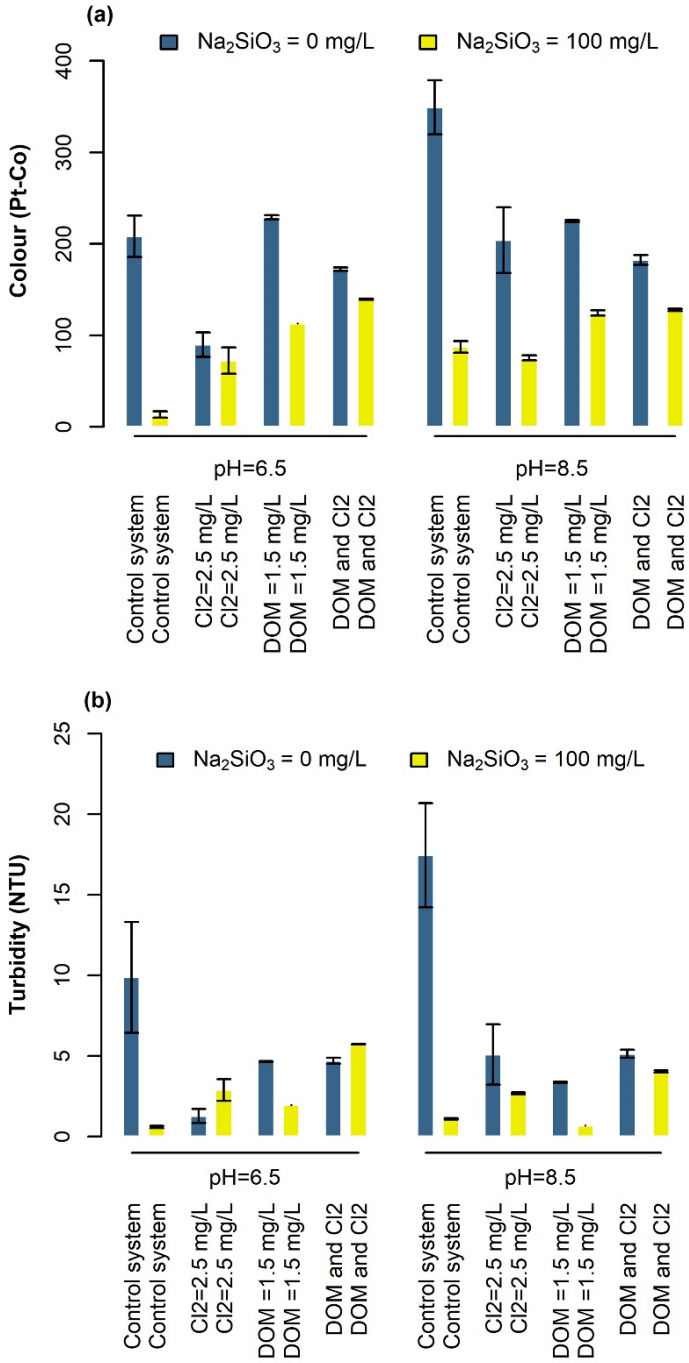

Figure 59 Effect of sodium silicate on the formation of iron particle suspension (a) colour and (b) turbidity in $NaHCO_3$ buffered synthetic water at 21±1°C.

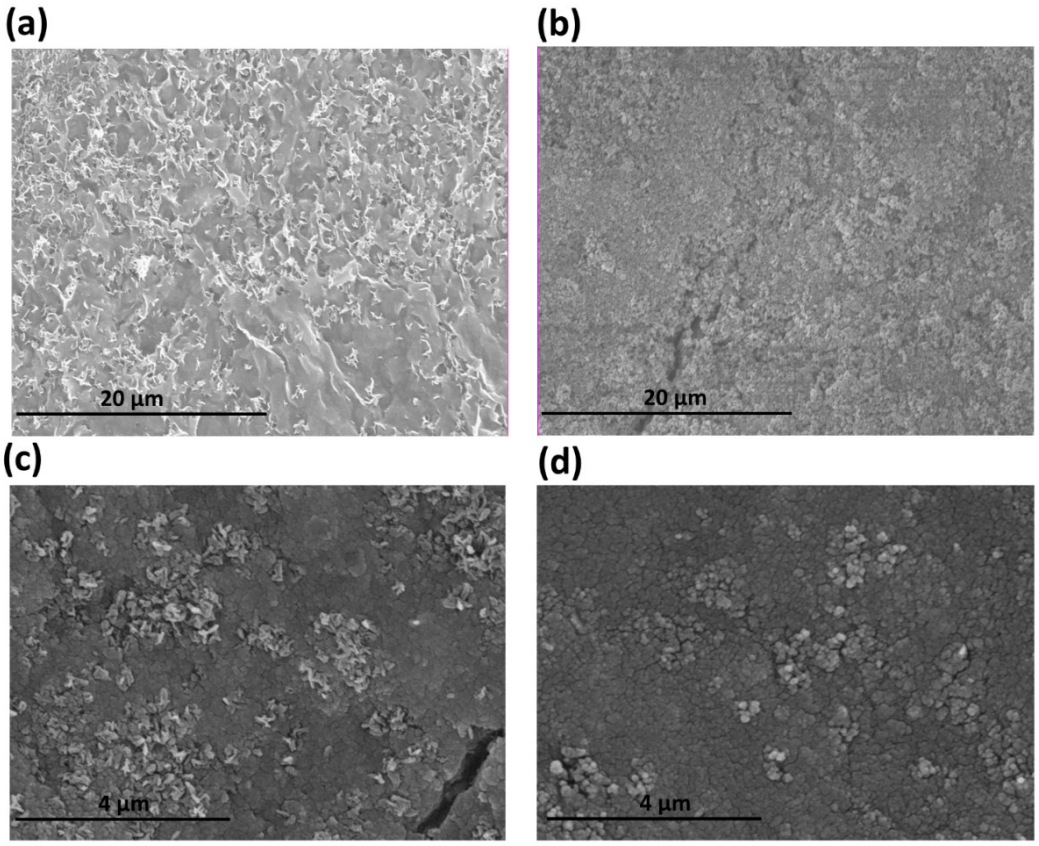

Figure 60 Scanning electron microscopy-energy dispersive X-ray spectroscopies (SEM-EDS) of (a) control system (Fe); (b) system in the presence of sodium silicate (60 mg/L) (Fe-Si); (c) system in the presence of DOM (3 mg TOC/L) and chlorine (2.5 mg/L) (Fe-DOM-Cl_2); and (d) system in the presence of DOM (3 mg TOC/L), chlorine (2.5 mg/L) and sodium silicate (60 mg/L) (Fe-DOM-Cl_2-Si).

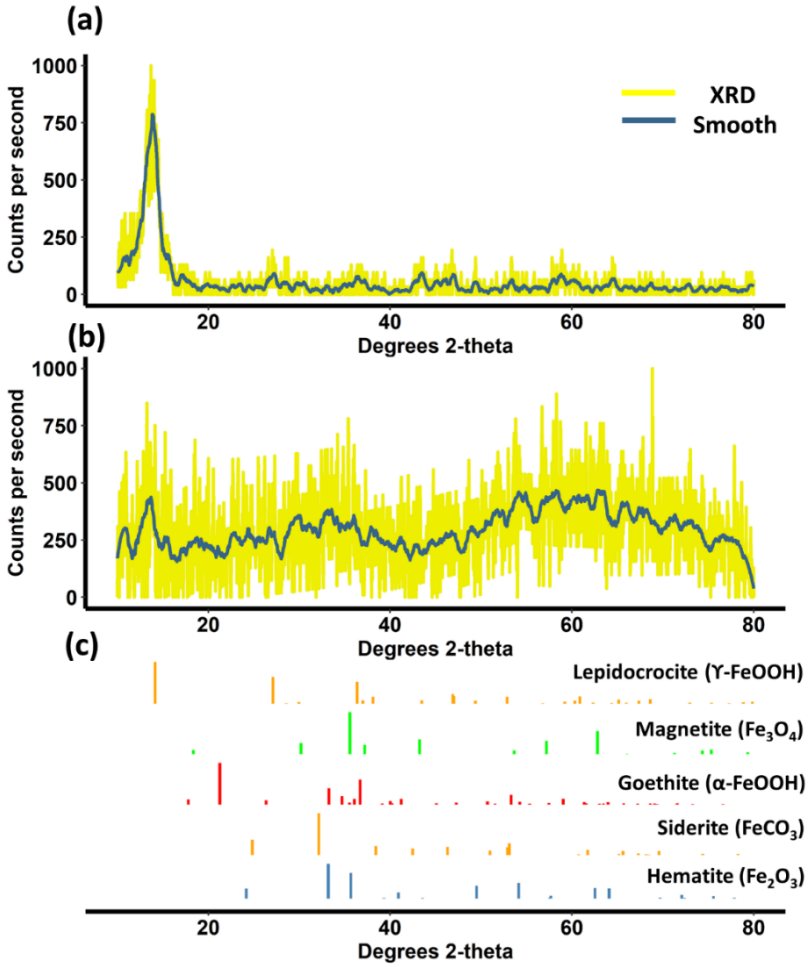

Figure 61 X-ray powder diffraction (XRD) of (a) control system (Fe); (b) system in the presence of sodium silicate (60 mg/L) (Fe-Si) and (c) XRD standard curves.

Characteristics of Goethite and Magnetite

Goethite (FeOOH): Particle size distribution in the range of 0.314-7.64 μm (>1%) using laser diffraction Surface area 10.97 m2/g using BET-N2

Magnetite (Fe_3O_4): Particle size distribution in the range of 0.991-35.3 μm (>1%) using laser diffraction Surface area 6.77 m2/g using BET-N2

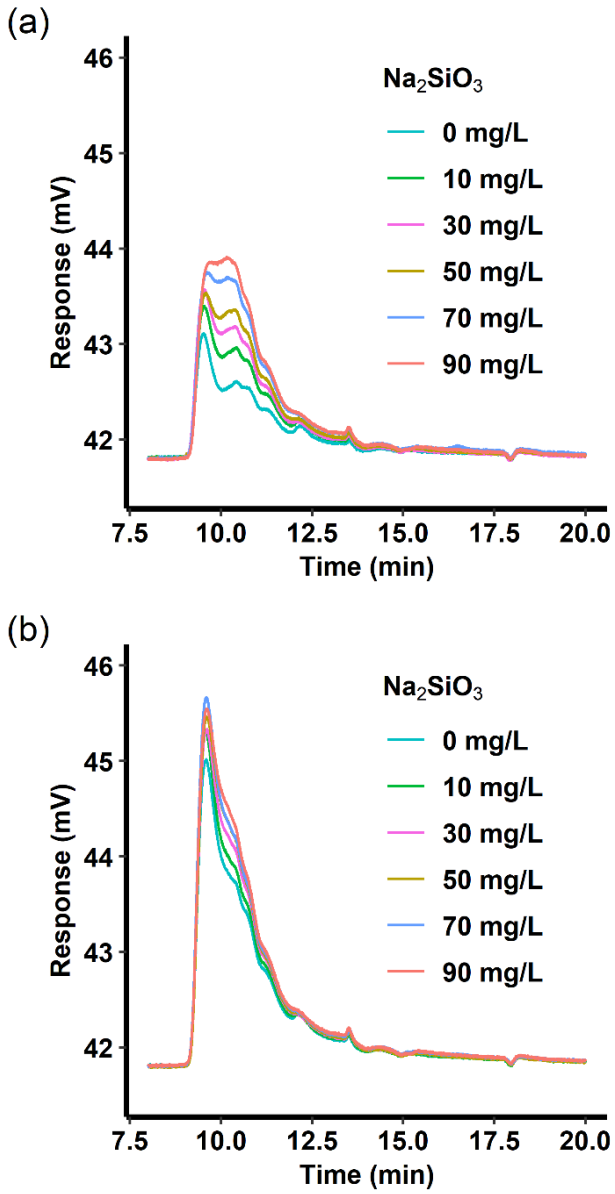

Figure 62 Molecular weight distribution of residual DOM at sodium silicate dosages of 0-90 mg/L with (a) goethite and (b) magnetite using high performance size exclusion chromatogphy (SEC-HPLC).

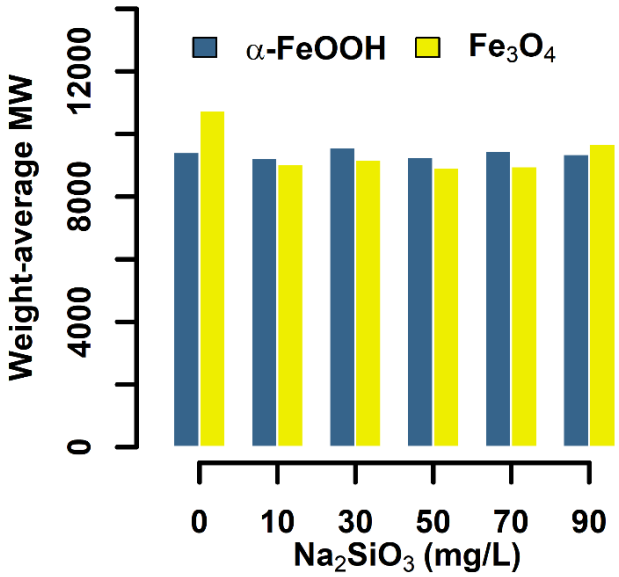

Figure 63 Weight-average molecular weight of matter in the presence of 0.3 g/L of goethite or magnetite. Data summarized from high performance size exclusion chromatogram results.

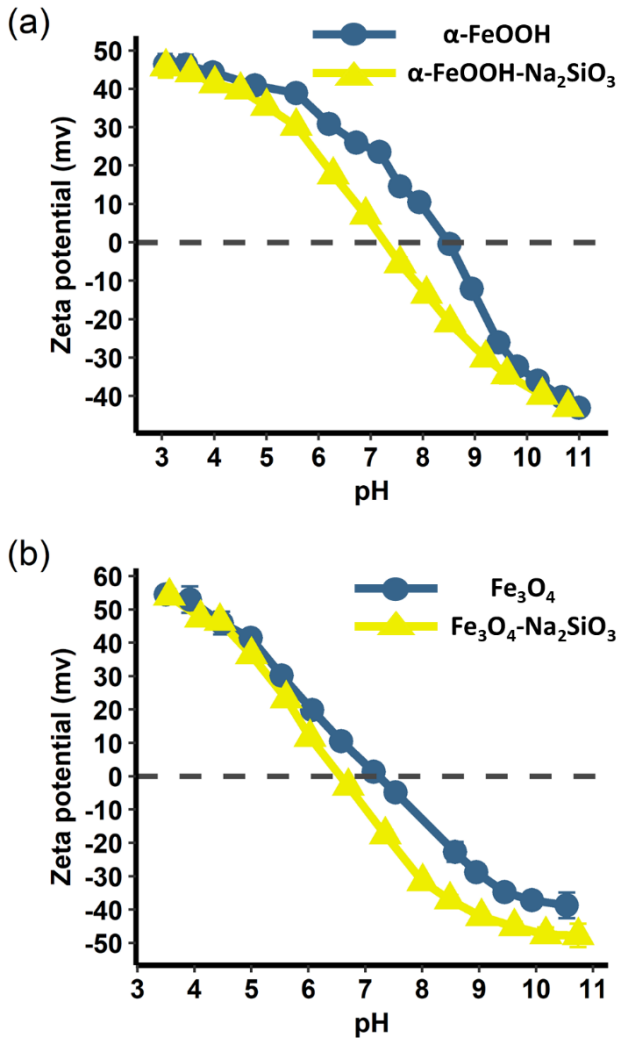

Figure 64 Effect of sodium silicate (20 mg/L) on the Zeta potential of (a) goethite (0.3 mg/L) and (b) magnetite (0.3 mg/L) at pH 6.5 and 21±1°C in a 0.01M NaCl solution.

Appendix E: Copyright Permissions

Impact of sodium silicate on lead release and colloid size distributions in drinking water

Author: Bofu Li,Benjamin F. Trueman,Sebastian Munoz,Javier A. Locsin,Graham A. Gagnon

Publication: Water Research

Publisher: Elsevier

Date: Available online 30 November 2020

Understanding the impacts of sodium silicate on water quality and iron oxide particles

B. Li, B. F. Trueman, M. S. Rahman, Y. Gao, Y. Park and G. A. Gagnon, *Environ. Sci.: Water Res. Technol.*, 2019, **5**, 1360
DOI: 10.1039/C9EW00257J